

University of Central Florida

**STARS**

---

Electronic Theses and Dissertations

---

2009

## An Integrated Hydrology/hydraulic And Water Quality Model For Watershed-scale Simulations

Cheng Wang

*University of Central Florida*



Part of the [Civil Engineering Commons](#)

Find similar works at: <https://stars.library.ucf.edu/etd>

University of Central Florida Libraries <http://library.ucf.edu>

This Doctoral Dissertation (Open Access) is brought to you for free and open access by STARS. It has been accepted for inclusion in Electronic Theses and Dissertations by an authorized administrator of STARS. For more information, please contact [STARS@ucf.edu](mailto:STARS@ucf.edu).

---

### STARS Citation

Wang, Cheng, "An Integrated Hydrology/hydraulic And Water Quality Model For Watershed-scale Simulations" (2009). *Electronic Theses and Dissertations*. 3852.

<https://stars.library.ucf.edu/etd/3852>

AN INTEGRATED HYDROLOGY/HYDRAULIC AND WATER QUALITY  
MODEL FOR WATERSHED-SCALE SIMULATIONS

by

CHENG WANG  
M.S. Iowa State University, 2007  
B.S. Wuhan University of Technology, 1997

A dissertation submitted in partial fulfillment of the requirements  
for the degree of Doctor of Philosophy  
in the Department of Civil, Environmental, & Construction Engineering  
in the College of Engineering and Computer Science  
at the University of Central Florida  
Orlando, Florida

Fall Term  
2009

Major Professor: Gour-Tsyh (George) Yeh

© 2009 Cheng Wang

## ABSTRACT

This dissertation presents the design of an integrated watershed model, WASH123D version 3.0, a first principle, physics-based watershed-scale model of integrated hydrology/hydraulics and water quality transport. This numerical model is comprised of three modules: (1) a one-dimensional (1-D) simulation module that is capable of simulating separated and coupled fluid flow, sediment transport and reaction-based water quality transport in river/stream/canal networks and through control structures; (2) a two-dimensional (2-D) simulation module, capable of simulating separated and coupled fluid flow, sediment transport, and reactive biogeochemical transport and transformation in two-dimensional overland flow systems; and (3) a three-dimensional (3-D) simulation module, capable of simulating separated and coupled fluid flow and reactive geochemical transport and transformation in three-dimensional variably saturated subsurface systems.

The Saint Venant equation and its simplified versions, diffusion wave and kinematic wave forms, are employed for surface fluid flow simulations and the modified Richards equation is applied for subsurface flow simulation. The reaction-based advection-dispersion equation is used as the governing equation for water quality transport. Several physically and mathematically based numerical options are provided to solve these governing equations for different application purposes.

The surface-subsurface water interactions are considered in the flow module and simulated on the basis of continuity of interface. In the transport simulations, fast/equilibrium reactions are decoupled from slow/kinetic reactions by the decomposition of reaction networks; this enables

robust numerical integrations of the governing equation. Kinetic variables are adopted as primary dependent variables rather than biogeochemical species to reduce the number of transport equations and simplify the reaction terms. In each time step, hydrologic/hydraulic variables are solved in the flow module; kinetic variables are then solved in the transport module. This is followed by solving the reactive chemical system node by node to yield concentrations of all species. Application examples are presented to demonstrate the design capability of the model.

This model may be of interest to environmental scientists, engineers and decision makers as a comprehensive assessment tool to reliably predict the fluid flow as well as sediment and contaminant transport on watershed scales so as to evaluate the efficacy and impact of alternative watershed management and remediation techniques prior to incurring expense in the field.

## ACKNOWLEDGMENTS

First and foremost, I would like to express my deepest gratitude to my advisor, Dr. Gour-Tsyh (George) Yeh, for his invaluable guidance and support throughout my Ph.D study with his patience and knowledge.

My special thanks is to my dissertation committee members, Dr. Ni-Bin Chang, Dr. David Cooper, Dr. Scott Hagen, and Dr. Xin Lin for their effort and contribution to this work.

Many thanks to Mrs. Shu-Shen Yeh for her encouragement. I would also like to thank my friends, Jae-Young Lee, Nitin Gawande, Stephen Medeiros, Fan Zhang, Dr. Qiyu Sun and Meiling Liu for their help. I am indebted to my family for the support and encouragement that enabled me to successfully complete this work. Especially, I am grateful to my wife Lili for her love, support and encouragement during my study. I would like to thank my sons, Daniel and Eric, for their love and joy they brought me which is the most precious property in my life.

## TABLE OF CONTENTS

LIST OF FIGURES .....	9
LIST OF TABLES .....	11
CHAPTER 1 INTRODUCTION .....	1
1.1 Background.....	1
1.2 Objective And Scope Of Work.....	6
1.3 Format And Content.....	7
1.4 References.....	8
CHAPTER 2 ISSUES IN INTEGRATED MODELING AND WASH123D MODEL .....	11
2.1 Hydrological Models .....	11
2.2 Water Quality Models.....	12
2.3 Coupling hydrodynamics and water quality transport.....	14
2.4 Coupling between transport and biogeochemical reactions.....	16
2.5 WASH123D .....	18
2.6 References.....	21
CHAPTER 3 AN INTEGRATED HYDROLOGY/HYDRAULIC AND WATER QUALITY MDOEL FOR RIVER/STREAM NETWORKS .....	28
3.1 Abstract.....	28
3.2 Introduction.....	29
3.3 Theory and mathematical basis.....	31
3.3.1 Water flow in one-dimensional river/stream/canal network .....	32
3.3.2 Sediment transport in one-dimensional river/stream/canal network.....	33
3.3.3 Biogeochemical transport in one-dimensional river/stream/canal network .....	37
3.3.4 Diagonalization of reactive transport governing equation .....	38
3.4 Numerical approaches.....	44
3.4.1 Approaches for the coupled transport and chemistry equations.....	44
3.4.2 Discretization schemes .....	47
3.4.3 Coupling of fluid flow with reactive water quality transport.....	57
3.5 Model verification.....	58
3.5.1 Example.....	59
3.5.2 Case study.....	72

3.6	Conclusion .....	76
3.7	Reference .....	77
CHAPTER 4 AN INTEGRATED HYDROLOGY/HYDRAULIC AND WATER QUALITY MODEL FOR OVERLAND SHALLOW WATER SYSTEMS .....		82
4.1	Abstract .....	82
4.2	Introduction .....	83
4.3	Theory and mathematical basis .....	85
4.3.1	Water flow in 2-D overland regime .....	85
4.3.2	Bed Sediment Transport in 2-D Overland Regime .....	87
4.3.3	Suspended Sediments .....	87
4.3.4	Reactive water quality transport in 2-D overland regime .....	90
4.3.5	Diagonalization of 1-D Reactive Transport Governing Equations .....	91
4.4	Numerical approaches .....	98
4.4.1	Finite Difference Method to Bed Sediment Transport .....	98
4.4.2	Numerical approaches for Suspended Sediment Transport .....	98
4.4.3	Strategies for the coupling of transport and biogeochemical reactions .....	98
4.4.4	Discretization schemes .....	100
4.5	Model verification .....	109
4.5.1	Example 1 .....	110
4.5.2	Example 2 .....	117
4.6	Conclusion .....	129
4.7	References .....	130
CHAPTER 5 AN INTEGRATED HYDROLOGY/HYDRAULIC AND WATER QUALITY MODEL FOR SUBSURFACE WATER SYSTEMS .....		134
5.1	Abstract .....	134
5.2	Introduction .....	135
5.3	Theory and mathematical basis .....	136
5.3.1	Water flow in subsurface system .....	136
5.3.2	Reactive Chemical Transport In Subsurface Systems .....	137
5.3.3	Diagonalization of Species Transport Equations .....	140
5.4	Numerical approaches .....	146
5.4.1	Strategies for the coupling transport and biogeochemical reactions .....	146

5.4.2	Discretization schemes .....	148
5.5	Model verification.....	156
5.6	Conclusion .....	168
5.7	References.....	169
CHAPTER 6	SUMMARY AND FUTURE WORK.....	174
6.1	Summary .....	174
6.2	Future works .....	176
6.3	References.....	177

## LIST OF FIGURES

Figure 2.1	Basic components, physical basis, and numerical approaches in WASH123D	21
Figure 3.1	Boundary condition and initial condition	60
Figure 3.2	Velocity profile from the two models	61
Figure 3.3	Simulated water depth at day 2, 6, and 12	61
Figure 3.4	Velocity at node 2 and 8	62
Figure 3.5	Water depths at node 2 and 8	62
Figure 3.6	Dissolved oxygen concentration profile for the two models	68
Figure 3.7	Phytoplankton concentration profile for the two models	68
Figure 3.8	Nitrate concentration profile for the two models	69
Figure 3.9	Dissolved organics concentration profile the two models	69
Figure 3.10	Variation of dissolved oxygen concentration at two locations	70
Figure 3.11	Variation of phytoplankton concentration at two locations	71
Figure 3.12	Variation of nitrate concentration at two locations	71
Figure 3.13	Variation of dissolved organics concentration at two locations	72
Figure 3.14	Schematic of the Des Moines River study area, Iowa, USA	74
Figure 3.15	Upstream discharge data from USGS gauge station	74
Figure 3.16	Comparison of model results with observed data	76
Figure 4.1	Simulated depth at t = half day	111
Figure 4.2	Simulated depth at t = half day	112
Figure 4.3	Concentration distribution of CMW1	115
Figure 4.4	Concentration distribution of CIMW1	116

Figure 4.5	Discretization, open boundary, and point sources.....	118
Figure 4.6	Simulated water depth.....	121
Figure 4.7	Simulated velocity profile.....	122
Figure 4.8	Simulated NO <sub>3</sub> concentration profile.....	127
Figure 4.9	Simulated concentration profile of PHYT.....	128
Figure 5.1	Simulation domain and discretization.....	157
Figure 5.2	Velocity simulated by two the two models at year 1.....	161
Figure 5.3	Simulated velocity at year 100.....	162
Figure 5.4	Simulated pressure head at year 1.....	163
Figure 5.5	Simulated pressure head at year 100.....	164
Figure 5.6	Simulated Tracer concentration at year 100.....	165
Figure 5.7	simulated aqueous Uranium concentration at year 100.....	166
Figure 5.8	Simulated adsorbed Uranium concentration year 100.....	167

## LIST OF TABLES

Table 3.1	Initial and boundary conditions for the reactive water quality simulation .....	63
Table 3.2	Reaction Coefficients used in the example .....	64
Table 3.3	The 6 equilibrium chemical reactions in the system.....	64
Table 3.4	The 32 kinetic chemical Reactions in the system .....	65
Table 3.5	The parameters in reaction rate formulation .....	66
Table 3.6	Chemical Species in Example.....	75
Table 4.1	Chemical Reactions Considered in Example 1 .....	114
Table 4.2	The 32 kinetic chemical Reactions in the system .....	123
Table 4.3	The 6 equilibrium chemical reactions in the system.....	124
Table 4.4	Initial and boundary conditions for the reactive water quality simulation .....	124
Table 4.5	Reaction Coefficient.....	125
Table 4.6	The reaction rate parameters .....	125
Table 5.1	Reactions in the example .....	160

# CHAPTER 1 INTRODUCTION

## 1.1 Background

*“Water is limited resource in increasingly short supply. The ability of watersheds to provide sufficient water quantity and quality is threatened in the face increasing population growth and human activities in the watershed.”*

*(Vadineanu et al., 2007)*

Surface water and groundwater are crucial to the human being as sources of water, ecologic diversity, and environmental benefit. Concurrently, human being and their associated behaviors impact the water cycle. For instance, the dramatic withdrawal of water from a system aquifer or the discharge and disposal of pollutants from point and non-point sources will reduce the self-recovery capability of the water resources system. This will result in degradation of water sources in both quantity and quality if no appropriate mitigation actions are taken. In the recent centuries, water resources, especially those suitable for human use, have become scarce due to the dramatic increasing demands for domestic, agricultural, industrial, and other uses, and due to an increasing pollution of surface and groundwater as a result of rapid growth of population, urbanization, and economic development. It has been fully recognized that efficient and sustainable management of water resources has become essential to alleviate the negative impact of human activities and to ensure that the needs of economic development are met.

Several important tools have been used to help researchers and engineers understand and manage water resources, among which are monitoring and modeling. Each has advantages and limitations. While monitoring quantifies the current condition of water resources and its response to development strategies and identifies the location and extent of problems in water resources, a comprehensive monitoring program can cost significantly. For example, it would be difficult and expensive to construct a satisfactory picture of soil leakage and water transport based solely on measurements; consequently some kind of model must be applied. Another drawback of a strictly monitoring approach is that it can never quantitatively predict the impact of a management strategy before its implementation, which is just the advantage of a modeling approach. One of the most important advantages of modeling is that it is cost-saving and has the capability of assessing potential water resources management strategies before taking action. If the models are developed well and used properly, they are capable of predicting the potential response of water resources from the implement of the alternative management strategies. A modeling approach can also be used to optimize the location of monitoring site distribution. However, no models, even those that are comprehensive and accurate, are able to simulate the natural processes fully. The calibration and validation of models rely on monitoring data. An ideal tool for water resources management is the use of monitoring and modeling approaches in conjunction.

Watershed models typically represent the hydrologic cycle processes within watersheds physically or conceptually including but not limited to the following aspects: water flow movement as well as the transport of salinity, heat, sediment, reactive-chemical, and nutrients. Watershed models have been serving in hydrologic studies and water resources engineering as an important tool since the development of unit hydrograph concept by Sherman and the infiltration

theory by Horton in 1930's (Singh and Frevert, 2006). Most of the early models focused mainly on single component of water flow simulations of the hydrologic cycle until the 1960's, when the Stanford Watershed Model (SWM) (Crawford and Linsley, 1966) was developed. Since then many empirical and lumped watershed models have been developed, such as the Storm Water Management Model (SWMM) (Metcalf and Eddy et al., 1971) and the Precipitation-Runoff Modeling system (PRMS) (Leavesley et al., 1983). This was mainly due to the computational limitations or lack of sufficient monitoring data which is a precondition for more comprehensive models. Many of these models and their improved successors may adequately simulate the discharge of a watershed; however, they cannot assess the management strategies or provide useful information for water quality simulation, i.e. they cannot answer the "what if" questions. Two limitations of these lumped models are the requirement for the model calibration with historical data for each individual watershed, and the fact that they cannot account for the water interaction among different media and processes. It has been recognized that only a true physics-based, distributed watershed model has these capabilities and could avoid the limitations of lumped models, although with an increase in the cost of computational effort and input data collection.

Numerous models have been developed at different comprehension levels and based on different numerical approaches with the advances in the development of computer technology and numerical methods. Among these models, some emphasize water quantity while the others focus on water quality. However, the increasing water resources problems and the recognition that the interaction of different components of hydrologic processes sometimes play an important role require more comprehensive management of water resources and, in turn, demands improved

tools based on sound scientific principles and efficient technologies among which are an integrated description of the entire land phase of the hydrological cycle and an integrated description of water quantity, quality and ecology.

Besides the demand for more comprehensive and accurate models, the rapid development in science and technology, such as deeper understand of hydrologic processes, faster computer processors, larger capacity in computer storage, GIS, remote sensing, and numerical methods, has made these models possible. Significant progresses in distributed watershed model development have been made since Freeze and Harlan (1969) outlined the first blueprint of a distributed watershed model. A number of distributed watershed models have been developed recently, such as MIKE SHE (Refsgaard and Storm, 1995), IHDM (Beven et al., 1987), InHM (VanderKwaak, 1999). Most current distributed watershed models are able to physically simulate the water flow in each media, but fail to physically account for the interactions between different media. The empirical linkage terms introduced in most currently existing watershed models downgrade them into non-physics-based model (Huang and Yeh, 2009; Yeh et al., 2006).

While water quantity is still a major concern, water quality and ecologic issues have become increasingly important concerns since due to the effects of population growth, urbanization and industrialization on water quality appeared, and the requirements of the Clean Water Act. Many water quality management programs, such as Total Daily Maximum Load (TMDL), Best Management Practice (BMP), and Low Impact Development (LID), have been implemented to protect water resources from further pollution and increase sustainable development. This leads to the change in water resource management system, and hence it requires that water quality

simulation be included in the watershed models. On the one hand, hydrodynamic of water flow has an significant impact on water quality transport; on the other hand, the transport of water quality also has feedback on water flow movement. For example, the redistribution of water density due to the water quality transport and biogeochemical reactions within water flow may cause the stratification in salty water systems. Most of the current water quality models only consider water quality simulation and are linked to hydrologic or hydraulic models indirectly. For instance, WASP5 (Ambrose et al., 1993b) was linked with DYNHYD5 (Ambrose et al., 1993a) in this way. In these models, the dynamic feedback effect of sediment and reactive chemical transport processes on hydrological flow cannot be reflected. In addition, simulation with these models may require large amount of computer memory to pass the flow information to water quality simulation models, especially when applied to large watersheds or multidimensional simulations, e.g. long term subsurface water and quality simulation for a large watershed. Some models do simulate water quality and water flow concurrently (e.g. Cole and Buchak (1995)), but most of them fail to handle equilibrium reactions and kinetic reactions together in the complete system. Some of them assume the reactions to be locally in equilibrium, while others only cover the kinetically-controlled reactions in the system. Some of the most recently developed distributed watershed models are able to simulate sediment transport and chemical transport and reactions, e.g. InHM (VanderKwaak, 1999), Mike 11/Mike SHE (Refsgaard and Storm, 1995); however, they use an ad hoc rate formulation that limits the reaction system with a limited number of chemical species. Such approaches and assumptions certainly limit the generality of these water quality models. The reaction-based water quality simulation approach with an arbitrary number of reactions and biogeochemical species taken into

account has the potential to handle a full range of water quality simulations.

The preceding brief review of the current watershed models indicates that an integrated physics-based watershed model is needed to overcome the shortcomings and missing links in most of the existing watershed models. These models should be able to simulate each hydrological component alone, furthermore, they should physically consider the interaction among different media, between water quantity and quality simulation, and between water quality transport and the full range of biogeochemical reactions.

## 1.2 Objective And Scope Of Work

The objective of this dissertation to develop a new version of WASH123D by incorporating a transport paradigm (Zhang, 2005) into the existing model, WASH123D version 1.5, so as to make the model more robust by including a wide range of simulation capabilities, such as the capability to simulate the coupled water flow and sediment and reactive-biochemical transport dynamically. WASH123D version 1.5, a modification of its previous version (Yeh et al., 1998), is an integrated physics-based watershed model that can be used to simulate water flow in surface water (river/stream/canal network and overland runoff) and subsurface water for the corresponding medium alone or dynamically by considering the interaction between surface water and subsurface water.

Following the development of the model program, numerical experiments will be conducted to demonstrate the correctness of the model, the design capabilities of the model, the performance of the numerical algorithms. This work is expected to contribute immediately in both the

research and application fields by providing a first principle, physics-based watershed model capable of simulating density-dependent water flow alone, sediment, and chemical transport in surface water system, alone or together, and of simulating density-dependent water flow and chemical transport and transformation, alone or combined, in a subsurface system. The interaction of water flow between surface water and subsurface water is also considered in the model.

One unique feature included in the newly developed model is its inclusion of several levels of integration or coupling. They are (1) coupling of water flow and water quality simulations, providing the model with a full range of simulation capability, allowing density-dependent water flow simulation, and saving significant computer storage compared to the commonly used external link of water flow model and water quality model; (2) coupling of surface and groundwater flow simulation, which allows the model to include the interaction of water flow from 1-D, 2-D and 3-D media, so that the users can conduct complete watershed-based simulations; (3) coupling of water quality transport with an arbitrary number of mixed equilibrium and kinetic reactions, which makes the model general and flexible enough to simulate water quality problems subject to any number of chemical reactions.

### 1.3 Format And Content

This thesis is organized as follows. First, a literature review of numerical watershed models and issues in the integrated model development is given in Chapter 2. Then the major findings of this research are presented in the form of three journal articles, self titled as Chapter 3 through 5.

Chapter 3 presents the development of the one-dimensional integrated hydrodynamic and water quality model for river/stream network of watershed systems. Chapter 4 describes the development of the two-dimensional integrated hydrodynamic and water quality model for land surface. Chapter 5 discusses the development of the three-dimensional integrated fluid flow and water quality model for groundwater systems. Finally, the conclusions and some suggested future work are discussed in Chapter 6.

#### 1.4 References

- Ambrose, R.B., Wool, T.A. and Martin, J.L., 1993a. The dynamic estuary model hydrodynamic program DYNHYD 5 documentation and user manual. Environmental Research Laboratory, US Environmental Protection Agency, Athens, GA
- Ambrose, R.B., Wool, T.A. and Martin, J.L., 1993b. The water quality analysis simulation program, WASP5 Part A: model documentation Environmental Research Laboratory, US Environmental Protection Agency, Athens, GA.
- Beven, K., Calver, A. and Morris, E.M., 1987. The institute of hydrology distributed model. Report 98, Institute of Hydrology Wallingford, UK.
- Cole, T.M. and Buchak, E.M., 1995. CE-QUAL-W2: A two-dimensional, laterally averaged hydrodynamic and water quality model, version 2.0, User Manual. Instruction Report EI-95, Vicksburg, MS.
- Crawford, N.H. and Linsley, R.K., 1966. Digital simulation in hydrology: Stanford Watershed

- Model IV. Tech. Rep. No. 39, Stanford University Palo Alto, CA.
- Freeze, R.A. and Harlan, R.L., 1969. Blueprint for a physically-based digitally simulated hydrologic response model. *Journal of Hydrology*, 9: 237-258.
- Huang, G.B. and Yeh, G.T., 2009. A Comparative Study of Coupling Approaches for Surface Water and Groundwater Interactions. *Journal of Hydrologic Engineering*, ASCE, 14(5): 453-462.
- Leavesley, G.H., Litchy, R.W., Troutman, B.M. and Saindon, L.G., 1983. Precipitation-runoff modeling system-User's manual. Water Resources Investigations Report 83-4238, U.S. Geological Survey, Denver, CO.
- Metcalf and Eddy Inc., University of Florida, and Water Resources Engineers Inc., 1971. Storm water management model. EPA Report 11024DOC7/71 (NITS PB-203289), Washington D.C.
- Refsgaard, J.C. and Storm, B., 1995. Mike SHE. In: V.J. Singh (Editor), *Computer models in watershed hydrology*. Water Resources Publications
- Singh, V.P. and Frevert, D.K., 2006. *Watershed models*. Taylor & Francis, Boca Raton, 653 pp.
- Vadineanu, A. et al., 2007. Land-based sources, water quality and management. In: I.E. Gonenc, A. Vadineanu, J.P. Wflin and R.C. Russo (Editors), *Sustainable Use and development of watersheds*. Springer, AA Dordrecht, The Netherlands, pp. 483-512.
- VanderKwaak, J.E., 1999. *Numerical Simulation of Flow and Chemical Transport in Integrated Surface Subsurface Hydrologic Systems*, University of Waterloo, Ontario, Canada.
- Yeh, G.T., Cheng, H.P., Cheng, J.R. and Jerry, H.L., 1998. A Numerical Model to Simulate Water Flow and Contaminant and Sediment Transport in Watershed Systems of 1-D

Stream-River Network, 2-D Overland Regime, and 3-D Subsurface Media (WASH123D: Version 1.0). Technical Report CHL-98-19, Waterways Experiment Station, U. S. Army Corps of Engineers, Vicksburg, MS 39180-6199.

Yeh, G.T., Huang, G., Cheng, H.P., Zhang, F., Lin, H.C., Edris, E. and Richards, D., 2006. A first-principle, physics-based watershed model: WASH123D. In: V.P. Singh and D.K. Frevert (Editors), Watershed Models. CRC Press, Boca Raton, FL.

Zhang, F., 2005. A New Paradigm of Modeling Watershed Water Quality, Ph.D Dissertation. Dept. of Civil and Environmental Engineering, University of Central Florida, Orlando, 237 pp.

## CHAPTER 2 ISSUES IN INTEGRATED MODELING AND WASH123D MODEL

There are essentially three core issues in the integrated modeling of watersheds: 1) the coupling between different hydrological process components, e.g. simulating the interaction flow between surface water and groundwater; 2) the coupling of water flow and reactive water quality transport, and 3) the coupling the advection-dispersion water quality transport and the biogeochemical reactions occurring during the transport. The discussion of the first issue is beyond the scope of this thesis. The detailed approaches and discussion can be found in Huang and Yeh (2009), Panday and Huyakorn (2004), and the references therein. This thesis presents the second and third issues in the next sections followed by the brief review of water flow and reactive water transport models.

### 2.1 Hydrological Models

Hydrological models can be classified into two categories: deterministic and stochastic models. Deterministic hydrological models can be further classified into three main categories on the basis of the spatial representation: empirical models, lumped conceptual models, and distributed models. Empirical models, also called black box models, treat watersheds as a single unit where the parameters and the input do not vary spatially within the basin and the basin response is evaluated only at the outlet. The lumped conceptual models, also called grey box models, use physically sound structures and equations together with semi-empirical ones (Refsgaard, 1996).

It is necessary to estimate the parameters from calibration which perhaps is one of the key disadvantages of this type of models from the computational point of view (Yeh et al., 2006). Examples of this type of conceptual model include HSPF (Bicknell et al., 2001), SWRRBWQ (Arnold et al., 1991).

Distributed models represent spatial heterogeneity in all variable and parameters. Among the distributed models, physics-based models give a detailed and potentially more correct description of hydrological processes in the watershed (Refsgaard, 1996; Yeh et al., 2006). Examples of physics-based watershed model can be found in VanderKwaak (1999) and Yeh et al.(2006). Many researchers have compared the different categories of models in various conditions (Boyle et al., 2001; Carpernter and Georgakakos, 2006; Koren et al., 2004; Michaud, 1994; Refsgaard and Knudsen, 1996); their comparison indicated that distributed hydrological models, sometimes even without calibration (Shah et al., 1996), perform better than empirical and conceptual models in their studies.

## 2.2 Water Quality Models

Similar to hydrological models, two approaches have been used to estimate the reactive water quality transport traditionally, empirical models and mechanistic models. In mechanistic water quality models, all processes are described based on physical, chemical, and biological laws, whereas in conceptual models, only the most prominent processes are described and other processes may be lumped into a single expression.

Mechanistic water quality models allow scientists and engineers to gain insights and increased

understanding of the water quality of a particular stream, lake or estuary as well as provide a predictive capability that is not available in purely empirical models (Martin and McCutcheon, 1999). Mechanistic reactive water quality models are based on conservation of mass, which, for a finite period of time, can be conceptually expressed as

$$\text{Accumulation} = (\text{advection} + \text{dispersion}) \pm \text{source/sink} \pm \text{reactions} \quad (2.1)$$

Examples of mechanistic surface water quality models include CE-QUAL-ICM/TOXI, EFDC, and WASP5-TOXI5. These models, linked with hydrologic and hydrodynamic models, have been used to address water quality issues including eutrophication, sediment transport, contaminant fate and bioaccumulation. The common limitation of these models is that they only simulate a specific reaction system, i.e. a finite number of chemical species in a system. New program components must be added in when new water quality parameters need to be included. For instance, routine TOXI has been developed for WASP model to allow it simulate toxics issues. This could result in extensive modification of computer code if all reactions in the model including currently existing reactions and the new reaction describing the new water quality parameters need to be formulated mechanistically. While surface water quality models are still focused on developing more components into the existing model structure so as to simulate more water quality parameters and to extend the capability of currently existing models, groundwater solute transport models seem to be one step ahead. Many mechanistic transport models have been developed, e.g. HYDROGEOCHEM (Yeh et al., 2009), which, perhaps the most advanced groundwater model currently, is capable of formulating the reaction rate in a more general and flexible way so that any number of species and any type reactions can be taken into account based on the reaction network rather than a specific set of reactions in the model to simulate a

certain set of water quality parameters. This kind of physics-based, process-level chemical transport provides a promising potential to simulate a full range of water quality issues. This is closely related to the third issue in integrated modeling.

### 2.3 Coupling hydrodynamics and water quality transport

Water flow is a fundamental mechanism that controls a significant amount of the variability of water quality in streams, lakes, and estuaries. Generally, water flow variations have a large impact on water quality (through the advection and dispersion term in the continuity equation for reactive chemical transport). Water quality, however, has feedback to water flow through its effect on water properties such as density and viscosity. Therefore, a fully integrated model should take into account a strong coupling of water flow and transport (Cheng and Yeh, 1998). A full range of water flow and transport formulations may include the continuity equation and momentum equation describing the fluid flow, advection-dispersion-reaction equation describing the reactive water quality transport, and equation of state describing the density of water which can be expressed as a function of temperature and concentration of chemical species in the water system (Cheng and Yeh, 1998; Martin and McCutcheon, 1999, pp. 40). These equations, ideally, should be solved simultaneously or iteratively in order to take all hydrological, advection-dispersion, and biogeochemical processes into account. This, however, certainly requires much more computational effort. On the other hand, for the majority of cases in surface water systems, water quality does not have an significant impact on flow variations (Martin and McCutcheon, 1999). This fact often permits the decoupling of water quality from water quantity in surface water simulation, which as a result reduces much of the computational effort. Whether

the hydrodynamic and transport models must be implicitly coupled or whether they can be run in series depends on if the influence of chemical concentration on the variation of water flow properties is significant.

From the programming point of view, there are essentially two approaches to link the water flow models and reactive water quality models: the direct link approach and indirect link approach (Cheng and Yeh, 1998; Lung, 2001; Martin and McCutcheon, 1999). In the direct approach, the water flow module and reactive water quality transport module are embedded in one computer code so that the two simulation processes proceed concurrently and dynamically. Whereas in the indirect link approach, the two components are separated in different computer codes and they are simulated in sequence. When both simulations are needed, the water flow module is run first and the simulated flow field is saved as input for the water quality simulation in the next step. So normally they are used in pairs, i.e. FEMWATER (Yeh, 1999) + LEWASTE (Yeh et al., 1992), and WASP (Ambrose et al., 1993b)+ DYHYD (Ambrose et al., 1993a). The advantage of indirect coupling approach is that it saves computation time; however, it also has several drawbacks. First, it requires much computer storage to save the flow data for water quality simulation use, particularly for long term multidimensional applications. Second, the spatial and temporal average of flow information is often involved in the indirect linking approach due to the different spatial and temporal resolution used in water flow and quality models. This has never been proven to be satisfactory (Lung, 2001). Third, it can never catch the feedback of water quality on water flow. This feedback is sometimes important, for example, in the case of seawater intrusion. The direct approach can overcome all of the problems encountered by indirect approach with a cost of more computational effort; fortunately, this is now less

significant with the advances in computer technology. However, it should be noted that there should be little difference between the solution obtained using the direct (weak) approach and or indirect approach if the transport information from the flow model is passed to a water quality model using the same spatial grid/mesh and simulation time step.

The direct approach can be further categorized into strong coupling and weak coupling. Strong coupling takes into account the influence of the chemical concentration on flow, while weak coupling simulates the water flow and transport in sequence (one direction) (Cheng and Yeh, 1998) with the same spatial grid/mesh and time step in the same computer code. There are several strongly coupled models available, e.g. MECCA (Hess, 1989), but only a few include the transport and kinetics of water quality constituents that do not impact circulation. Some directly and weakly linked hydrologic/hydrodynamic models with water quality model have already been developed (Dai and Labadie, 2001; Krysanova et al., 1998).

#### 2.4 Coupling between transport and biogeochemical reactions

In the advection-dispersion-reaction equation governing the reactive water quality transport, one of the key issues is how to deal with the reaction term that includes formulating the reaction rate in the reactions so that the coupled reactive transport equation can be solve numerically. Consideration of equilibrium geochemistry, kinetic geochemistry, and microbiology as well as hydrologic transport is needed to reflect the complexity of many real systems (Yeh et al., 2009).

The coupling of transport and biogeochemical has been an active research topic in the groundwater community. It doesn't command as much attention in surface water quality

simulations, perhaps because hydrologic transport moves solutes much faster than chemical reactions can occur (Kimbali et al., 1994).

Many groundwater models couple transport with equilibrium geochemistry (Cheng, 1995; Parkhurst and Appelo, 1999; Yeh and Tripathi, 1991), while some models couple transport with kinetic biogeochemistry (Cheng and Yeh, 1994; Lichtner, 1996; Steefel and Yabusaki, 1996; Szecsody et al., 1998; Wood et al., 1994; Yeh and Tripathi, 1990).

General reactive transport models capable of handling a complete suite of geochemical reaction processes (aqueous complexation, adsorption, precipitation-dissolution, acid-base, and reduction-oxidation phenomena) and allow any individual reaction for any of these geochemical processes to be handled as either equilibrium or kinetic have been developed (Bacon et al., 2000; Xu et al., 2003; Yeh et al., 1996; Yeh et al., 2001). Most of these models can only simulate a limited reaction network. Fang et al. (2003) proposed a reaction-based batch model, BIOGEOCHEM, capable of handling any number of mixed equilibrium and kinetic reactions. Several models have coupled BIOGEOCHEM with transport successfully (Yeh et al., 2004; Zhang et al., 2007). These models have extensive flexibility and provide a promising generality.

The strategy for solving coupled hydrologic transport and mixed geochemical equilibrium/kinetic reaction problems is to solve the two subsystems of equations iteratively (Yeh, 2000). Three major approaches are generally used to model such coupled processes. The first one is fully implicit approach (Zysset et al., 1994; Freedman and Ibaraki, 2002; Kanney et al., 2003a), where transport and reaction are solved in a single, tightly coupled system of equations. The second is predictor-corrector approach (Cheng et al., 2000; Dresback and Kolar,

2000). The third is operator-splitting approach (Herzer and Kinzelbach, 1989; Yeh and Tripathi, 1989; Valocchi and Malmstead, 1992; Miller and Rabideau, 1993; Steefel and MacQuarrie, 1996; Barry et al., 1996a,b, 1997, 2000; Leeming et al., 1998; Prommer et al., 1999; Xu et al., 1999; Kanney et al., 2003b). Since Yeh and Tripathi's work in 1989, the operator-splitting approach has been used extensively in transport codes.

## 2.5 WASH123D

WASH123D (WATERSHed Systems of 1-D Stream-River Network, 2-D Overland Regime, and 3-D Subsurface Media) is a first-principle, physics-based watershed model that is developed to have the design capability to simulate density-dependent water flow, thermal and salinity transport, and sediment and water quality transport in watershed systems of river/stream/canal networks, overland regime, and subsurface media. It can simulate problems of various spatial and temporal scales as long as the assumptions of continuum are valid.

The model incorporates management structures such as storage ponds, pumping stations, culverts, and levees in the overland regime and in river/stream/canal networks. WASH123D is also designed to deal with physics-based multi-processes occurring in watersheds. The processes include (1) evaporation from surface waters (rivers, lakes, reservoirs, ponds, etc) in the terrestrial environment; (2) evportranspiration from plants, grass, and forest from the land surface; (3) infiltration to vadose zone through land surface and recharges (percolations) to groundwater through water tables; (4) overland flow and thermal and salinity transport in surface runoff; (5) hydraulics and hydrodynamics and thermal and salinity transport in river networks; and (6)

subsurface flow and thermal and salinity transport in both vadose and saturated zones.

WASH123D is comprised of three major modules: (1) one-dimensional river/stream network module, (2) two-dimensional overland module, (3) three-dimensional subsurface module. For the surface modules, the model is capable of simulating coupled fluid flow and thermal, salinity, sediment transport, and reactive chemical transport in river networks and surface runoff. For the subsurface module, the model is capable of simulating the same coupled processes as in the surface modules except for sediment transport. Routines are included in the program to simulate the interaction between surface water and groundwater.

The Saint Venant equation and its simplified versions (diffusive and kinematic wave forms) are employed for surface fluid flow simulations and the modified Richards equation is applied for subsurface flow. These governing equations are solved with several physically and mathematically based numerical options. For sediment transport, both suspended and bed sediments of various size fractions are considered, and phenomenological equations for erosions and depositions are used. For reactive biogeochemical transport, reaction rate equations are provided based on mechanisms (pathways) or empirical formulations using experimental data for every slow reaction.

To provide robust and efficient numerical solutions of the governing equations, many options and strategies are provided in WASH123D so that a wide range of application-dependent circumstances can be simulated. For surface flow problems, the semi-Lagrangian method (backward particle tracking) was used to solve kinematic wave equations. The diffusion wave models were numerically approximated with the Galerkin finite element method or the

semi-Lagrangian method. The dynamic wave model was first mathematically transformed into characteristic wave equations. Then it was numerically solved with the Lagrangian-Eulerian method. The subsurface flow-governing equations were discretized with the Galerkin finite element method. For scalar transport equations such as thermal, salinity, sediment, and reactive chemical transport, either finite element methods or hybrid Lagrangian-Eulerian methods were used to approximate the governing equations.

For scalar transport equations including thermal, salinity, sediment, and reactive chemical transport, either finite element methods or hybrid Lagrangian-Eulerian methods were used to approximate the governing equations. Three strategies were employed to handle the coupling between transport and biogeochemical reactions: (1) fully implicit scheme, (2) mixed predictor-corrector and operator-splitting methods, and (3) operator-splitting schemes. For the fully implicit scheme, one iteratively solves the transport equations and reaction equations. For the mixed predictor-corrector and operator-splitting method, the advection-dispersion transport equation is solved with the source/sink term evaluated at the previous time in the predictor step. The implicit finite difference was used to solve the system of ordinary equations governing the chemical kinetic and equilibrium reactions in the corrector step. The nonlinearity in flow and sediment transport equations is handled with the Picard method, while the nonlinear chemical system is solved using the Newton-Raphson method. Figure 2.1 illustrates the major component of WASH123D program, the physical basis, and numerical approaches.

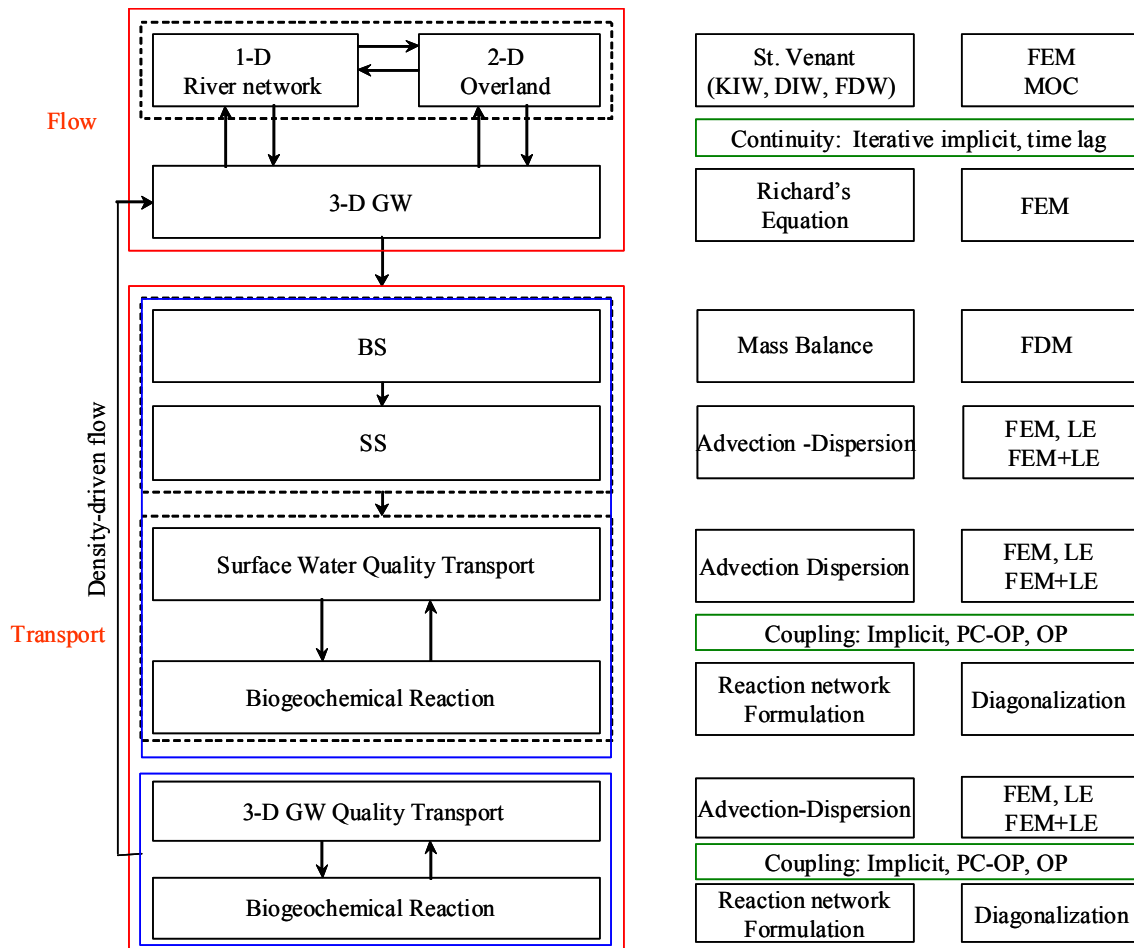


Figure 2.1 Basic components, physical basis, and numerical approaches in WASH123D

## 2.6 References

Ambrose, R.B., Wool, T.A. and Martin, J.L., 1993a. The dynamic estuary model hydrodynamic program DYNHYD5 documentation and user manual. Environmental Research Laboratory, US Environmental Protection Agency, Athens, GA

Ambrose, R.B., Wool, T.A. and Martin, J.L., 1993b. The water quality analysis simulation program, WASP5 Part A: model documentation. Environmental Research Laboratory, US

Environmental Protection Agency, Athens, GA.

Arnold, J.G., Williams, J.R., Griggs, R.H. and Sammons, N.B., 1991. SWRRBWQ - A basin scale model for assessing management impact on water quality, Grassland, Soil, and Water Research laboratory, Temple, TX.

Bacon, D.H., White, M.D. and McGrail, B.P., 2000. Subsurface Transport Over Reactive Multiphases (STORM): A General, Coupled, Nonisothermal Multiphase Flow, Reactive Transport, and Porous Medium Alternation Simulator, Version 2, User's Guide. PNNL-13108, Pacific Northwest national Laboratory, Richland, WA.

Bicknell, B.R., Imhoff, J.C., Kittle, J.L., Jobs Jr., T.H. and Donigian Jr., A.S., 2001. HYDROLOGICAL SIMULATION PROGRAM - FORTRAN, Version 12, User's manual, AQUA TERRA Consultants.

Boyle, D.B., Gupta, H.V., Sorooshian, S., Koren, V., Zhang, Z. and Smith, M., 2001. Toward improved streamflow forecasts, value of semi-distributed modeling. Water Resources Research, 37(11): 2749-2759.

Carpernter, T.M. and Georgakakos, K.P., 2006. Intercomparison of lumped versus distributed hydrologic model ensemble simulations on operational forecast scales. journal of Hydrology, 329: 174-185.

Cheng, H.P., 1995. Development and Application of a Three-Dimensional Finite Element Model of Subsurface Flow, Heat Transfer, and Reactive Chemical Transport, Ph.D Dissertation. The Pennsylvania State University, University Park, PA.

Cheng, H.P. and Yeh, G.T., 1998. Development of a three-dimensional model of subsurface flow, heat transfer, and reactive chemical transport: 3DHYDROGEOCHEM. Journal of

- Contaminant Hydrology, 34: 47-83.
- Cheng, H.P., Yeh, G.T. and Cheng, J.R., 2000. A numerical model simulating reactive transport in shallow water domains: model development and demonstrative applications. *Advances in Environmental Research*, 4: 187-209.
- Cheng, J.R. and Yeh, G.T., 1994. Modeling three-dimensional subsurface flow, fate and transport of microbes and chemicals (3DFATMIC), X-th Int. Conf. on Numerical Methods in Water Resources, Heidelberg, Germany, pp. 217-224.
- Dai, T. and Labadie, J.W., 2001. River basin network model for integrated water quantity/water quality management. *Journal of Water Resources Planning and Management*, 127(5): 295-305.
- Dresback, K.M. and Kolar, R.L., 2000. An implicit time-marching algorithm for 2D GWC shallow water models. In: Bentley et al (Editor), XIII International Conference on Computational Methods in Water Resources, pp. 913-920.
- Fang, Y.L., Yeh, G.T. and Burgos, W.D., 2003. A Generic Paradigm to Model Reaction-Based Biogeochemical Processes in Batch Systems. *Water Resources Research*, 33(4): 1083-1118.
- Hess, N.S., 1989. MECCA programs documentation. NOAA technical report NESDIS 46, NOAA.
- Huang, G.B. and Yeh, G.T., 2009. Comparative Study of Coupling Approaches for Surface Water and Subsurface Interactions. *Journal of Hydrologic Engineering*, 14(5): 453-462.
- Kimballi, B.A., Broshears, R.E., Bencala, K.E. and McInlght, D.M., 1994. Coupling of Hydrologic Transport and Chemical Reactions in a Stream Affected by Acid Mine

- Drainage. *Environmental Science and Technology*, 26: 2065-2073.
- Koren, V., Reed, S., Smith, M., Zhang, Z. and Seo, D.-J., 2004. Hydrology Laboratory Research Modeling System (HL-RMS) of the U.S. National Weather Service *Journal of Hydrology*, 291(3-4): 297-318.
- Krysanova, V., Muler-Wohlfeil, D.-I. and Becker, A., 1998. Development and test of a spatially distributed hydrological/water quality model for mesoscale watersheds. *Ecological Modelling*, 106(2-3): 261-289.
- Lichtner, P.C., 1996. Continuum Formulation of Multicomponent-Multiphase Reactive Transport. In: P.C. Lichtner, C.I. Steefel and E.H. Oelkers (Editors), *Reactive Transport in Porous Media, Reviews in Mineralogy*. Mineralogical Society of America, Washington, D.C.
- Lung, W.S., 2001. *Water quality modeling for wasteload allocations and TMDLs*. John Wiley & Sons, Inc, New York.
- Martin, J.L. and McCutcheon, S.C., 1999. *Hydrodynamics and transport for water quality modeling*. CRC Press Inc., Boca Raton, Florida.
- Michaud, J., 1994. Comparison of simple versus complex distributed runoff models on a midsized semiarid watershed. *Water Resources Research*, 30(30): 593-605.
- Panday, S. and Huyakorn, S.P., 2004. A fully coupled physically-based spatially-distributed model for evaluating surface/subsurface flow. *Advances in Water Resources*, 27: 361-382.
- Parkhurst, D.L. and Appelo, C.A.J., 1999. *User's guide to PHREEQC - a computer program for speciation, reaction-path, 1D-transport, and Inverse Geochemical Calculations*, U.S. Geological Survey, USA.

- Refsgaard, J.C., 1996. Terminology, modelling protocol and classification of hydrological model codes. In: M.B. Abbott and J.C. Refsgaard (Editors), Distributed hydrological modelling. Kluwer Academic Publishers, Dordrecht, the Netherlands.
- Refsgaard, J.S. and Knudsen, J., 1996. Operational validation and intercomparison of different types of hydrological models. *Water Resources Research*, 32(7): 2189-2202.
- Shah, S.M.S., O'Connell, P.E. and Hosking, J.R.M., 1996. Modelling the effects of spatial variability in rainfall on catchment response, 2, experiments with distributed and lumped models. *Journal of Hydrology*, 175: 89-111.
- Steeffel, C.I. and Yabusaki, S.B., 1996. OS3D/GIMRT, Software for Modeling Multi-Component-Multidimensional Reactive Transport, Pacific Northwest Laboratory, Richland, WA.
- Szecsody, J.E., Zachara, J.M., Chilakapati, A., Jardine, P.M. and Ferency, A.S., 1998. Importance of flow and particle-scale heterogeneity on Co(II/III)EDTA reactive transport. *Journal of Hydrology*, 209(1): 112-136.
- VanderKwaak, J.E., 1999. Numerical Simulation of Flow and Chemical Transport in Integrated Surface Subsurface Hydrologic Systems, University of Waterloo, Ontario, Canada.
- Wood, B.D., Dawson, C.N., Szecsody, J.E. and Streile, G.P., 1994. Modeling contaminant transport and biodegradation in a layered porous media system. *Water Resources Research*, 30(6): 1833-1845.
- Xu, T., E., Sonnenthal, E., Spycher, N. and Pruess, S., 2003. TOUGHREACT Use's guide: A simulation program for non-isothermal multiphase reactive geochemical transport in variably saturated geologic media.

- Yeh, G.T., Fang, Y., Zhang, F., Sun, J., Li, Y., Li, M.-H. and Siegel, M.D., 2009. Numerical modeling of coupled fluid flow and thermal and reactive biogeochemical transport in porous and fractured media. *Computational Geosciences*. DOI: 10.1007/s10596-009-9140-3
- Yeh, G.T., Huang, G., Cheng, H.-P., Zhang, F., Lin, H.-C., Edris, E. and Richards, D., 2006. A first-principle, physics-based watershed model: WASH123D. In: V.P. Singh and D.K. Frevert (Editors), *Watershed Models*. CRC Press, Boca Raton, FL.
- Yeh, G.T., 1999. *Users' Manual: A 3-Dimensional Finite Element Model of WATER Flow through Saturated-Unsaturated Media: Version 2.0*.
- Yeh, G.T., 2000. *Computational subsurface hydrology: reactions, transport, and fate*. Kluwer Academic Publishers, 318 pp.
- Yeh, G.T., Salvage, K. and Choi, W.H., 1996. Reactive Multispecies-Multicomponent Chemical Transport Controlled by both Equilibrium and Kinetic Reactions, XI-th Int. Conf. on Numerical Methods in Water Resources, Cancun, Mexico, pp. 585-592.
- Yeh, G.T., Sharp-Hansen, S., Lester, B., Strobl, R. and Searbrough, J., 1992. 3DFEMEATER/3DLEWASTE: numerical codes for delineating wellhead protection areas in agricultural regions based on the assimilative capacity criterion. . EPA/600/R-92/223, Environmental Research Laboratory, U.S. Environmental Protection Agency, Athens, Georgia.
- Yeh, G.T., Siegel, M.D. and Li, M.H., 2001. Numerical Modeling of Coupled Fluid Flows and Reactive Transport Including Fast and Slow Chemical Reactions. *Journal of Contaminant Hydrology*, 47: 379-390.

- Yeh, G.T., Sun, J., Jardine, P.M., Burgos, W.D., Fang, Y.L., Li, M.H. and Siegel, M.D., 2004. HYDROGEOCHEM 5.0: A Three-Dimensional Model of Coupled Fluid Flow, Thermal Transport, and HYDROGEOCHEMical Transport through Variably Saturated Conditions - Version 5.0, Oak Ridge National Laboratory, Oak Ridge, Tennessee.
- Yeh, G.T. and Tripathi, V.S., 1990. HYDROGEOCHEM: a coupled model of hydrologic transport and geochemical equilibrium in reactive multicomponent systems. ORNL-6371., Oak Ridge National Laborator, Environmental Sciences Division. Oak Ridge, Tennessee.
- Yeh, G.T. and Tripathi, V.S., 1991. A model for simulating transport of reactive multispecies components: model development and demonstration. *Water Resources Research*, 27: 3075-3094.
- Zhang, F., Yeh, G.T., Parker, J.C., Brooks, S.C., Pace, M.N., Kim, Y.J., Jardine, P.M. and Watson, D.B., 2007. A reaction-based paradigm to model reactive chemical transport in groundwater with general kinetic and equilibrium reactions. *Journal of Contaminant Hydrology*, 92(1-2): 10-32.

## CHAPTER 3 AN INTEGRATED HYDROLOGY/HYDRAULIC AND WATER QUALITY MDOEL FOR RIVER/STREAM NETWORKS

### 3.1 Abstract

This chapter presents an integrated one-dimensional cross section averaged numerical model simulating water flow and sediment and reactive contaminant transport for dendritic river networks, with emphasis on the mathematic formulation of reactive water quality transport. This model is comprised of two major physics-based modules: water flow module and reactive transport module; both are physics-based. The water flow module adopts the well developed current version of WASH123D, while the transport module is based on a newly developed general paradigm for water quality simulation. The St. Venant equation and its simplified versions, diffusion wave and kinematic wave models, are employed for water flow simulation while the reactive advection-dispersion equation is used as the governing equation for water quality transport. The surface-subsurface water interactions are considered in the flow module and simulated on the basis of continuity of interface. In the transport simulations, fast/equilibrium reactions are decoupled from slow/kinetic reactions by the decomposition of reaction networks; this enables robust numerical integrations of the governing equation. Kinetic variables are adopted as primary dependent variables rather than biogeochemical species to reduce the number of transport equations and simplify the reaction terms. In each time step, hydrologic/hydraulic variables are solved in the flow module; kinetic variables are then solved in the transport module. This is followed by solving the reactive chemical system node by node to yield concentrations of

all species. One example is presented to verify the model and one case study is conducted to demonstrate the design capability of the model.

### 3.2 Introduction

The last two decades have witnessed a rapid growth in watershed models. With the advances in the development of computer technology, numerical methods, and deeper understanding of hydrological processes and water quality transport, numerous models have been developed to simulate fluid flow alone, sediment and water quality alone, or both in river networks. There are two basic issues. One is the linkage between hydrodynamic models and water quality models and the other is the generality and flexibility of the water quality models that requires the mechanistically coupling of transport with biogeochemical reactions.

Although there are many models that have both water flow and water quality modules, they, mostly, emphasize one. Some emphasize hydrodynamics, e.g., DYNHYD5 (Ambrose et al., 1993a), UNET (Barkau, 1992) and EFDC (Hamrick, 1996); some can simulate nutrients transport such as nitrogen and phosphorus, e.g. QUAL2E (Barnwell and Brown, 1987) or its updated version QUAL2K (Chapra and Pelletier, 2003), and CE-QUAL-W2 (Cole and Wells, 2003). Some models are able to simulate more comprehensive water quality issues in addition to eutrophication such as sediment and toxics, e.g. WASP5 (Ambrose et al., 1993b), EFDC (Hamrick, 1996), HSPF (Bicknell et al., 2001), DELFT3D (Roelvink, 2003). These well developed models are often linked to others so that they can be extended to a wider use. For instance, EFDC and CE-QUAL-W2 have strength in the water fluid simulation and there are

water quality modules in them; however, they are still linked with WASP5 because it is capable of simulating comprehensive quality issues in a mechanistic way. Due to the limitations of the computer resources in the past, hydrodynamic and water quality models were not linked together using the same temporal and spatial resolutions (Lung and Hwang, 1989). For example, the hydrodynamic models often use finite difference methods or finite elements method while many of water quality models are based on the finite segment approach. Therefore, the linkage of these two types of models requires temporally and spatially averages of the hydrodynamic model results. As Lung (2001) pointed out that such an approach never proved satisfactory because efforts are needed to perform the averaging procedure. The significant improvements in computer technology have made it possible to link the two models in the same spatial grid/mesh, and time step if necessary. Some recently developed models allow hydrodynamic and sediment and water quality simulation to be performed concurrently on the same spatial and temporal basis (grid or mesh size), e.g. CCHE1D\_WQ (Vieira and Wu, 2002). These models have strong water flow and water quality modules and remove the linkage issues in the models. They can be applied for a broad range of water quality simulation issues; however, they have the limitation of only being able to simulate some specific bio-chemicals or reactions.

Among the water quality models many mechanistic-based models are able to simulate a broad range of water quality parameters, such as WASP5 and CE-QUAL-ICM (Cercio and Cole, 1995). However, they can only simulate the specific bio-chemicals or reactions written into the computer codes. Every time when a new water quality parameter simulation is needed, one or more new routines are needed to handle these new water quality parameters. The new reaction involved in the new parameter simulation may have to be formulated by *ad hoc* approaches in

the add-in routines; however, they may have an effect on the current built-in reaction networks in the model. From the mechanistic simulation point of view, the whole reaction network in the model should be reformulated so that the effect of new reactions can be taken into account.

It has been pointed out that the reaction-based water quality simulation approach with an arbitrary number of reactions and biogeochemical species taken into account has the potential to handle a full range of water quality simulations (Steeffel and van Cappellen, 1998; Yeh et al., 2001). Some reaction-based models have been developed to simulate contaminant transport subject to kinetically controlled chemical reactions (Cheng et al., 2000; Yeh et al., 1998). In particular, one reaction-based general paradigm for water quality has been developed by Zhang et al (2007).

This chapter presents an integrated one-dimensional cross section averaged numerical model simulating water flow and reactive contaminant and sediment transport for dendritic river networks, with emphasis on the mathematic formulation of reactive water quality transport. This model comprises two major physics-based modules: water flow module and reactive transport module; both are physics-based. The water flow module adopts the well developed current version of WASH123D, while the transport module is based on a general paradigm (Zhang et al., 2007) for water quality simulation.

### 3.3 Theory and mathematical basis

The governing equations of water flow and sediment and water quality transport are presented in this section. It is assumed that the variation of the variable within a cross-section is not

significant, and the model equations were written in a one-dimensional, longitudinal form.

The water flow is governed by various forms of the Saint-Venant equations under different conditions. Kinematic waves dominate the water flow when the inertial and pressure forces are negligible, while diffusive waves may be more applicable when pressure forces are important. The dynamic waves must be used when inertial and pressure forces and feedback effects to upstream are significant, e.g., in mild-sloped rivers. The reaction-based advection-dispersion equation is adopted for the sediment and water quality transport simulation.

### 3.3.1 Water flow in one-dimensional river/stream/canal network

Neglecting the spatial variation in velocity across the channel and with respect to the depth, the cross-section-averaged Saint-Venant equations of continuity and momentum for variable-density flow in channel/stream networks can be written as equations (3.1) and (3.2), respectively, in conservative form (Huang and Yeh, 2009).

$$\frac{\partial A}{\partial t} + \frac{\partial Q}{\partial x} = S_S + S_R - S_E + S_I + S_1 + S_2 \quad (3.1)$$

where  $t$  is time [T];  $x$  is the axis along the river/stream/canal direction [L];  $A$  is the cross-sectional area of the river/stream [ $L^2$ ];  $Q$  is the flow rate of the river/stream/canal [ $L^3/T$ ];  $S_S$  is the human-induced source [ $L^3/T/L$ ];  $S_R$  is the source due to rainfall [ $L^3/T/L$ ];  $S_E$  is the sink due to evapotranspiration [ $L^3/T/L$ ];  $S_I$  is the source due to exfiltration from the subsurface media [ $L^3/T/L$ ];  $S_1$  and  $S_2$  are the source terms contributed by overland flow [ $L^3/T/L$ ].

$$\frac{\partial Q}{\partial t} + \frac{\partial VQ}{\partial x} = -gA \frac{\partial(Z_o + h)}{\partial x} - \frac{gAh}{c\rho} \frac{\partial \Delta\rho}{\partial x} - \frac{\partial F_x}{\partial x} + \left(M_S + M_R - M_E + M_I + M_1 + M_2\right) + \frac{B\tau^s - P\tau^b}{\rho} \quad (3.2)$$

where  $h$  is the water depth [L];  $V$  is the river/stream/canal velocity [L/T];  $g$  is gravity [L/T<sup>2</sup>];  $Z_o$  is bottom elevation [L];  $\Delta\rho = \rho - \rho_o$  is the density deviation [M/L<sup>3</sup>] from the reference density ( $\rho_o$ ), which is a function of temperature and salinity as well as other chemical concentrations;  $c$  is the shape factor of the cross-sectional area;  $F_x$  is the momentum flux due to eddy viscosity [L<sup>4</sup>/T<sup>2</sup>];  $M_S$  is the external momentum-impulse from artificial sources/sinks [L<sup>3</sup>/T<sup>2</sup>];  $M_R$  is the momentum-impulse gained from rainfall [L<sup>3</sup>/T<sup>2</sup>];  $M_E$  is the momentum-impulse lost to evapotranspiration [L<sup>3</sup>/T<sup>2</sup>];  $M_I$  is the momentum-impulse gained from the subsurface due to exfiltration [L<sup>3</sup>/T<sup>2</sup>];  $M_1$  and  $M_2$  are the momentum-impulse gained from the overland flow [L<sup>3</sup>/T<sup>2</sup>];  $\rho$  is the water density [M/L<sup>3</sup>];  $B$  is the top width of the cross-section [L];  $\tau^s$  is the surface shear stress [M/T<sup>2</sup>/L];  $P$  is the wet perimeter [L]; and  $\tau^b$  is the bottom shear stress [M/T<sup>2</sup>/L], which can be assumed proportional to the flow rate as  $\tau^b/\rho = \kappa V^2$  where  $\kappa = gn^2/R^{1/3}$  and  $R$  is the hydraulic radius (L) and  $n$  is the Manning's roughness.

Depending on the simplification of the momentum equation, Eq.(3.2), three approaches may be used, fully dynamic wave model, diffusive model, and kinematic wave model. Yeh et al. (2005) presents the detail of each approach and the associated initial and boundary conditions.

### 3.3.2 Sediment transport in one-dimensional river/stream/canal network

The governing equations for bed sediment are derived based on mass balance of sediments on river bed while the governing equations for suspended sediments are derived based on the mass

conservation law. They are given as Eq.(3.3) and (3.4), respectively (Yeh et al., 2005; Zhang et al., 2008).

$$\frac{\partial(PM_n)}{\partial t} = P(D_n - R_n), \quad n \in [1, N_s] \quad (3.3)$$

$$\frac{\partial(AS_n)}{\partial t} + \frac{\partial(QS_n)}{\partial x} - \frac{\partial}{\partial x} \left( AK_x \frac{\partial S_n}{\partial x} \right) = M_n^{as} + M_n^{os1} + M_n^{os2} + (R_n - D_n)P, \quad n \in [1, N_s] \quad (3.4)$$

where  $P$  is the river/stream cross-sectional wetted perimeter [L],  $M_n$  is the wetted perimeter-averaged concentration of the  $n$ -th bed sediment in mass per unit bed area [ $M/L^2$ ],  $D_n$  is the deposition rate of the  $n$ -th sediment in mass per unit bed area per unit time [ $M/L^2/T$ ],  $R_n$  is the erosion rate of the  $n$ -th sediment in mass per unit bed area per unit time [ $M/L^2/T$ ],  $N_s$  is the total number of sediment size fractions,  $S_n$  is the cross-sectional-averaged concentration of the  $n$ -th suspended sediment in the unit of mass per unit column volume [ $M/L^3$ ],  $K_x$  is the dispersion coefficient [ $L^2/T$ ],  $M_n^{as}$  is the artificial source of the  $n$ -th suspended sediment [ $M/L/T$ ], and  $M_n^{os1}$  and  $M_n^{os2}$  are overland sources of the  $n$ -th suspended sediment from river bank 1 and 2, respectively [ $M/L/T$ ]. The deposition and erosion rates in equation (3.3) and (3.4) for cohesive (e.g. silt and clay with grain size less than  $63\mu m$ ) and non-cohesive (e.g. silt and clay with grain size greater than  $63\mu m$ ) sediments, are quantified, respectively, by the well established formulations. The current version of WASH123D program adopted the equations estimating deposition and erosion rate for cohesive and non-cohesive sediments by Yeh et al. (1998).

Concentration of every sediment fraction needs to be given initially either from field measurement or from the simulation of steady-state version of (3.3) and(3.4). No boundary condition is needed for bed sediments while four types of boundary conditions (Yeh et al., 1998)

are taken into account for suspended sediments, i.e. Dirichlet, Variable, Cauchy, and Neumann boundary conditions (Yeh et al., 2006).

Initial Condition

$$M_n = M_n(x, 0), n \in [1, N_s] \quad (3.5)$$

$$S_n = S_n(x, 0), n \in [1, N_s] \quad (3.6)$$

where  $M_n(x, 0)$  and  $S_n(x, 0)$  is the initial cross-section averaged concentration of n-th bed sediment and suspended sediment over the domain,  $[M/L^3]$ .

Dirichlet boundary condition:

Dirichlet boundary conditions are prescribed on the boundary where the suspended sediment concentration is known,

$$S_n = S_n(x_b, t) \quad (3.7)$$

where  $x_b$  is the axis coordinate of the boundary node  $[L]$ , and  $S_n(x_b, t)$  is a time-dependent concentration on the boundary  $[M/L^3]$ .

Neumann boundary condition:

This boundary condition is used when the diffusive material flow rate is known at the boundary node.

$$-\mathbf{n}AK_x \frac{\partial S_n}{\partial x} = Q_{S_n}(x_b, t) \quad (3.8)$$

where  $Q_{S_n}(x_b, t)$  is a time-dependent diffusive material flow rate at the boundary [M/T].

Cauchy boundary condition:

This boundary condition is employed when the total material flow rate is given. Usually, this boundary is an upstream flux boundary.

$$\mathbf{n} \left( QS_n - AK_x \frac{\partial S_n}{\partial x} \right) = Q_{S_n}(x_b, t) \quad (3.9)$$

where  $Q_{S_n}(x_b, t)$  is a time-dependent material flow rate at the boundary [M/t].

Variable boundary condition:

Variable boundary conditions are normally specified on the boundary where the flow direction can change with time or on any open boundary. On the variable boundary, when the flow is directed into the region of the interest, the mass rate into the region is given by the product of the flow rate and concentration of the incoming fluid. When the flow is directed out of the region, the sediment mass is assumed to be carried out through advection. Mathematically, a variable boundary condition is given as

$$\mathbf{n} \left( QS_n - AK_x \frac{\partial S_n}{\partial x} \right) = \mathbf{n}QS_n(x_b, t) \quad \text{if} \quad \mathbf{n}Q \leq 0 \quad (3.10)$$

$$-nAK_x \frac{\partial S_n}{\partial x} = 0 \quad \text{if} \quad nQ > 0 \quad (3.11)$$

where  $n$  is a unit outward direction, and  $S_n(x_b, t)$  is a time-dependent concentration at the boundary that is associated with the incoming flow [M/L<sup>3</sup>].

### 3.3.3 Biogeochemical transport in one-dimensional river/stream/canal network

The biogeochemical species include chemical species in bed sediment phase, suspended sediment phase, immobile phase, and mobile phase, and also precipitated particulate, and bed precipitate. The biogeochemical reactions among these species are mostly subject to two types of reactions, fast or equilibrium reactions and slow or kinetic reactions (Rubin, 1983). Fast reactions are sufficiently fast compared to transport time scale and reversible so that local equilibrium could be assumed; this assumption does not hold for slow reactions.

The general continuity equation for M biogeochemical species in river/stream/canal network is given by (3.12)

$$\frac{\partial(A\rho_i C_i)}{\partial t} + \alpha_i L(\rho_i C_i) = Ar_i \Big|_N \quad i \in M \quad (3.12)$$

where

$$L(\rho_i C_i) = \frac{\partial(Q\rho_i C_i)}{\partial x} - \frac{\partial}{\partial x} \left[ AK_x \frac{\partial(\rho_i C_i)}{\partial x} \right] - (M_i^{as} + M_i^{rs} + M_i^{os1} + M_i^{os2} + M_i^{is}) \quad (3.13)$$

where A is river/stream/canal cross-sectional area [L<sup>2</sup>];  $\rho_i$  is the density of the phase associated with species i [M/L<sup>3</sup>];  $C_i$  is the concentration of species i in the unit of chemical mass per unit phase mass [M/M];  $\alpha_i$  is the index of mobility of the i-the species, 0 for immobile species and 1 for mobile species; L is the advection-diffusion transport operator, defined as Eq.(3.13);  $M_i^{as}$  is the artificial source of species i [M/L/T];  $M_i^{rs}$  is the rainfall source of species i [M/L/T],  $M_i^{os1}$  and  $M_i^{os2}$  are the overland sources of species i from river bank 1 and 2, respectively [M/L/T]; and  $M_i^{is}$  is the source of species i from subsurface [M/L/T]; and  $r_i \Big|_N$  is the production rate of species i due to all N reactions in the unit of chemical mass per column volume per time [M/L<sup>3</sup>/T].

### 3.3.4 Diagonalization of reactive transport governing equation

In equation (3.12) the determination of  $r_i|_N$  for computation is a primary challenge in the numerical computation of the equation. It can be formulated by an ad hoc method (e.g. (Ambrose et al., 1993b) and (Brown and Barnwell, 1987)), and reaction-based formulations e.g. (Steeffel and van Cappellen, 1998) and (Fang et al., 2003). Yeh et al. (2001) highlighted that ad-hoc reaction parameters are only applicable to the experimental conditions tested. Reaction-based formulation is used in WASH123D and the fast reactions are decoupled from slow reactions in order to provide an efficient and reliable numerical solution to Eq.(3.12).

In a reaction-based formulation,  $r_i|_N$  is given by the summation of rates of all reactions that the  $i$ -th species participates in,

$$r_i|_N = \frac{\partial(\rho_i C_i)}{\partial t}|_{reaction} = \sum_{k=1}^N [(v_{ik} - \mu_{ik})r_k], \quad i \in M \quad (3.14)$$

where  $v_{ik}$  is the reaction stoichiometry of the  $i$ -th species in the  $k$ -th reaction associated with products,  $\mu_{ik}$  is the reaction stoichiometry of the  $i$ -th species in the  $k$ -th reaction associated with the reactants, and  $r_k$  is the rate of the  $k$ -th reaction.

The mass balance equation for species  $i$  is given by substituting equation (3.14) into (3.12),

$$\frac{\partial(A\rho_i C_i)}{\partial t} + \alpha_i L(\rho_i C_i) = A \sum_{k=1}^N [(v_{ik} - \mu_{ik})r_k], \quad i \in M; \quad or \quad \mathbf{U} \frac{\partial \mathbf{C}_A}{\partial t} + \boldsymbol{\alpha} L(\mathbf{C}) = A \mathbf{v} \mathbf{r} \quad (3.15)$$

where  $\mathbf{U}$  is a unit matrix,  $\mathbf{C}_A$  is a vector with its components representing  $M$  species concentrations multiplied the cross section area of the river [M/L],  $\boldsymbol{\alpha}$  is a diagonal matrix with  $\alpha_i$  as its diagonal component,  $\mathbf{C}$  is a vector with its components representing  $M$  species

concentrations  $[M/L^3]$ ,  $v$  is the reaction stoichiometry matrix, and  $r$  is the reaction rate vector with  $N$  reaction rates as its components.

Because numerical solutions to (3.15) still encounters significant challenges and the approach has been proven inadequate (Fang et al., 2003; Yeh et al., 2001), fast reactions must be decoupled from (3.15) and mass conservation must be enforced. The diagonalization of the reactive transport system equation (3.15) is employed. This approach was used by Fang et al. (2003) in a reactive batch system.

First, remove the redundant reactions from the reaction network. A “redundant reaction” is defined as a fast reaction that is linearly dependent on other fast reactions, and an “irrelevant reaction” is a kinetic reaction that is linearly dependent on only equilibrium reactions. Consider a reaction system that consists of  $N_e$  fast/equilibrium reactions and  $N_k$  slow/kinetic reactions among  $M$  chemical species. Among  $N_e$  fast/equilibrium reactions are  $N_E$  independent equilibrium reactions and there are  $N_K$  kinetic reactions among the  $N_k$  kinetic reactions that are independent to  $N_E$  equilibrium reaction, in other words, there are  $N_e - N_E$  redundant reactions and  $N_k - N_K$  irrelevant reactions in the system. Finally the reaction network only includes  $N_E$  equilibrium reactions and  $N_K$  kinetic reactions after removing the redundant and irrelevant reactions. Second, decomposition of the system results in decoupling the equilibrium reactions from kinetic reactions. After decomposition by pivoting on the  $N_E$  equilibrium reactions using Gaussian-Jordan decomposition, the system consists of two sub-system of equations,  $N_E$  equations for equilibrium variables, and  $N_{KI} (= M - N_E)$  equations for kinetic variables that include  $N_{KI}$  kinetic variables corresponding to the  $N_{KI}$  kinetic reactions independent of any other kinetic

reactions among the  $N_K$  kinetic reactions, and  $N_C$  ( $N_C=M-N_E-N_{KI}$ ) component variables. The system can be written as equation(3.16),

$$\begin{bmatrix} \mathbf{A}_{11} & \mathbf{0}_{12} \\ \mathbf{A}_{21} & \mathbf{U}_{22} \end{bmatrix} \begin{Bmatrix} \frac{\partial \mathbf{C}_{A1}}{\partial t} \\ \frac{\partial \mathbf{C}_{A2}}{\partial t} \end{Bmatrix} + \begin{bmatrix} \mathbf{B}_{11} & \mathbf{0}_{12} \\ \mathbf{B}_{21} & \boldsymbol{\alpha}_{22} \end{bmatrix} \mathbf{L} \left( \begin{Bmatrix} \mathbf{C}_1 \\ \mathbf{C}_2 \end{Bmatrix} \right) = \mathbf{A} \begin{bmatrix} \mathbf{D}_{11} & \mathbf{K}_{12} \\ \mathbf{0}_{21} & \mathbf{K}_{22} \end{bmatrix} \begin{Bmatrix} \mathbf{r}_1 \\ \mathbf{r}_2 \end{Bmatrix} \quad (3.16)$$

where  $\mathbf{A}_{11}$  and  $\mathbf{A}_{21}$  are the submatrices of the reduced  $\mathbf{U}$  matrix with size of  $N_E \times N_E$  and  $N_{KIV} \times N_E$ , respectively (note that  $N_{KIV} = M - N_E = N_{KI} + N_C$ );  $\mathbf{0}_{12}$  and  $\mathbf{U}_{22}$  are the zero- and unit-submatrices, respectively, of the reduced  $\mathbf{U}$  matrix with size of  $N_E \times N_{KIV}$  and  $N_{KIV} \times N_{KIV}$ , respectively;  $\mathbf{C}_{A1}$  and  $\mathbf{C}_{A2}$  are the subvectors of the vector  $\mathbf{C}_A$  with sizes of  $N_E$  and  $N_{KIV}$ , respectively;  $\mathbf{B}_{11}$  and  $\mathbf{B}_{21}$  are the submatrices of the reduced  $\boldsymbol{\alpha}$  matrix with sizes of  $N_E \times N_E$  and  $N_{KIV} \times N_E$ , respectively;  $\mathbf{0}_{12}$  and  $\boldsymbol{\alpha}_{22}$  are the zero- and unit- submatrices, respectively, of the reduced  $\boldsymbol{\alpha}$  matrix with size of  $N_E \times N_{KIV}$  and  $N_{KIV} \times N_{KIV}$ , respectively;  $\mathbf{C}_1$  and  $\mathbf{C}_2$  are the subvectors of the vector  $\mathbf{C}$  with sizes of  $N_E$  and  $N_{KIV}$ , respectively;  $\mathbf{D}_{11}$  is the diagonal submatrix of the reduced  $\mathbf{v}$  matrix with size of  $N_E \times N_E$  and  $\mathbf{K}_{12}$  is the submatrix of the reduced  $\mathbf{v}$  matrix with size of  $N_E \times N_{KIV}$ ;  $\mathbf{0}_{21}$  is the zero submatrix of the reduced  $\mathbf{v}$  matrix with size of  $N_{KIV} \times N_E$  and  $\mathbf{K}_{22}$  is the submatrix of the reduced  $\mathbf{v}$  matrix with size of  $N_{KIV} \times N_E$ ;  $\mathbf{r}_1$  and  $\mathbf{r}_2$  are the subvectors of the vector  $\mathbf{r}$  with sizes of  $N_E$  and  $N_{KIV}$ , respectively.

The system of Equation (3.16) can be further decomposed by pivoting on  $N_{KI}$  independent kinetic reactions.

$$\begin{bmatrix} \mathbf{A}_{11} & \mathbf{A}_{12} & \mathbf{0}_{13} \\ \mathbf{A}_{21} & \mathbf{A}_{22} & \mathbf{0}_{23} \\ \mathbf{A}_{31} & \mathbf{A}_{32} & \mathbf{U}_{33} \end{bmatrix} \begin{Bmatrix} \frac{\partial \mathbf{C}_{A1}}{\partial t} \\ \frac{\partial \mathbf{C}_{A2}}{\partial t} \\ \frac{\partial \mathbf{C}_{A3}}{\partial t} \end{Bmatrix} + \begin{bmatrix} \mathbf{B}_{11} & \mathbf{B}_{12} & \mathbf{0}_{13} \\ \mathbf{B}_{21} & \mathbf{B}_{22} & \mathbf{0}_{23} \\ \mathbf{B}_{31} & \mathbf{B}_{32} & \boldsymbol{\alpha}_{33} \end{bmatrix} \mathbf{L} \begin{Bmatrix} \mathbf{C}_1 \\ \mathbf{C}_2 \\ \mathbf{C}_3 \end{Bmatrix} = \mathbf{A} \begin{bmatrix} \mathbf{D}_{11} & \mathbf{K}_{12} & \mathbf{K}_{13} \\ \mathbf{0}_{21} & \mathbf{D}_{22} & \mathbf{K}_{23} \\ \mathbf{0}_{31} & \mathbf{0}_{32} & \mathbf{0}_{33} \end{bmatrix} \begin{Bmatrix} \mathbf{r}_1 \\ \mathbf{r}_2 \\ \mathbf{r}_3 \end{Bmatrix} \quad (3.17)$$

where  $\mathbf{A}_{11}$  is the submatrix of the reduced  $\mathbf{U}$  matrix with size of  $N_E \times N_E$ ,  $\mathbf{A}_{21}$  is the submatrix of the reduced  $\mathbf{U}$  matrix with size of  $N_{KI} \times N_E$ , and  $\mathbf{A}_{31}$  is the submatrix of the reduced  $\mathbf{U}$  matrix with size of  $N_C \times N_E$ ;  $\mathbf{A}_{12}$  is the submatrix of the reduced  $\mathbf{U}$  matrix with size of  $N_E \times N_{KI}$ ,  $\mathbf{A}_{22}$  is the submatrix of the reduced  $\mathbf{U}$  matrix with size of  $N_{KI} \times N_{KI}$ , and  $\mathbf{A}_{32}$  is the submatrix of the reduced  $\mathbf{U}$  matrix with size of  $N_C \times N_{KI}$ ;  $\mathbf{0}_{13}$  is the zero submatrix of the reduced  $\mathbf{U}$  matrix with size of  $N_E \times N_C$ ,  $\mathbf{0}_{23}$  is the submatrix of the reduced  $\mathbf{U}$  matrix with size of  $N_{KI} \times N_C$ , and  $\mathbf{U}_{33}$  is the unit submatrix of the reduced  $\mathbf{U}$  matrix with size of  $N_C \times N_C$ ;  $\mathbf{C}_{A1}$ ,  $\mathbf{C}_{A2}$ , and  $\mathbf{C}_{A3}$  are the subvectors of the vector  $\mathbf{C}_A$  with sizes of  $N_E$ ,  $N_{KI}$ , and  $N_C$ , respectively;  $\mathbf{B}_{11}$  is the submatrix of the reduced  $\boldsymbol{\alpha}$  matrix with size of  $N_E \times N_E$ ,  $\mathbf{B}_{12}$  is the submatrix of the reduced  $\boldsymbol{\alpha}$  matrix with size of  $N_E \times N_{KI}$ ,  $\mathbf{B}_{21}$  is the submatrix of the reduced  $\boldsymbol{\alpha}$  matrix with size of  $N_{KI} \times N_E$ , and  $\mathbf{B}_{31}$  is the submatrix of the reduced  $\boldsymbol{\alpha}$  matrix with size of  $N_C \times N_E$ ;  $\mathbf{A}_{22}$  is the submatrix of the reduced  $\boldsymbol{\alpha}$  matrix with size of  $N_{KI} \times N_{KI}$ , and  $\mathbf{B}_{32}$  is the submatrix of the reduced  $\boldsymbol{\alpha}$  matrix with size of  $N_C \times N_{KI}$ ;  $\mathbf{0}_{13}$  is the zero submatrix of the reduced  $\boldsymbol{\alpha}$  matrix with size of  $N_E \times N_C$ ,  $\mathbf{0}_{23}$  is the submatrix of the reduced  $\boldsymbol{\alpha}$  matrix with size of  $N_{KI} \times N_C$ , and  $\boldsymbol{\alpha}_{33}$  is the diagonal submatrix of the reduced  $\boldsymbol{\alpha}$  matrix with size of  $N_C \times N_C$ ;  $\mathbf{C}_1$ ,  $\mathbf{C}_2$ , and  $\mathbf{C}_3$  are the subvectors of the vector  $\mathbf{C}$  with sizes of  $N_E$ ,  $N_{KI}$ , and  $N_C$ , respectively;  $\mathbf{D}_{11}$  is the diagonal submatrix of the reduced  $\mathbf{v}$  matrix with size of  $N_E \times N_E$ ,  $\mathbf{K}_{12}$  is the submatrix of the reduced  $\mathbf{v}$  matrix with size of  $N_E \times N_{KI}$ , and  $\mathbf{K}_{13}$  is the submatrix of the reduced  $\mathbf{v}$  matrix with size of  $N_E \times N_{KD(k)}$ ;  $\mathbf{0}_{21}$  is the zero submatrix of the reduced  $\mathbf{v}$  matrix

with size of  $N_{KI} \times N_E$ ,  $\mathbf{D}_{22}$  is the diagonal submatrix of the reduced  $\mathbf{v}$  matrix with size of  $N_{KI} \times N_{KI}$ , and  $\mathbf{K}_{23}$  is the submatrix of the reduced  $\mathbf{v}$  matrix with size of  $N_{KI} \times N_{KD(k)}$ ;  $\mathbf{0}_{13}$  is the zero submatrix of the reduced  $\mathbf{v}$  matrix with size of  $N_C \times N_E$ ,  $\mathbf{0}_{32}$  is the zero submatrix of the reduced  $\mathbf{v}$  matrix with size of  $N_C \times N_{KI}$ , and  $\mathbf{0}_{33}$  is the zero submatrix of the reduced  $\mathbf{v}$  matrix with size of  $N_C \times N_{KD(k)}$ ;  $\mathbf{r}_1$ ,  $\mathbf{r}_2$ , and  $\mathbf{r}_3$  are the subvectors of the vector  $\mathbf{r}$  with sizes of  $N_E$ ,  $N_{KI}$ , and  $N_{KD(k)}$ , respectively.

The two subsets of equations in (3.16) are further defined as follows,

Algebraic Equations for NE Equilibrium Reactions

$$\frac{\partial(AE_i)}{\partial t} + L(E_i^m) = AD_{1ii}r_i + A \sum_{j=1}^{N_K} K_{1ij}r_{2j}, \quad i \in N_E \quad (3.18)$$

which is replaced with a thermodynamically consistent equation

$$K_i^e = \prod_{j \in M} A_j^{\nu_j} / \prod_{j \in M} A_j^{\mu_j} \quad \text{or} \quad F_i(C_1, \dots, C_M; p_1, p_2, \dots) = 0 \quad (3.19)$$

where  $E_i = \sum_{j=1}^{N_E} A_{1ij} C_{1j}$  and  $E_i^m = \sum_{j=1}^{N_E} B_{1ij} C_{1j}$

where  $K_i^e$  is the equilibrium constant of the  $i$ -th fast reaction,  $A_j$  is the activity of the  $j$ -th species,  $F_i(C_1, \dots, C_M; p_1, p_2, \dots)$  is an empirical function of all species and a number of parameters  $p_1, p_2, \dots$  for the  $i$ -th fast reaction.

Transport Equations for  $N_{KIV}$  Kinetic-Variables

$$\frac{\partial(AE_i)}{\partial t} + L(E_i^m) = A \sum_{j=1}^{N_K} K_{2nj} r_{2j}, \quad i \in N_{KIV} = M - N_E \quad (3.20)$$

where  $E_i = \sum_{j=1}^{N_E} (A_{21})_j (C_{A1})_j + (C_{A2})_j$  and  $E_i^m = \sum_{j=1}^{N_E} (B_{21})_{ij} C_{1j} + (\alpha_{22})_{ij} C_{2i}$

where  $E_i$  is called kinetic variable (Fang, et al., 2003) and is subject to only kinetic reactions in the system. For the  $N_C$  component variables among the  $N_{KIV}$  kinetic variables, the right hand side of equation (3.20) is zero.

Only  $M-N_E$  kinetic variables needs to be included in the transport computation, which should be less than or equal to the number of M in Eq.(3.15). And the governing equation (3.12) for reactive chemical transport in 1-D river/stream network can be replaced by a set of NE algebraic equations (Eq. (3.19) ) and  $M-N_E$  partial differential equations for kinetic variables as written in equation (3.21) by explicitly expressing the transport operator.

$$\begin{aligned} \frac{\partial(AE_i)}{\partial t} + \frac{\partial(QE_i^m)}{\partial x} - \frac{\partial}{\partial x} \left( AK_x \frac{\partial E_i^m}{\partial x} \right) = M_{E_i}^{as} + M_{E_i}^{rs} \\ + M_{E_i}^{os1} + M_{E_i}^{os2} + M_{E_i}^{is} + AR_i, \quad i \in N_{KIV} \end{aligned} \quad (3.21)$$

where  $E_i$  is the concentration of the i-th kinetic-variable [ $M/L^3$ ],  $E_i^{im}$  is the concentration of mobile part of the i-th kinetic-variable [ $M/L^3$ ],  $M_{E_i}^{as}$  is the artificial source of the i-th kinetic-variable [ $M/L/T$ ],  $M_{E_i}^{rs}$  is the rainfall source of the i-th kinetic-variable [ $M/L/T$ ],  $M_{E_i}^{os1}$  and  $M_{E_i}^{os2}$  are overland sources of the i-th kinetic-variable from river banks 1 and 2, respectively [ $M/L/T$ ],  $M_{E_i}^{is}$  is the mass rate of the source of the i-th kinetic-variable in river/stream from subsurface [ $M/L/T$ ],  $R_i$  is the production rate of i-th kinetic-variable due to

biogeochemical reactions  $[M/L^3/T]$ , and  $N_{KIV}$  is the number of kinetic variables.

The initial concentration of each species including immobile species (bed precipitates, particulate sorbed onto bed sediment, and dissolved chemical in the immobile water phase), and mobile species (dissolved chemical in mobile water phase, suspended precipitates, and particulate sorbed onto suspended sediment), should be obtained either by field measurement or by simulating the steady state of the system. No boundary conditions are needed for immobile species, while four types of boundary conditions are taken into account for mobile species, Dirichlet, Neumann, Cauchy, and Variable boundary conditions (Yeh et al., 2006), which are similar to the boundary conditions for suspended sediments transport presented in section 3.2.2.

### 3.4 Numerical approaches

In this section, we present the numerical approaches employed to solve the governing equations of sediment of reactive transport in 1-D river/stream networks addressed in the preceding section. The numerical approaches for the governing equations of water flow have been addressed in detail elsewhere (Yeh et al., 2005).

#### 3.4.1 Approaches for the coupled transport and chemistry equations

The three options usually used are fully implicit scheme, operator-splitting scheme, and mixed operator-splitting/predictor-corrector scheme.

Defining the advection-dispersion operator  $L$  as

$$L(\bullet) = \frac{\partial(Q \cdot \bullet)}{\partial x} - \frac{\partial}{\partial x} \left[ AK_x \frac{\partial(\bullet)}{\partial x} \right] - (M_i^{as} + M_i^{rs} + M_i^{os1} + M_i^{os2} + M_i^{is}) \quad (3.22)$$

The reactive transport equation of kinetic-variables, equations (3.21) can be simplified as

$$A \frac{\partial E_n}{\partial t} + \frac{\partial A}{\partial t} E_n + L(E_n^m) = AR_{E_n} \quad (3.23)$$

Equation (3.23) is approximated by the following equations at the (n+1)-th time step,

$$A \frac{(E_n)^{n+1} - (E_n)^n}{\Delta t} + \frac{\partial A}{\partial t} E_n + L(E_n^m) = AR_{E_n} \quad (3.24)$$

### Fully Implicit Scheme

For the fully implicit scheme, Equation (3.24) is separated into the following equations,

$$A \frac{(E_n)^{n+1/2} - (E_n)^n}{\Delta t} + \frac{\partial A}{\partial t} E_n + L(E_n^m) = AR_{E_n} \quad (3.25)$$

$$\frac{(E_n)^{n+1} - (E_n)^{n+1/2}}{\Delta t} = 0 \quad (3.26)$$

where the superscripts n, n+1/2, and n+1 represent the old, intermediate, and new time step, respectively, and terms without superscript is the corresponding average values calculated with time weighting factors.

In fully implicit scheme,  $E^{n+1/2}$  is solved through Equation (3.25) first, and then  $E^{n+1}$  is solved through Equation (3.26) together with algebraic equations for equilibrium reactions using BIOGEOCHEM model (Fang et al., 2003) so as to obtain the species concentrations. Iterations

between Equation (3.25) and Equation (3.26) are performed.

### Mixed Predictor-Corrector/Operator-Splitting Scheme

For the mixed predictor-corrector/operator-splitting scheme, Equation (3.24) is separated into two equations as follows,

$$A \frac{(E_n^m)^{n+1/2} - (E_n^m)^n}{\Delta t} + \frac{\partial A}{\partial t} E_n^m + L(E_n^m) = AR_{E_n^n} - A \frac{\partial(\ell n A)}{\partial t} (E_n^{im})^n \quad (3.27)$$

$$\frac{E_n^{n+1} - [(E_n^m)^{n+1/2} + (E_n^{im})^n]}{\Delta t} = R_{E_n^{n+1}} - R_{E_n^n} - \frac{\partial(\ell n A)}{\partial t} (E_n^{im})^{n+1} + \frac{\partial(\ell n A)}{\partial t} (E_n^{im})^n \quad (3.28)$$

In the predictor-corrector/operator-splitting scheme,  $E_n^{n+1/2}$  is solved through Equation (3.27) and then Equation (3.28) is solved together with the algebraic equations for equilibrium reactions using the BIOGEOCHEM model (Fang et al., 2003) to obtain  $E_n^{n+1}$  and individual species concentration.

### Operator-Splitting Scheme

For the Operator-Splitting scheme, Equation (3.24) is separated into two equations as follows,

$$A \frac{(E_n^m)^{n+1/2} - (E_n^m)^n}{\Delta t} + \frac{\partial A}{\partial t} E_n^m + L(E_n^m) = 0 \quad (3.29)$$

$$\frac{E_n^{n+1} - [(E_n^m)^{n+1/2} + (E_n^{im})^n]}{\Delta t} = R_{E_n^{n+1}} - \frac{\partial(\ell n A)}{\partial t} (E_n^{im})^{n+1} \quad (3.30)$$

Equation (3.29) is solved first to obtain  $E_n^{n+1/2}$ , then Equation (3.30) together with the algebraic equations for equilibrium reactions are solved using the BIOGEOCHEM model (Fang et al.,

2003) to obtain  $E_m^{n+1}$  and individual species concentration.

### 3.4.2 Discretization schemes

Under each framework of the three coupling strategies dealing with the coupling of reaction and advection-dispersion terms in the kinetic-variable transport equation, five spatial discretization schemes are included in the model, namely, (1) Finite Element Method (FEM) on the conservative form of the transport equation, (2) FEM on the advective form of the transport equation, (3) modified Lagrangian-Eulerian (LE) approach to the transport equation, (4) LE approach for all interior nodes and downstream boundary + FEM on conservative form of the transport equations for upstream boundary, and (5) LE approach for all interior nodes and downstream boundary + FEM on advective form of the transport equations for upstream boundary. The backward finite difference scheme is used for temporal discretization. In summary, 15 numerical options that provide a very wide range of efficiency and accuracy are available for use. In this section we use the case of operator-splitting strategy as an example to illustrate the five discretization options.

FDM to bed sediment in 1-D river/stream/canal network

At  $n+1$ -th time step, the continuity equation for 1-D bed sediment transport, Eq.(3.3), is approximated as follows:

$$\frac{P^{n+1}M_n^{n+1} - P^n M_n^n}{\Delta t} = W_1 P^{n+1} (D_n^{n+1} - R_n^{n+1}) + W_2 P^n (D_n^n - R_n^n) \quad (3.31)$$

where  $W_1$  and  $W_2$  are time weighting factors satisfying  $W_1 + W_2 = 1$ ,  $0 < W_1 < 1$ , and  $0 < W_2 < 1$  So that

$$M_n^{n+1} = \left\{ P^n M_n^n + \left[ W_1 P^{n+1} (D_n^{n+1} - R_n^{n+1}) + W_2 P^n (D_n^n - R_n^n) \right] \Delta t \right\} / P^{n+1} \quad (3.32)$$

Numerical schemes for suspended sediment for 1-D river/stream network

Five spatial discretization schemes are provided for 1-D suspended sediment simulation. these five , (1) Finite Element Method (FEM) on the conservative form of the transport equation, (2) FEM on the advective form of the transport equation, (3) modified Lagrangian-Eulerian (LE) approach to the Lagrangian form of the transport equation, (4) LE approach for all interior nodes and downstream boundary + FEM on conservative form of the transport equations for upstream boundary, and (5) LE approach for all interior nodes and downstream boundary + FEM on advective form of the transport equations for upstream boundary. The backward finite difference scheme is used for temporal discretization. The formulation of these five numerical schemes is the similar to the ones for the reactive transport with the operator-splitting coupling strategy that is presented in the following section.

Numerical Schemes for Kinetic Variable Transport in 1-D river/stream network

*FEM On the conservative form Of 1-D Transport Governing Equation*

The governing equations for the kinetic variables in 1-D river/stream network are given by Eq. (3.29), which is rewritten as follows:

$$A \frac{(E_n^m)^{n+1/2} - (E_n^m)^n}{\Delta t} + \frac{\partial A}{\partial t} E_n^m + L(E_n^m) = 0 \quad (3.33)$$

Assigning

$$R_{HSn} = 0 \quad \text{and} \quad L_{HSn} = 0 \quad (3.34)$$

and  $R_{HSn}$  and  $L_{HSn}$  are continuously calculated as follows,

$$M_{E_n}^{rs} = \begin{cases} S_R \times E_{n^{rs}}, & \text{if } S_R > 0 \Rightarrow R_{HSn} = R_{HSn} + M_{E_n}^{rs} \\ S_R \times E_n^m, & \text{if } S_R \leq 0 \Rightarrow L_{HSn} = L_{HSn} - S_R \end{cases} \quad (3.35)$$

$$M_{E_n}^{as} = \begin{cases} S_S \times E_{n^{as}}, & \text{if } S_S > 0 \Rightarrow R_{HSn} = R_{HSn} + M_{E_n}^{as}, \\ S_S \times E_n^m, & \text{if } S_S \leq 0 \Rightarrow L_{HSn} = L_{HSn} - S_S \end{cases} \quad (3.36)$$

$$M_{E_n}^{os1} = \begin{cases} S_1 \times E_{n^{os1}}, & \text{if } S_1 > 0 \Rightarrow R_{HSn} = R_{HSn} + M_{E_n}^{os1} \\ S_1 \times E_n^m, & \text{if } S_1 \leq 0 \Rightarrow L_{HSn} = L_{HSn} - S_1 \end{cases} \quad (3.37)$$

$$M_{E_n}^{os2} = \begin{cases} S_2 \times E_{n^{os2}}, & \text{if } S_2 > 0 \Rightarrow R_{HSn} = R_{HSn} + M_{E_n}^{os2} \\ S_2 \times E_n^m, & \text{if } S_2 \leq 0 \Rightarrow L_{HSn} = L_{HSn} - S_2 \end{cases} \quad (3.38)$$

$$M_{E_n}^{is} = \begin{cases} S_I \times E_{n^{is}}, & \text{if } S_I > 0 \Rightarrow R_{HSn} = R_{HSn} + M_{E_n}^{is} \\ S_I \times E_n^m, & \text{if } S_I \leq 0 \Rightarrow L_{HSn} = L_{HSn} - S_I \end{cases} \quad (3.39)$$

where  $E_{n^{rs}}$  is the concentration of En in the rainfall source,  $E_{n^{es}}$  is the concentration of En in the evaporation source,  $E_{n^{as}}$  is the concentration of En in the artificial source,  $E_{n^{os1}}$  is the concentration of En in the overland source from bank 1,  $E_{n^{os2}}$  is the concentration of En in the overland source from bank 2, and  $E_{n^{is}}$  is the concentration of En in the exfiltration source from the subsurface media.

Substituting  $R_{HSn}$  and  $L_{HSn}$  into Eq.(3.33), the equation is simplified as

$$A \frac{(E_n^m)^{n+1/2} - (E_n^m)^n}{\Delta t} + \frac{\partial A}{\partial t} E_n^m + \frac{\partial(QE_n^m)}{\partial x} - \frac{\partial}{\partial x} \left( K_x A \frac{\partial E_n^m}{\partial x} \right) + \left( L_{HSn} + \frac{\partial A}{\partial t} \right) E_n^m = R_{HSn} \quad (3.40)$$

After applying Galerkin or Petrov-Galerkin FEM to spatially discretize Eq.(3.40) and appropriate mathematic manipulation, Eq.(3.40) can be approximated by the following equation in matrix form,

$$([L1]+[L2]+[L3])\{E_n^m\}+[M]\left\{\frac{dE_n^m}{dt}\right\}=\{S\}+\{B\} \quad (3.41)$$

where

$$L1_{ij} = -\int_{x_1}^{x_N} \frac{dW_i}{dx} QN_j dx, \quad L2_{ij} = \int_{x_1}^{x_N} \frac{dN_i}{dx} K_x A \frac{dN_j}{dx} dx \quad (3.42)$$

$$L3_{ij} = \int_{x_1}^{x_N} N_i \left( L_{HSn} + \frac{\partial A}{\partial t} \right) N_j dx, \quad M_{ij} = \int_{x_1}^{x_N} N_i A N_j dx \quad (3.43)$$

$$S_i = \int_{x_1}^{x_N} N_i R_{HSn} dx, \quad B_i = -\mathbf{n} \left( W_i Q E_n^m - N_i K_x A \frac{\partial E_n^m}{\partial x} \right)_b \quad (3.44)$$

where  $N_j$  is the base function (linear function used in the model) at the  $j$ -th node;  $N_i$  is the weighting function with the same order as  $N_j$  at the  $j$ -th node; and  $W_i$  is the weighting function with the same order (in Galerkin FEM) as or one order higher (in Petrov-Galerkin FEM)  $N_j$  at the  $j$ -th node.

For interior nodes,  $B_i$  is zero, while for boundary nodes  $i=b$ ,  $B_i$  is calculated based on the boundary conditions by Eq. (3.45). Four types of boundary conditions are taken into account in

the model.

$$B_i = -\mathbf{n} \left( QE_n^m - K_x A \frac{\partial E_n^m}{\partial x} \right)_b \quad (3.45)$$

Dirichlet Boundary Condition

$$E_n^m = E_n^m(x_b, t) \quad (3.46)$$

Cauchy boundary condition

$$-\mathbf{n}AK_x \frac{\partial E_n^m}{\partial x} = Q_{En}(x_b, t) \Rightarrow B_i = -\mathbf{n}QE_n^m - Q_{En}(x_b, t) \quad (3.47)$$

Neumann boundary condition

$$n \left( QE_n^m - AK_x \frac{\partial E_n^m}{\partial x} \right) = Q_{En}(x_b, t) \Rightarrow B_i = -Q_{En}(x_b, t) \quad (3.48)$$

Variable boundary condition

When flow is coming in from outside ( $nQ < 0$ )

$$\mathbf{n} \left( QE_n^m - AK_x \frac{\partial E_n^m}{\partial x} \right) = \mathbf{n}QE_n^m(x_b, t) \Rightarrow B_i = -\mathbf{n}QE_n^m(x_b, t) \quad (3.49)$$

When Flow is going out from inside ( $nQ > 0$ )

$$-\mathbf{n}AK_x \frac{\partial E_n^m}{\partial x} = 0 \Rightarrow B_i = -\mathbf{n}QE_n^m \quad (3.50)$$

*FEM On The Advective Form Of 1-D Transport Governing Equation*

Converting the conservative form of the governing equation for 1-D transport, Eq.(3.33), into its

advective form given the continuity equation of water flow for 1-D river/stream, we obtain

$$A \frac{\partial E_n}{\partial t} + \frac{\partial A}{\partial t} E_n + Q \frac{\partial E_n^m}{\partial x} - \frac{\partial}{\partial x} \left( K_x A \frac{\partial E_n^m}{\partial x} \right) - \left[ \frac{\partial A}{\partial t} - (S_S + S_R + S_I + S_1 + S_2) \right] E_n^m \quad (3.51)$$

$$= M_{E_n}^{as} + M_{E_n}^{rs} + M_{E_n}^{is} + M_{E_n}^{os1} + M_{E_n}^{os2} + AR_{E_n}$$

Assign

$$R_{HSn} = 0 \quad \text{and} \quad L_{HSn} = (S_S + S_R + S_I + S_1 + S_2) - \frac{\partial A}{\partial t} \quad (3.52)$$

Following the same formulation for  $R_{HSn}$  and  $L_{HSn}$  as that in equations (3.35) through (3.39), equation **Error! Reference source not found.** can be rewritten as

$$A \frac{\partial E_n}{\partial t} + \frac{\partial A}{\partial t} E_n + Q \frac{\partial E_n^m}{\partial x} - \frac{\partial}{\partial x} \left( K_x A \frac{\partial E_n^m}{\partial x} \right) + L_{HSn} E_n^m = R_{HSn} + AR_{E_n} \quad (3.53)$$

Applying Galerkin or Petrov-Galerkin FEM method to spatially discretize equation (3.53), we obtain

$$([L1] + [L2] + [L3]) \{E_n^m\} + [M] \left\{ \frac{\partial E_n^m}{\partial t} \right\} = \{S\} + \{B\} \quad (3.54)$$

where [L2], [L3], [M], and {S} are defined the same as those in section 3.4.2.1, while [L1] and {B} are defined as follows.

$$L1_{ij} = \int_{x_i}^{x_N} W_i Q \frac{dN_j}{dx} dx \quad (3.55)$$

$$B_i = \mathbf{n} \left( N_i K_x A \frac{\partial E_n^m}{\partial x} \right)_b \quad (3.56)$$

For interior nodes,  $B_i$  is zero, while for boundary nodes  $i=b$ ,  $B_i$  is calculated based on the boundary conditions by Eq. (3.57),

$$B_i = \mathbf{n} \left[ K_x A \frac{\partial E_n^m}{\partial x} \right]_b \quad (3.57)$$

Dirichlet, Neumann, Cauchy, and Variable boundary conditions are taken into account and the corresponding  $B_i$  can be obtained based on Eq. (3.57). All the boundary conditions can be addressed the same as the ones for FEM on the conservative form except for the variable boundary condition.

Variable boundary condition

When flow is coming in from outside ( $nQ < 0$ )

$$n \left( QE_n^m - AK_x \frac{\partial E_n^m}{\partial x} \right) = nQE_n^m(x_b, t) \Rightarrow B_i = nQE_n^m - nQE_n^m(x_b, t) \quad (3.58)$$

When Flow is going out from inside ( $nQ > 0$ )

$$-nAK_x \frac{\partial E_n^m}{\partial x} = 0 \Rightarrow B_i = 0 \quad (3.59)$$

*Modified LE Approach For 1-D Transport Governing Equation*

Assign the true transport velocity  $V_{true}$ ,

$$V_{true} = Q / A \quad (3.60)$$

Equation (3.53) can be rewritten as

$$A \frac{(E_n^m)^{n+1/2} - (E_n^m)^n}{\Delta t} + AV_{true} \frac{\partial E_n^m}{\partial x} - \frac{\partial}{\partial x} \left( K_x A \frac{\partial E_n^m}{\partial x} \right) + \left( L_{HS_n} + \frac{\partial A}{\partial t} \right) E_n^m = R_{HS_n} \quad (3.61)$$

Equation (3.61) is written in Lagrangian and Eulerian forms as equation (3.62) and (3.63), respectively.

$$\frac{dE_n^m}{d\tau} = \frac{(E_n^m)^{n+1/2} - (E_n^m)^n}{\Delta t} + V_{true} \frac{\partial E_n^m}{\partial x} = 0 \quad (3.62)$$

$$A \frac{dE_n^m}{d\tau} - \frac{\partial}{\partial x} \left( K_x A \frac{\partial E_n^m}{\partial x} \right) + \left( L_{HS_n} + \frac{\partial A}{\partial t} \right) E_n^m = R_{HS_n} \quad (3.63)$$

Equation (3.62) is solved first to obtain the Lagrangian values of  $E_n^m$  first by particle tracking, and then equation (3.63) is dealt with finite element method. The diffusive term equation (3.63) is defined as equation (3.64). Galerkin FEM is applied to approximate the diffusive term as follows.

$$D = \frac{1}{A} \frac{\partial}{\partial x} \left( K_x A \frac{\partial E_n^m}{\partial x} \right) \quad (3.64)$$

$$\{D\} = -[QE]\{E_n^m\} + \{B\} \quad (3.65)$$

where

$$A1_{ij} = \int_{x_1}^{x_N} N_i A N_j dx, \quad A2_{ij} = \int_{x_1}^{x_N} \frac{dN_i}{dx} (K_{true} A) \frac{dN_j}{dx} dx \quad (3.66)$$

$$B1_i = \left( \mathbf{n} N_i K_{true} A \frac{\partial E_n^m}{\partial x} \right)_b \quad (3.67)$$

Lumping matrix [A1], and assign

$$QE_{ij} = A2_{ij} / A1_{ii}, \quad B_i = B1_i / A1_{ii} \quad (3.68)$$

Substitution equation (3.64) and (3.65) into equation (3.63), and the integration of equation (3.63) along a characteristic line yields the approximation of  $E_n^m$  as follows.

$$[CMATRIX] \left\{ (E_n^m)^{n+1/2} \right\} = \{RLD\} \quad (3.69)$$

where

$$[CMATRIX] = \frac{[U]}{\Delta\tau} + W_1[QE^{n+1}] + W_1[K^{n+1}] \quad (3.70)$$

$$\{RLD\} = \frac{[U]}{\Delta\tau} \left\{ (E_n^m)^* \right\} - W_2 \left\{ (KE_n^m)^* \right\} + W_2 \{D^*\} + W_1 \{R_L^{n+1}\} + W_2 \{R_L^*\} + W_1 \{B^{n+1}\} \quad (3.71)$$

where the superscript \* corresponds to the previous time step value at the location where node I is backwardly tracked in the Lagrangian step; and

$$K = \frac{(L_{HS_n})}{A}, \quad R_L = \frac{R_{HS_n}}{A} \quad (3.72)$$

For boundary node  $i=b$ , the boundary term  $\{B^{n+1}\}$  in equation (3.71) is calculated as follows.

Dirichlet Boundary Condition: the following equation is used for Dirichlet boundary node rather than Eq.(3.71).

$$E_n^m = E_n^m(x_b, t) \quad (3.73)$$

Variable boundary condition:

When flow is coming in from outside ( $nQ < 0$ ), equation (3.71) cannot be applied because  $\Delta\tau$

equals to zero. Applying boundary condition, we have

$$n \left[ Q(E_n^m)_i - AK_x \frac{(E_n^m)_j - (E_n^m)_i}{\Delta x} \right] = \mathbf{n} Q E_n^m(x_b, t) \quad (3.74)$$

where j is the interior node connected to the boundary node i.

when flow is going out from inside ( $nQ > 0$ ), the boundary term  $\{B^{n+1}\}$  in equation (3.71) is calculated as follows

$$-\mathbf{n} AK_x \frac{\partial E_n^m}{\partial x} = 0 \Rightarrow B_i = 0 \quad (3.75)$$

Cauchy boundary condition: equation (3.71) cannot be applied because  $\Delta\tau$  equals to zero.

Applying the boundary condition, we have

$$\mathbf{n} \left[ Q(E_n^m)_i - AK_x \frac{(E_n^m)_j - (E_n^m)_i}{\Delta x} \right] = Q_{Sn}(x_b, t) \quad (3.76)$$

where j is the interior node connected to the boundary node i.

Neumann boundary:

$$-\mathbf{n} AK_x \frac{\partial E_n^m}{\partial x} = Q_{E_n^m}(x_b, t) \Rightarrow B_i = -Q_{E_n^m}(x_b, t) / A1_{ii} \quad (3.77)$$

### *Mixed LE and FEM schemes*

Because the conventional LE method cannot be performed at the upstream boundary nodes, two mixed LE and FEM schemes are considered to overcome the conventional LE scheme's inaccuracy at upstream boundary nodes. The first option applies LE method for all interior nodes

and downstream boundary nodes, and FEM to the conservative form of the governing equations for upstream boundary nodes. The second option is the same as the first one except that in the Eulerian step FEM is applied to the advective form of the governing equation for upstream boundary nodes.

For the mixed predictor-corrector/operator-splitting strategy, all five spatial schemes are formulated the same as those for operator-splitting scheme, as preceding illustration, except for that the vector  $\{S\}$  in the two FEM approaches, and matrix  $[K]$  and vector  $\{R_L\}$  in LE approach are formulated as follows

$$S_i = \int_{x_1}^{x_N} N_i \left( R_{HS_n} + AR_{E_n}^n - \frac{\partial A}{\partial t} (E_n^{im})^n \right) dx \quad (3.78)$$

$$K = \frac{\left( L_{HS_n} + \frac{\partial A}{\partial t} \right)}{A}, \quad R_L = \frac{R_{HS_n} + AR_{E_n}^n - \frac{\partial A}{\partial t} (E_n^{im})^n}{A} \quad (3.79)$$

For the implicit strategy, the primary dependent variables should be transformed to  $E_n$  by expressing  $E_n^m$  in terms of  $(E_n^m/E_n) \cdot E_n$  or  $E_n - E_n^{im}$ . Then a similar procedure can then be followed to formulate five options of discretization formulation.

### 3.4.3 Coupling of fluid flow with reactive water quality transport

Two methods are often used to couple the hydrodynamic module and water quality transport module, direct linkage and indirect linkage. In the indirectly linked models, a water quality model takes hydrodynamic model output and uses it as input. This linkage usually requires large amount of computer storage to store and pass the flow information to the water quality model. Many models have been linked this way by modifying one code slightly so that the necessary

information for another model can be accepted or passed properly. In this case, the two models are used as a pair. The direct linkage can avoid this inconvenience by coding the two models into a single computer program so that they can run concurrently. This provides the efficiency and furthermore a promising potential to incorporate the feed back of water quality on hydrodynamic pattern. This model directly links the water flow and water quality so that the two components can be simulated simultaneously based on the same spatial mesh and time step.

### 3.5 Model verification

The model verification basically is comprised of three major steps in order.

(1) Verify the flow module stand alone: In this step the flow module alone is run and the results are compared with those obtained from WASH123D version 1.5, with the exact the same simulation conditions and numerical options. The results are expected to be identical if the flow module is correct.

(2) Verify the reactive chemical transport module: In this step, the reactive transport module is run alone with the flow field read in. The flow field is obtained from the first step. The results are compared with those using a general water quality paradigm (Zhang et al., 2008) where the same conditions are specified and the same flow field is input. Since this paradigm is adopted and incorporated into the current version of WASH123D, we expect no different in solution from the comparison.

(3) Verify the fully coupled model: In this step, the flow module and reactive transport module

are run concurrently and the flow field and chemical species concentrations are obtained simultaneously, with the same flow and transport boundary and initial conditions and numerical approaches taken. The simulated flow results should be the same as the ones from the first step, and the simulated reactive water quality is also expected to be nearly identical to the ones in step two if the same time step is used.

Two examples are presented in this section to demonstrate the correctness of the coupling of the hydrodynamic and reactive water quality transport components in the model. The first example is a hypothetical problem where 22 chemical species are involved in a complex reaction networks as described in WASP5 model (Ambrose et al., 1993b). The second is a case study of Des Moines River in Iowa, U.S.A.

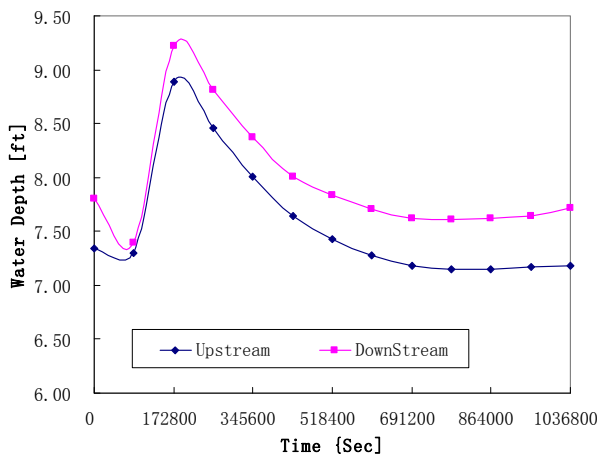
### 3.5.1 Example

This example problem presents one-dimensional problem of flow and reactive water quality transport modeling. The canal of interest was 15545 ft long with width of 15~40 ft and a very small bottom slope where Manning's roughness coefficient is assumed to be 0.02. The canal was discretized into 9 elements with sizes of 1690~1801 ft. In the flow simulation, the initial conditions were given and the Dirichlet boundary conditions were specified for up and downstream. Figure 3.1 shows the boundary conditions for the up and downstream nodes and the initial conditions. The dynamic wave model is employed. A twelve days simulation was performed with a fixed time step size of 6 minutes.

Figure 3.2 shows the simulated flow velocities on day 2, 6, and 12, by the proposed model and WASH123D version1.5, respectively. Compared with the WASH123D version 1.5, the proposed

model gives identical results when the dynamic wave model was used. Figure 3.3 shows the water depths along the distance on day 2, 6, and 12 using the two models. The velocities and the water depths are identical for the two models as expected.

Figure 3.4 and Figure 3.5 show the variation of velocity and water depths respectively at node 2 and 8. Again the two model results are identical. The velocity and the water depth between day 1 and 2 is high which also corresponds to the increase in the head at the boundaries as per model input.



Node	Distance ft	Water depth ft	Velocity ft/s
1	0	7.34	1.20
2	1690	7.39	0.68
3	3381	7.45	0.83
4	5183	7.49	0.89
5	6924	7.56	0.97
6	8666	7.59	0.92
7	10406	7.66	0.83
8	12148	7.70	0.86
9	13847	7.77	0.75
10	15545	7.81	0.78

Figure 3.1 Boundary condition and initial condition  
 Left: boundary conditions      Right: initial condition

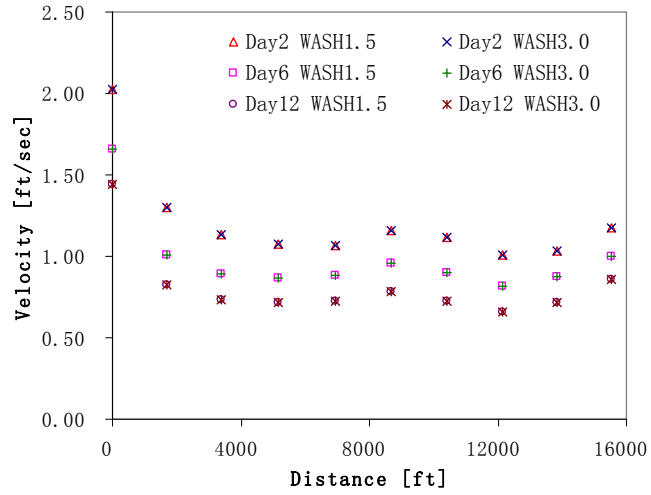


Figure 3.2 Velocity profile from the two models

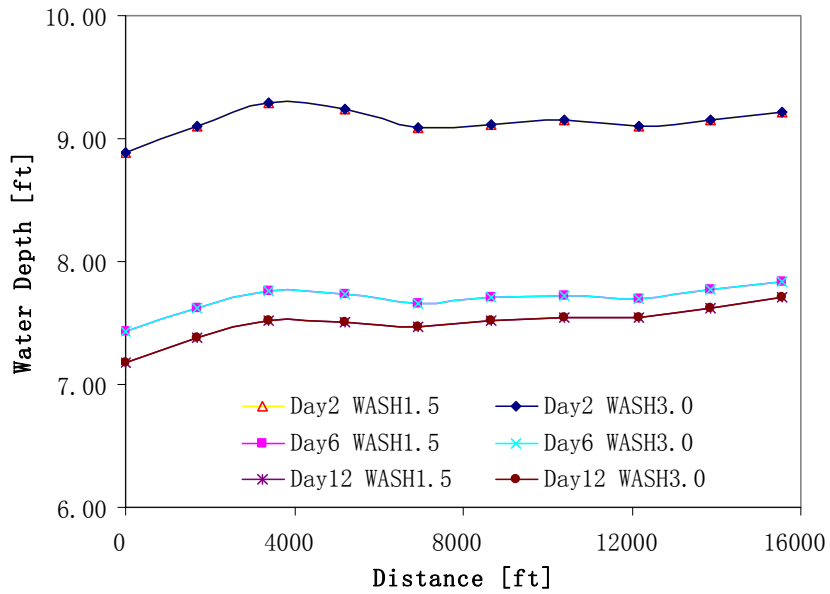


Figure 3.3 Simulated water depth at day 2, 6, and 12

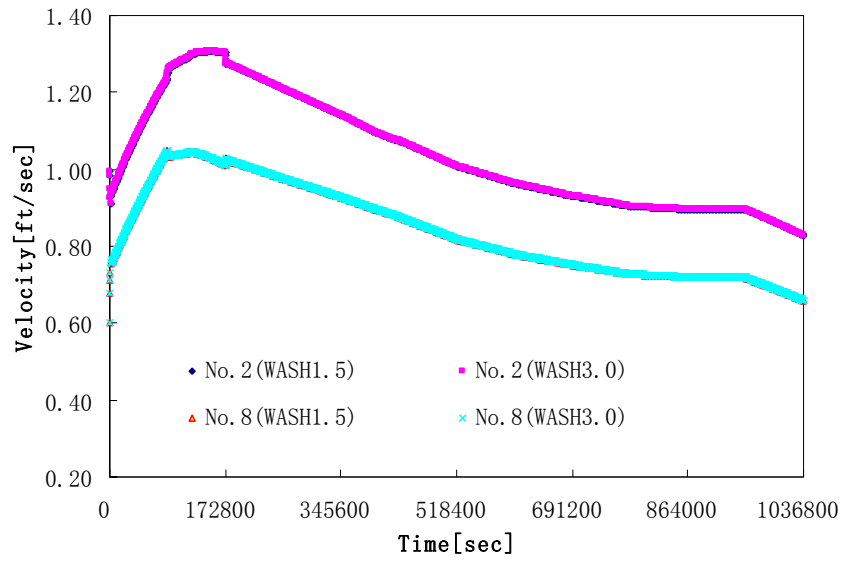


Figure 3.4 Velocity at node 2 and 8

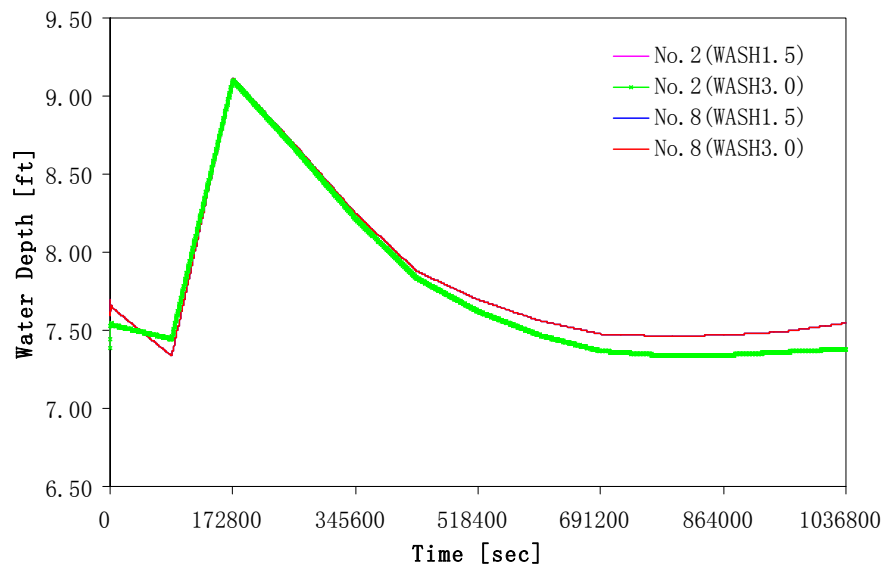


Figure 3.5 Water depths at node 2 and 8

In modeling the reactive water quality transport for the present example, the reactions used to formulate the reaction system were adopted from WASP5 (Ambrose et al., 1993b); this reaction network had been recast into the general paradigm (Zhang et al., 2008). There are 22 chemical species in the system involving 6 equilibrium and 32 kinetic reactions, as shown in Table

### 3.2 Reaction Coefficients used in the example

Description	Variable	Value	Unit
Phytoplankton nitrogen-carbon ratio	$a_{nc}$	0.25	mgN/mgC
Phytoplankton phosphorus-carbon ratio	$a_{pc}$	0.025	mgP/mgC
Phytoplankton oxygen-carbon ratio	$a_{oc}$	2.67	mgO <sub>2</sub> /mgC

Table 3.3 and Table 3.4 respectively. The reaction coefficients and rate parameters are listed in Table 3.2 and Table 3.5, respectively. The temperature is assumed to be 15°C, suspended sediment concentration SS is 1g/m<sup>3</sup>, and bed sediment concentration BS is 15 g/m<sup>2</sup> throughout the canal. A Dirichlet boundary condition is applied to the upstream boundary node. Flow-out variable boundary condition is applied to the downstream boundary node. Initial concentrations of all species and Dirichlet boundary concentrations of mobile species are listed in Table 3.1. The longitudinal dispersivity is 90 m. The FEM in conservative form is applied for spatial discretization and the operator-splitting scheme is used to deal with the coupling of transport and reaction. In order to test the transport module alone, the flow field obtained from the first step, verification of water flow module, is used as known input for the transport module and for the general water quality paradigm developed by Zhang (2008). As in flow simulation, a 12-day simulation is performed with a fixed time step size of 6 minutes. A relative error of 10<sup>-4</sup> is used to determine the convergence for iterations involved in the computation.

Table 3.1 Initial and boundary conditions for the reactive water quality simulation

Notation	Conc.	Initial Conditions	Boundary Conditions	$\rho_i$
NH <sub>3</sub>	C <sub>1</sub>	0.1 mg N/kg	1 mg N/kg	$\rho_w$
NH <sub>3(b)</sub>	C <sub>2</sub>	0.1 mg N/kg	-	$Ph_b\rho_{wb}\theta_b/A$
NO <sub>3</sub>	C <sub>3</sub>	0.1 mg N/kg	1 mg N/kg	$\rho_w$

NO <sub>3(b)</sub>	C <sub>4</sub>	0.1 mg N/kg	-	Ph <sub>b</sub> ρ <sub>wb</sub> θ <sub>b</sub> /A
OPO <sub>4</sub>	C <sub>5</sub>	0.01 mg P/kg	0.1 mg P/kg	ρ <sub>w</sub>
OPO <sub>4(b)</sub>	C <sub>6</sub>	0.01 mg P/kg	-	Ph <sub>b</sub> ρ <sub>wb</sub> θ <sub>b</sub> /A
PHYT	C <sub>7</sub>	0.2 mg C/kg	2 mg C/kg	ρ <sub>w</sub>
PHYT <sub>(b)</sub>	C <sub>8</sub>	0.2 mg C/kg	-	Ph <sub>b</sub> ρ <sub>wb</sub> θ <sub>b</sub> /A
CH <sub>2</sub> O	C <sub>9</sub>	1.0 mg O <sub>2</sub> /kg	10 mg O <sub>2</sub> /kg	ρ <sub>w</sub>
CH <sub>2</sub> O <sub>(p)</sub>	C <sub>10</sub>	1.0 mg O <sub>2</sub> /mg	10 mg O <sub>2</sub> /mg	SS
CH <sub>2</sub> O <sub>(b)</sub>	C <sub>11</sub>	1.0 mg O <sub>2</sub> /kg	-	Ph <sub>b</sub> ρ <sub>wb</sub> θ <sub>b</sub> /A
CH <sub>2</sub> O <sub>(bp)</sub>	C <sub>12</sub>	0.01 mg O <sub>2</sub> /mg	-	PBS/A
O <sub>2</sub>	C <sub>13</sub>	0.2 mg O <sub>2</sub> /kg	2 mg O <sub>2</sub> /kg	ρ <sub>w</sub>
O <sub>2(b)</sub>	C <sub>14</sub>	0.2 mg O <sub>2</sub> /kg	-	Ph <sub>b</sub> ρ <sub>wb</sub> θ <sub>b</sub> /A
ON	C <sub>15</sub>	0.2 mg N/kg	2 mg N/kg	ρ <sub>w</sub>
ON <sub>(p)</sub>	C <sub>16</sub>	0.0 mg N/mg	0 mg N/mg	SS
ON <sub>(b)</sub>	C <sub>17</sub>	0.2 mg N/kg	-	Ph <sub>b</sub> ρ <sub>wb</sub> θ <sub>b</sub> /A
ON <sub>(bp)</sub>	C <sub>18</sub>	0.0 mg N/mg	-	PBS/A
OP	C <sub>19</sub>	0.035 mg P/kg	0.35 mg P/kg	ρ <sub>w</sub>
OP <sub>(p)</sub>	C <sub>20</sub>	0.015 mg P/mg	0.15 mg P/mg	SS
OP <sub>(b)</sub>	C <sub>21</sub>	0.035 mg P/kg	-	Ph <sub>b</sub> ρ <sub>wb</sub> θ <sub>b</sub> /A
OP <sub>(bp)</sub>	C <sub>22</sub>	0.00015 mg P/mg	-	PBS/A

Note:  $\rho_w = \rho_{wb} = 1 \text{ kg/L}$ ,  $hb = 0.12 \text{ m}$ , and  $\theta_b = 0.6$

Table 3.2 Reaction Coefficients used in the example

Description	Variable	Value	Unit
Phytoplankton nitrogen-carbon ratio	a <sub>nc</sub>	0.25	mgN/mgC
Phytoplankton phosphorus-carbon ratio	a <sub>pc</sub>	0.025	mgP/mgC
Phytoplankton oxygen-carbon ratio	a <sub>oc</sub>	2.67	mgO <sub>2</sub> /mgC

Table 3.3 The 6 equilibrium chemical reactions in the system

No	Mechanism	Reaction	Reaction rate
E1	Carbonaceous sorption	CH <sub>2</sub> O → CH <sub>2</sub> O <sub>(p)</sub>	$f_{D5} = \frac{C_9}{C_9 + C_{10}}$
E2	Organic nitrogen sorption	ON → ON <sub>(p)</sub>	$f_{D7} = \frac{C_{15}}{C_{15} + C_{16}}$
E3	Organic phosphorous sorption	OP → OP <sub>(p)</sub>	$f_{D8} = \frac{C_{19}}{C_{19} + C_{20}}$
E4	Benthic carbonaceous sorption	CH <sub>2</sub> O <sub>(b)</sub> → CH <sub>2</sub> O <sub>(bp)</sub>	$f_{D5(\text{bed})} = \frac{C_{11}}{C_{11} + C_{12}}$
E5	Benthic organic nitrogen sorption	ON <sub>(b)</sub> → ON <sub>(bp)</sub>	$f_{D7(\text{bed})} = \frac{C_{17}}{C_{17} + C_{18}}$
E6	Benthic organic phosphorous sorption	OP <sub>(b)</sub> → OP <sub>(bp)</sub>	$f_{D8(\text{bed})} = \frac{C_{21}}{C_{21} + C_{22}}$

Table 3.4 The 32 kinetic chemical Reactions in the system

No.	Mechanism	Reaction	Reaction Rate
K1	PHYT growth	$a_{nc}NH_3 + a_{pc}OPO_4 + CO_2 + H_2O \rightarrow PHYT + \frac{32}{12}O_2$	$R_1 = G_p C_7$
K2	PHYT growth related nitrate reduction	$a_{nc}NO_3^- \rightarrow a_{nc}NH_3 + \frac{48}{12}O_2$	$R_2 = (1 - P_{NH_3})G_p C_7$
K3	PHYT death-endogenous respiration	$PHYT + \frac{32}{12}O_2 \rightarrow CO_2 + H_2O + a_{nc}ON + a_{pc}OP$	$R_3 = k_{ir} \Theta_{ir}^{T-20} C_7$
K4	PHYT death-parasitization	$PHYT \rightarrow a_{nc}CH_2O + a_{nc}ON + a_{pc}OP$	$R_4 = k_{id} C_7$
K5	PHYT death-herbivorous grazing	$PHYT \rightarrow a_{nc}CH_2O + a_{nc}ON + a_{pc}OP$	$R_5 = k_{ig} ZC_7$
K6	PHYT death-promoted oxidation of ON	$a_{nc}ON \rightarrow a_{nc}NH_3$	$R_6 = (1 - f_{on})(k_{ir} \Theta_{ir}^{T-20} C_7 + k_{id} C_7 + k_{ig} ZC_7)$
K7	PHYT death-promoted oxidation of OP	$a_{pc}OP \rightarrow a_{pc}OPO_4$	$R_7 = (1 - f_{op})(k_{ir} \Theta_{ir}^{T-20} C_7 + k_{id} C_7 + k_{ig} ZC_7)$
K8	Benthic PHYT decomposition	$PHYT_{(b)} \rightarrow a_{nc}CH_2O_{(b)} + a_{nc}ON_{(b)} + a_{pc}OP_{(b)}$	$R_8 = k_{pzd} \Theta_{pzd}^{T-20} C_8$
K9	PHYT(b) decomposition promoted oxidation of ON(b)	$a_{nc}ON_{(b)} \rightarrow a_{nc}NH_{3(b)}$	$R_9 = (1 - f_{on(bd)})k_{pzd} \Theta_{pzd}^{T-20} C_8 \cdot h_b P/A$
K10	PHYT(b) decomposition Promoted oxidation of OP(b)	$a_{pc}OP_{(b)} \rightarrow a_{pc}OPO_{4(b)}$	$R_{10} = (1 - f_{op(bd)})k_{pzd} \Theta_{pzd}^{T-20} C_8 \cdot h_b P/A$
K11	Phytoplankton settling	$PHYT \rightarrow PHYT_{(b)}$	$R_{11} = \frac{V_{s3}}{h_b} C_7 \cdot h_b P/A$
K12	Re-aeration	$O_{2(g)} \rightarrow O_2$	$R_{12} = k_2 \Theta_a^{(T-20)} (C_8 - C_{13})$
K13	Oxygen diffusion	$O_2 \rightarrow O_{2(b)}$	$R_{13} = \frac{E_{DIF}}{h_b} (C_{13} - C_{14}) \cdot h_b P/A$
K14	Carbonaceous oxidation	$CH_2O + O_2 \rightarrow CO_2 + H_2O$	$R_{14} = k_3 \Theta_a^{(T-20)} \left( \frac{C_{13}}{K_{BOD} + C_{13}} \right) (C_9 + C_{10})$
K15	Benthic carbonaceous oxidation	$CH_2O_{(b)} + O_{2(b)} \rightarrow CO_2 + H_2O$	$R_{15} = k_{D8} \Theta_{D8}^{T-20} (C_{11} + C_{12}) \cdot h_b P/A$
K16	Carbonaceous settling	$CH_2O_{(p)} \rightarrow CH_2O_{(bp)}$	$R_{16} = \frac{V_{s3}}{h_b} C_{10} \cdot h_b P/A$
K17	Carbonaceous re-suspension	$CH_2O_{(bp)} \rightarrow CH_2O_{(p)}$	$R_{17} = \frac{V_{R3}}{h_b} C_{12} \cdot h_b P/A$
K18	Carbonaceous diffusion	$CH_2O \rightarrow CH_2O_{(b)}$	$R_{18} = \frac{E_{DIF}}{h_b} (C_9 - C_{11}) \cdot h_b P/A$
K19	Nitrogen mineralization	$ON \rightarrow NH_3$	$R_{19} = k_{71} \Theta_{71}^{(T-20)} \left( \frac{C_7}{K_{mpe} + C_7} \right) (C_{15} + C_{16})$
K20	Nitrification	$NH_3 + \frac{64}{14} O_2 \rightarrow NO_3^- + H_2O + H^+$	$R_{20} = k_{12} \Theta_{12}^{(T-20)} \left( \frac{C_{13}}{K_{NIT} + C_{13}} \right) C_1$
K21	De-nitrification	$\frac{5}{4} CH_2O + \frac{14}{32} NO_3^- + H^+ \rightarrow \frac{5}{4} CO_2 + \frac{1}{2} N_2 + \frac{7}{4} H_2O$	$R_{21} = k_{2D} \Theta_{2D}^{(T-20)} \left( \frac{K_{NO_3}}{K_{NO_3} + C_{13}} \right) C_3 \cdot \frac{32}{14}$
K22	Benthic nitrogen mineralization	$ON_{(b)} \rightarrow NH_{3(b)}$	$R_{22} = k_{OND} \Theta_{OND}^{T-20} C_{17} \cdot h_b P/A$
K23	Benthic de-nitrification	$\frac{5}{4} CH_2O_{(b)} + \frac{14}{32} NO_3^-_{(b)} + H^+ \rightarrow \frac{5}{4} CO_2 + \frac{1}{2} N_2 + \frac{7}{4} H_2O$	$R_{23} = k_{2D} \Theta_{2D}^{(T-20)} C_4 \cdot \frac{32}{14} \cdot h_b P/A$
K24	Ammonia flux	$NH_{3(b)} \rightarrow NH_3$	$R_{24} = \frac{E_{DIF}}{h_b} (C_2 - C_1) \cdot h_b P/A$
K25	Nitrate flux	$NO_{3(b)} \rightarrow NO_3$	$R_{25} = \frac{E_{DIF}}{h_b} (C_4 - C_3) \cdot h_b P/A$
K26	Organic nitrogen settling	$ON_{(p)} \rightarrow ON_{(bp)}$	$R_{26} = \frac{V_{s3}}{h_b} C_{16} \cdot h_b P/A$
K27	Organic nitrogen flux	$ON_{(b)} \rightarrow ON$	$R_{27} = \frac{E_{DIF}}{h_b} (C_{17} - C_{15}) \cdot h_b P/A$
K28	Phosphorous mineralization	$OP \rightarrow OPO_4$	$R_{28} = k_{83} \Theta_{83}^{(T-20)} \left( \frac{C_7}{K_{mpe} + C_7} \right) (C_{19} + C_{20})$
K29	Benthic phosphorous mineralization	$OP_{(b)} \rightarrow OPO_{4(b)}$	$R_{29} = k_{OPD} \Theta_{OPD}^{T-20} C_{21} \cdot h_b P/A$
K30	Phosphorous flux	$OPO_{4(b)} \rightarrow OPO_4$	$R_{30} = \frac{E_{DIF}}{h_b} (C_6 - C_5) \cdot h_b P/A$
K31	Organic phosphorous setting	$OP_{(p)} \rightarrow OP_{(bp)}$	$R_{31} = \frac{V_{s3}}{h_b} C_{20} \cdot h_b P/A$
K32	Organic phosphorous flux	$OP_{(b)} \rightarrow OP$	$R_{32} = \frac{E_{DIF}}{h_b} (C_{21} - C_{19}) \cdot h_b P/A$

Table 3.5 The parameters in reaction rate formulation

Description	Variable	Value	Unit
Phytoplankton growth rate	$G_{PI}$	$k_{IC}X_{RT}X_{RI}X_{RN}$	day <sup>-1</sup>
Maximum phytoplankton growth rate	$k_{IC}$	2.0	day <sup>-1</sup>
Temperature adjustment factor for phytoplankton growth	$X_{RT}$	$\Theta_{IC}^{T-20}$	-
Temperature coefficient for phytoplankton growth	$\Theta_{IC}$	1.068	-
Light adjustment coefficient for phytoplankton growth	$X_{RI}$	$\min \{ef[e^{-(I_a/I_s)^{0.75}} - e^{-I_a/I_s}]/(K_e D), 1.0\}$	-
Light extinction coefficient	$K_e$	2	m <sup>-1</sup>
Fraction of day that is daylight	$F$	0.5	-
Average daily surface solar radiation	$I_a$	400	Langley/day
Saturating light intensity of phytoplankton	$I_s$	540	Langley/day
Nutrient limitation factor for phytoplankton growth	$X_{RN}$	$\text{Min}(DIN/(K_{mN} + DIN), DIP/(K_{mP} + DIP))$	-
Concentration of the dissolved inorganic nitrogen	$DIN$	$C_1 + C_3$	mg N/L
Half-saturation constant for nitrogen	$K_{mN}$	0.025	mg N/L
Dissolved inorganic phosphorus	$DIP$	$f_{D3}C_5$	mg P/L
Fraction of dissolved inorganic phosphorus	$f_{D3}$	0.85	-
Half-saturation constant for phosphorus	$K_{mP}$	0.001	mg P/L
Preference for ammonia uptake term	$P_{NH3}$	$[C_1 C_3 / (K_{mN} + C_1) + C_1 K_{mN} / (C_1 + C_3)] / (K_{mN} + C_3)$	-
Phytoplankton respiration rate constant	$k_{Ir}$	0.125	day <sup>-1</sup>
Temperature coefficient for Phytoplankton respiration	$\Theta_{Ir}$	1.045	-
Phytoplankton death rate constant	$k_{Id}$	0.02	day <sup>-1</sup>
Phytoplankton Grazing Rate Constant	$k_{Ig}$	0	L/mgC
Zooplankton Population	$Z$	0	mgC/L
Fraction of dead and respired PHYT recycled to ON	$f_{on}$	0.5	-
Fraction of dead and respired PHYT recycled to OP	$f_{op}$	0.5	-
Benthic phytoplankton decomposition rate constant	$k_{PZD}$	0.02	day <sup>-1</sup>
Temperature coefficient for benthic PHYT decomposition	$\Theta_{PZD}$	1.08	-
Benthic fraction of decomposed PHYT recycled to ON	$f_{on(bed)}$	0.5	-
Benthic fraction of PHYT recycled to the OP pool	$f_{op(bed)}$	0.5	-
Phytoplankton Settling Velocity	$V_{S4}$	0.1	m/day
Re-aeration rate constant	$k_2$	$\min[\text{Max}(k_a, k_w), 10.0]$	-
Flow-induced re-aeration rate coefficient	$k_q$	$5.049v^{0.97}h^{-1.67}$	-
Wind-induced re-aeration rate coefficient	$k_w$	0	-
Re-aeration rate temperature coefficient	$\Theta_a$	1.028	-
Dissolve oxygen saturation	$C_s$	$-139.34 + 1.5757 \times 10^6 T^{-1} - 6.6423 \times 10^7 T^{-2} + 1.2438 \times 10^{10} T^{-3} + 8.6219 \times 10^{11} T^{-4}$ $e^{-0.55358(0.031929 - 19.428 T^{-1} - 3868.3 T^{-2})}$	-
Oxygenation rate constant	$k_d$	0.185	day <sup>-1</sup>

Table 3.5 The parameters in reaction rate formulation (Continued)

Oxygenation rate Temperature coefficient	$\Theta_d$	1.047	-
Half saturation constant for oxygen limitation	$K_{BOD}$	0.5	mgO <sub>2</sub> /L
Benthic Oxygenation rate constant	$k_{DS}$	0.0004	day <sup>-1</sup>
Oxygenation rate Temperature coefficient	$\Theta_{DS}$	1.08	-
Organic matter settling velocity	$V_{S3}$	0.1	m/day
Organic matter re-suspension velocity	$V_{R3}$	0.01	m/day
Fraction of dissolved Carbonaceous	$f_{D5}$	0.5	-
Fraction of dissolved benthic Carbonaceous	$f_{D5(b)}$	0.5	-
Diffusive exchange coefficient is	$E_{DIF}$	0.0002	m <sup>2</sup> /day
Organic nitrogen mineralization rate constant	$k_{71}$	0.075	day <sup>-1</sup>
Organic nitrogen mineralization Temperature coefficient	$\Theta_{71}$	1.08	-
Half saturation constant for PHYT limitation of P recycle	$K_{mPc}$	1.0	mgC/L
Nitrification rate constant	$k_{12}$	0.105	day <sup>-1</sup>
Nitrification rate temperature coefficient	$\Theta_{12}$	1.08	
Half saturation for oxygen limitation of Nitrification	$K_{NIT}$	2.0	mgO <sub>2</sub> /L
De-nitrification rate constant	$K_{2D}$	0.09	day <sup>-1</sup>
De-nitrification rate temperature coefficient	$\Theta_{2D}$	1.045	-
Half saturation constant for oxygen of De-nitrification	$K_{NO3}$	0.1	mgO <sub>2</sub> /L
Benthic Organic nitrogen mineralization rate constant	$k_{OND}$	0.0004	day <sup>-1</sup>
Mineralization rate Temperature coefficient	$\Theta_{OND}$	1.08	-
Fraction of dissolved Organic Nitrogen	$f_{D7}$	1.0	-
Fraction of dissolved benthic Organic Nitrogen	$f_{D7(b)}$	1.0	-
Dissolved OP mineralization rate constant	$k_{83}$	0.22	day <sup>-1</sup>
Dissolved OP mineralization temperature coefficient	$\Theta_{83}$	1.08	-
Half saturation constant for PHYT limitation of P recycle	$K_{mPc}$	1.0	mgC/L
Benthic dissolved OP mineralization rate constant	$k_{OPD}$	0.0004	day <sup>-1</sup>
Benthic dissolved OP mineralization temperature coefficient	$\Theta_{OPD}$	1.08	-
Fraction of dissolved OP	$f_{D8}$	0.7	-
Fraction of dissolved benthic OP	$f_{D8(b)}$	0.7	-

The variation of dissolved oxygen, phytoplankton, nitrate, and organic matter, with time and space is presented in Figure 3.6 through Figure 3.9. As the variation of all these parameters is linked through the reaction scheme presented above, their trends are generally similar.

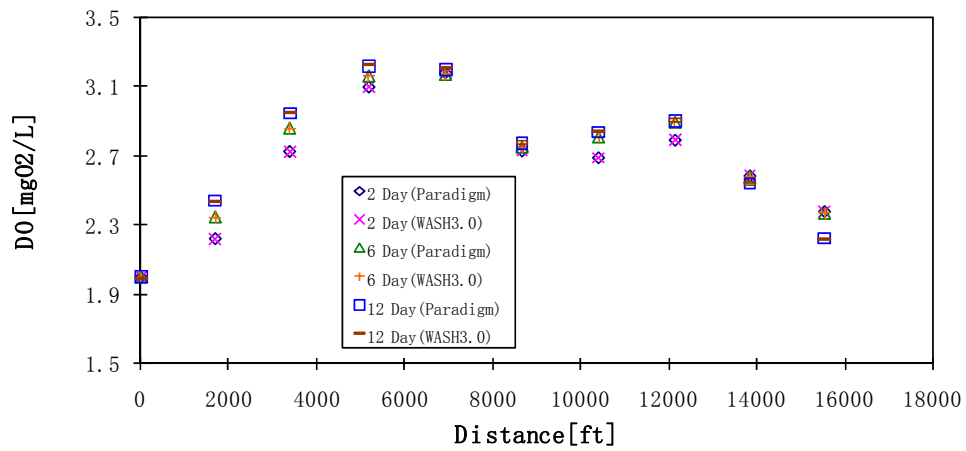


Figure 3.6 Dissolved oxygen concentration profile for the two models

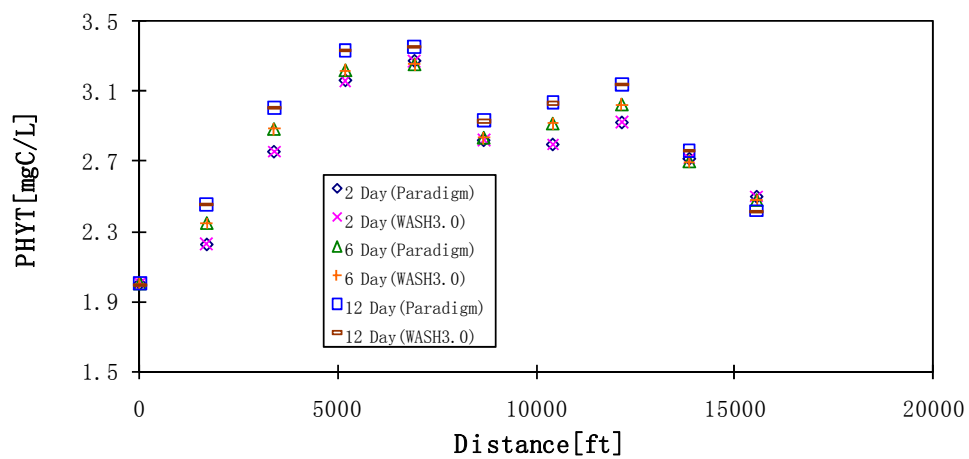


Figure 3.7 Phytoplankton concentration profile for the two models

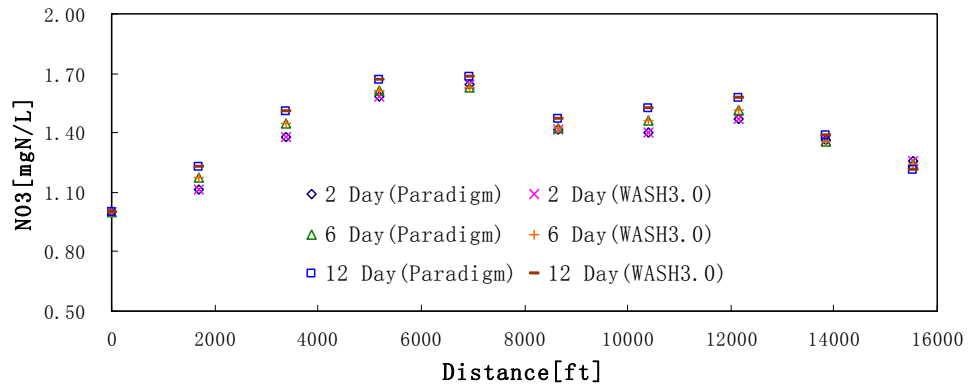


Figure 3.8 Nitrate concentration profile for the two models

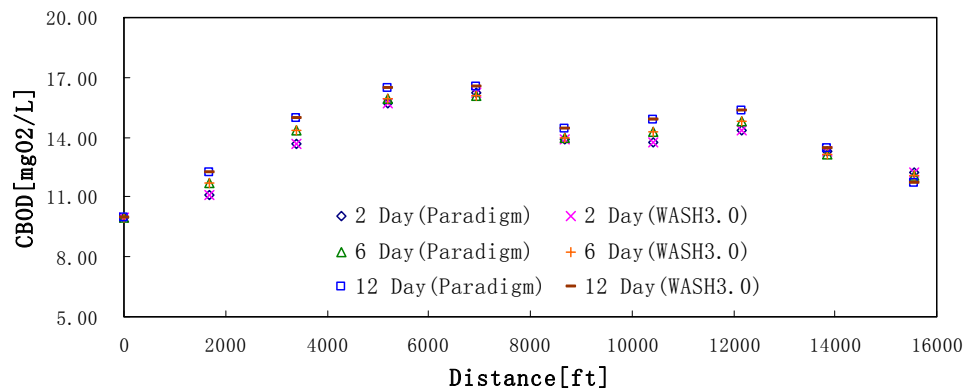


Figure 3.9 Dissolved organics concentration profile the two models

The variation of the four parameters at two locations with time also show identical trends as shown in Figure 3.10 through Figure 3.13. Through the comparison of the water quality output file from the proposed model and the general paradigm, we found the simulation results are identical.

The final step is to verify the fully coupled model. Both the water flow and water quality module in the new model are activated and a concurrent simulation of flow and water quality transport is performed. All initial conditions, boundary conditions, and numerical approaches are the same as in the first two steps. A 12-day simulation is performed with a fixed time step size of 6 minutes. A relative error of  $10^{-4}$  is used to determine the convergence for iterations involved in the computation. Since the same time step is used, the simultaneous simulation gives exactly the same solution as WASH123D version 1.5 and the general paradigm in the simulation of flow and water quality transport, respectively. The output is not plotted for presentation herein since they would be exactly the same as Figure 2 through 13 if the roundoff error is considered. As WASH123D version 1.5 has been tested in many aspects (Yeh et al., 2005), the well agreement of the simulations from present model with WASH123D validates the present model as well.

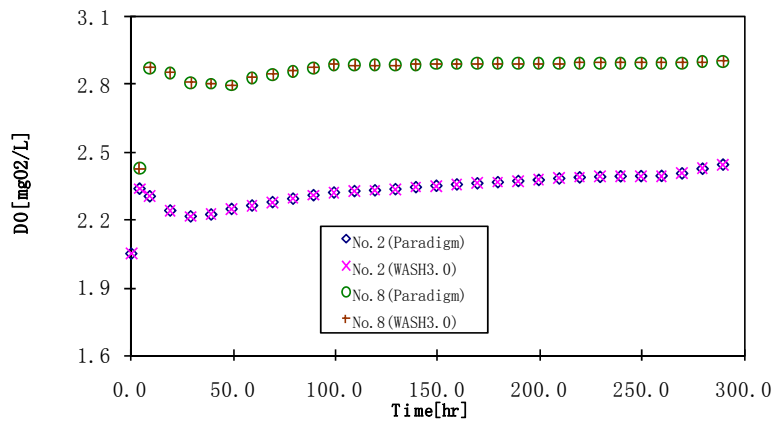


Figure 3.10 Variation of dissolved oxygen concentration at two locations

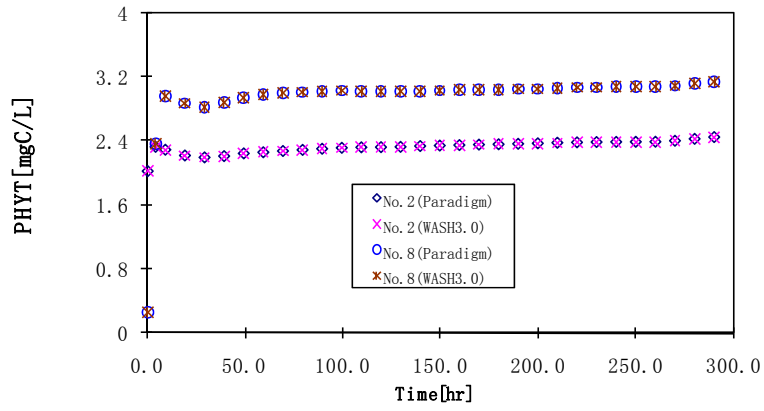


Figure 3.11 Variation of phytoplankton concentration at two locations

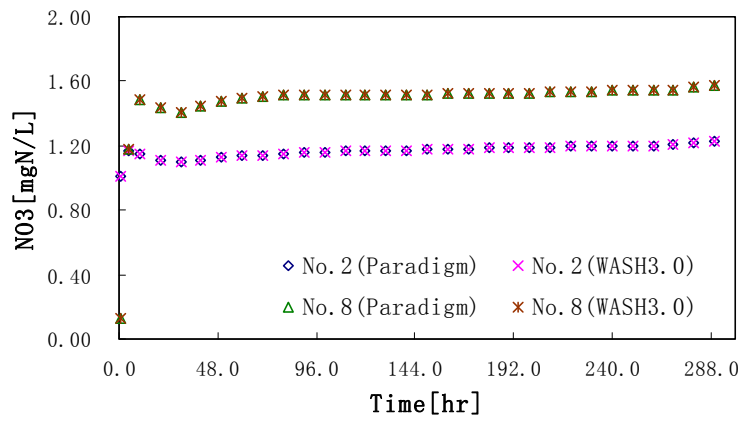


Figure 3.12 Variation of nitrate concentration at two locations

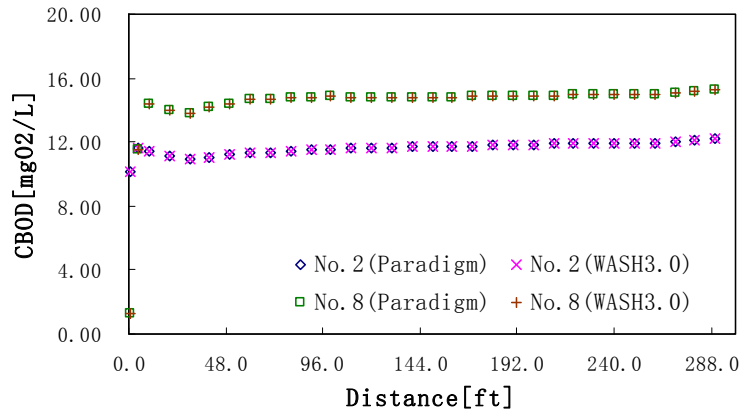


Figure 3.13 Variation of dissolved organics concentration at two locations

### 3.5.2 Case study

A case study of the Des Moines River water quality simulation is conducted in this section to demonstrate the capability of the integrated model. The study reach begins at the outfall of Des Moines Sewage Treatment Plant located upstream of water quality sampling station 6 and ends 38.6 km downstream at station 7 ( Figure 3.14) The drainage area of the reach is about 4600 km<sup>2</sup>. According to the historical flow records from US Geological Survey (USGS) gauging station located 3.5 km upstream of the reach, the stream basin experienced a severe drought condition in the summer of 1977. Gu and Dong (1998) successfully calibrated WASP5 with the low flow data during of a period of one week before July 13, 1977. A steady state stream flow rate of 2.5 m<sup>3</sup>/s for 7 days was assumed in that study. This case study use the same data as Gu and Dong (1998) and the chemical reactions used in this study are extracted from WASP5, as shown in Table 3.3 and Table 3.4; however, a transient simulation of water flow is performed simultaneously with water quality simulation.

The reach is assumed to have a triangular shaped cross-section with side slope of 1:22.9. This

38.6 km reach is discretized into 24 elements, each about 1600m long. The initial velocity in the river is assumed to be 0.00326 m/s and the initial water depth is assumed to be 2.59m initially. The incoming flux boundary condition is applied at the upstream end of the reach (Figure 3.15) and the Dirichlet boundary condition describing the water surface elevation is used. According to the monitoring station, the water temperature was 27.5 °C, suspended sediment concentration SS is 35 g/m<sup>3</sup>, and bed sediment concentration BS is 3.26 g/m<sup>2</sup>, these values are considered uniform throughout the reach. A Dirichlet boundary condition applied at the upstream end and a flow-out variable boundary condition is applied at the downstream boundary. The initial and boundary conditions are listed in Figure 3.16, longitudinal dispersivity is assumed to be 100 m. The diffusive model is applied for water flow simulation, and discretized by FEM method, the operator-splitting scheme is employed to handle the reaction term in the reactive transport equation and the FEM on conservative form is used discretize the advective-dispersive transport equation. A 7-day simulation is performed with a fixed time-step size of 1 hour. The reaction coefficients and the rate parameters used for this simulation are the same as shown in Table 3.2 and Table 3.5 except that the oxygenation rate constant  $k_d$  is adjusted to 0.16 day<sup>-1</sup> and the organic matter settling velocity  $V_{S3}$  is adjusted to zero.

Figure 3.16 shows the observed and simulated BOD, DO, and total nitrogen at 7 days, respectively. The simulated DO, BOD, and ammonia nitrogen concentration profiles all agree well with field measurements.

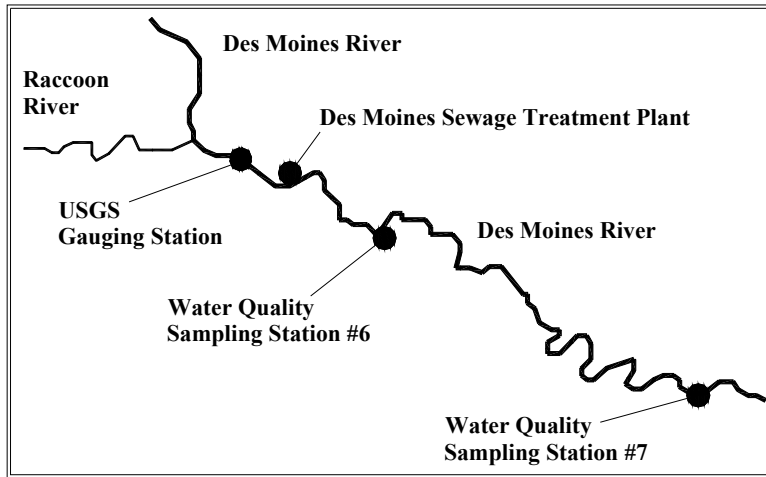


Figure 3.14 Schematic of the Des Moines River study area, Iowa, USA

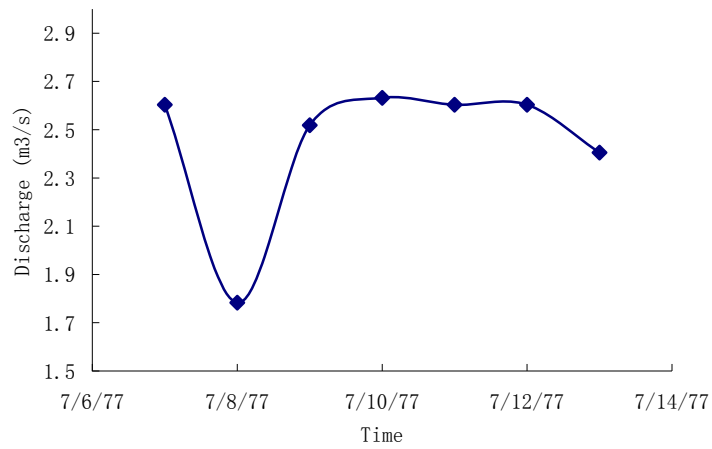


Figure 3.15 Upstream discharge data from USGS gauge station

Table 3.6 Chemical Species in Example

Notation	Concen.	Initial	Boundary
NH3	C1	8.2 mg N/kg	8.2 mg N/kg
NH3(b)	C2	8.2 mg N/kg	-
NO3	C3	0.35 mg N/kg	0.35 mg N/kg
NO3(b)	C4	0.35 mg N/kg	-
OPO4	C5	0.4 mg P/kg	0.4 mg P/kg
OPO4(b)	C6	0.4 mg P/kg	-
PHYT	C7	6.5 mg C/kg	6.5 mg C/kg
PHYT(b)	C8	6.5 mg C/kg	-
CH2O	C9	5.25 mg O2/kg	5.25 mg O2/kg
CH2O(p)	C10	0.15 mg O2/mg	0.15 mg O2/mg
CH2O(b)	C11	5.25 mg O2/kg	-
CH2O(bp)	C12	0.0136 mg O2/mg	-
O2	C13	3.6 mg O2/kg	3.6 mg O2/kg
O2(b)	C14	3.6 mg O2/kg	-
ON	C15	1.15 mg N/kg	1.15 mg N/kg
ON(p)	C16	0.0 mg N/mg	0 mg N/mg
ON(b)	C17	1.15 mg N/kg	-
ON(bp)	C18	0.0 mg N/mg	-
OP	C19	0.28 mg P/kg	0.28 mg P/kg
OP(p)	C20	0.00343 mg P/mg	0.00343 mg P/mg
OP(b)	C21	0.28 mg P/kg	-
OP(bp)	C22	0.00031 mg P/mg	-

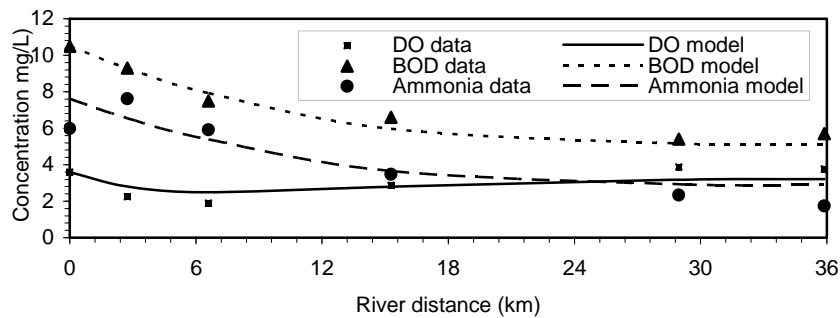


Figure 3.16 Comparison of model results with observed data

The simulation of actual observed data in the field validates the application of the present model to water quality simulation problems.

### 3.6 Conclusion

This chapter presents the development of a numerical model for water flow and sediment and reactive water quality transport simulation in river/stream networks by incorporating a general water quality simulation paradigm into the current version of WASH123D model. The model is one of three major components of an integrated hydrology/hydraulic water quality model for watershed scale simulations.

The coupling of water flow and water quality simulations provides the model with a full range of simulation capability and saves computer storage compared with the commonly used indirectly linked models. The coupling of water quality transport with an arbitrary number of mixed equilibrium and kinetic reactions makes the model general and flexible enough to simulate water

quality problems subject to any number of chemical reactions.

Through the diagonalization of the reactive transport equation via Gauss-Jordan column reduction of the chemical reaction network, equilibrium reactions are decoupled from the kinetic reactions. Species reactive transport equations are transformed into two sets: reactive transport equations of kinetic-variables and algebraic equations of equilibrium variables. Kinetic variable is adopted as primary dependent variable in solving the transport equation rather than individual species to reduce the number of transport equations and simplify the reaction terms. Three coupling strategies, fully implicit scheme, mixed predictor-corrector/operator-splitting scheme, and operator-splitting scheme, are included in the model to do with the coupling of transport and biogeochemical reactions at different levels of efficiency and accuracy. Five spatial discretization approaches are utilized to solve the advection-dispersion transport equation describing the kinetic variable transport.

In each time step, hydrologic/hydraulic variables are solved in the flow module; kinetic variables are then solved in the transport module. This is followed by solving the reactive chemical system node by node to yield concentrations of all species. One hypothetical example is employed to verify the correctness of the coupling between hydrodynamics and reactive water quality model. One case study in Des Moines River is conducted for the verification of the model.

### 3.7 Reference

Ambrose, R.B., Wool, T.A. and Martin, J.L., 1993a. The dynamic estuary model hydrodynamic

- program DYNHYD 5 documentation and user manual, Environmental Research Laboratory, US Environmental Protection Agency, Athens, GA.
- Ambrose, R.B., Wool, T.A. and Martin, J.L., 1993b. The water quality analysis simulation program, WASP5 Part A: model documentation. Environmental Research Laboratory, US Environmental Protection Agency, Athens, GA.
- Barkau, R.L., 1992. One-Dimensional Unsteady Flow Through a Full Network of Open Channels. (Computer Program). UNET, St. Louis, MO.
- Barnwell, T.O. and Brown, L.C., 1987. The Enhanced Stream Water Quality Models QUAL2E and QUAL2E-UNCAS: Documentation and User Manual., U.S. Environmental Protection Agency, Washington, DC.
- Barnwell, T.O. and Brown, L.C., 1987. The Enhanced Stream Water Quality Models QUAL2E and QUAL2E-UNCAS: Documentation and User Manual., U.S. Environmental Protection Agency, Washington, DC.
- Bicknell, B.R., Imhoff, J.C., Kittle, J.L., Jobs Jr., T.H. and Donigian Jr., A.S., 2001. HYDROLOGICAL SIMULATION PROGRAM - FORTRAN, Version 12, User's manual, AQUA TERRA Consultants.
- Bicknell, B.R., Imhoff, J.C., Kittle, J.L., Jobs Jr., T.H. and Donigian Jr., A.S., 2001. HYDROLOGICAL SIMULATION PROGRAM - FORTRAN, Version 12, User's manual, AQUA TERRA Consultants.
- Brown, L.C. and Barnwell, T.O., 1987. The enhanced stream water quality models QUAL2E and QUAL2E-UNCAS: Documentation and user Manual. EPA/600/3-87/007.
- Cerco, C.F. and Cole, T., 1995. User's Guide to the CE-QUAL-ICM Three-dimensional

- eutrophication model, release version 1.0. Technical Report EL-95-15, US Army Corps of Engineers Water Experiment Station, Vicksburg, MS.
- Chapra, S.C. and Pelletier, G.J., 2003. QUAL2K: A Modeling Framework for Simulating River and Stream Water Quality: Documentation and Users Manual, Civil and Environmental Engineering Department, Tufts University, Medford, MA.
- Cheng, H.P., Yeh, G.T. and Cheng, J.R., 2000. A numerical model simulation reactive transport in shallow water domains: model development and demonstrative applications. *Advances in Environmental Research*, 4: 187-209.
- Cole, T.M. and Wells, S.A., 2003. A two-dimensional, laterally averaged, Hydrodynamic and Water Quality Model, Version 3.1. Instruction Report EL-03-1, Army Engineer Waterways Experiment Station, Vicksburg, MS.
- Fang, Y.L., Yeh, G.T. and Burgos, W.D., 2003. A Generic Paradigm to Model Reaction-Based Biogeochemical Processes in Batch Systems. *Water Resources Research*, 33(4): 1083-1118.
- Fang, Y.L., Yeh, G.T. and Burgos, W.D., 2003. A Generic Paradigm to Model Reaction-Based Biogeochemical Processes in Batch Systems. *Water Resources Research*, 33(4): 1083-1118.
- Gu, R. and Dong, M., 1998. Water quality modeling in the watershed-based approach for water load allocations. *Water Science and Technology*, 38(10): 165-172.
- Hamrick, J.M., 1996. A user's manual for the environmental fluid dynamics computer code (EFDC), The College of William and Mary, Virginia Institute of Marine Science, Gloucester Point, VA.

- Huang, G.B. and Yeh, G.T., 2009. Comparative Study of Coupling Approaches for Surface Water and Subsurface Interactions. *Journal of Hydrologic Engineering*, 14(5): 453-462.
- Lung, W.S. and Hwang, C.C., 1989. Integrating hydrodynamic and water quality models for Patuxent Estuary. In: ASCE (Editor), *Estuarine and Coastal Engineering*. ASCE, New York, NY, pp. 420-429.
- Lung, W.S., 2001. *Water quality modeling for wasteload allocations and TMDLs*. John Wiley & Sons, Inc, New York.
- Roelvink, J.A., 2003. Implementation of roller model, draft Delft3D manual, Delft Hydraulics Institute.
- Rubin, J., 1983. Transport of reacting solutes in porous media: relation between mathematical nature of problem formulation and chemical nature of reactions. *Water Resources Research*, 38(11): 253-260.
- Steeffel, C.I. and van Cappellen, P., 1998. Preface: reactive transport modeling of natural systems. *Journal of Hydrology*, 209: 1-7.
- Vieira, D.A. and Wu, W., 2002. One-dimensional Channel network model CCHE1D version 3.0 - user's manual, University of Mississippi, University, MS.
- Yeh, G.-T., Burgosb, W.D. and Zacharac, J.M., 2001. Modeling and measuring biogeochemical reactions: system consistency, data needs, and rate formulations. *Advances in Environmental Research*, 5: 219-237.
- Yeh, G.T., Cheng, H.P., Cheng, J.R. and Jerry, H.L., 1998. A Numerical Model to Simulate Water Flow and Contaminant and Sediment Transport in Watershed Systems of 1-D Stream-River Network, 2-D Overland Regime, and 3-D Subsurface Media (WASH123D:

- Version 1.0). Technical Report CHL-98-19, Waterways Experiment Station, U. S. Army Corps of Engineers, Vicksburg, MS 39180-6199.
- Yeh, G.-T., Huang, G., Cheng, H.-P., Zhang, F., Lin, H.-C., Edris, E. and Richards, D., 2006. A first-principle, physics-based watershed model: WASH123D. In: V.P. Singh and D.K. Frevert (Editors), *Watershed Models*. CRC Press, Boca Raton, FL.
- Yeh, G.T., Huang, G., Zhang, F., Cheng, H.P. and Lin, H.-C., 2005. WASH123D: A numerical model of flow, thermal transport, and salinity, sediment, and water quality transport in WAterSHed systems of 1-D stream-river network, 2-D overland regime, and 3-D subsurface media, Office of Research and Development, Orlando, FL.
- Zhang, F., Yeh, G.T., Parker, J.C. and Jardine, P.M., 2008. A reaction-based river/stream water quality model: Model development and numerical schemes. *journal of Hydrology*, 348(3-4): 496-509.
- Zhang, F., Yeh, G.T., Parker, J.C., Brooks, S.C., Pace, M.N., Kim, Y.J., Jardine, P.M. and Watson, D.B., 2007. A reaction-based paradigm to model reactive chemical transport in groundwater with general kinetic and equilibrium reactions. *Journal of Contaminant Hydrology*, 92(1-2): 10-32.
- Zhang, F., Yeh, G.T., Parker, J.C., Brooks, S.C., Pace, M.N., Kim, Y.J., Jardine, P.M. and Watson, D.B., 2007. A reaction-based paradigm to model reactive chemical transport in groundwater with general kinetic and equilibrium reactions. *Journal of Contaminant Hydrology*, 92(1-2): 10-32.

## CHAPTER 4 AN INTEGRATED HYDROLOGY/HYDRAULIC AND WATER QUALITY MODEL FOR OVERLAND SHALLOW WATER SYSTEMS

### 4.1 Abstract

This chapter presents an integrated two-dimensional depth-averaged numerical model simulating water flow and reactive contaminant and sediment transport over the land surface, with emphasis on the mathematic formulation of reactive water quality transport. This model is comprised of two major modules: water flow module and reactive transport module. The water flow module is the well developed current version of WASH123D, while the transport module is on based on a newly developed a paradigm for water quality simulation. The St. Venant equation and its simplified versions, diffusion wave and kinematic wave models, are employed for water flow simulation while the reactive advection-dispersion equation is used as the governing equation for water quality transport. The surface-subsurface water interactions are considered in the flow module and simulated on the basis of continuity of interface. In the transport simulations, fast/equilibrium reactions are decoupled from slow/kinetic reactions by the decomposition of reaction networks; this enables robust numerical integrations of the governing equation. Kinetic variables are adopted as primary dependent variables rather than biogeochemical species to reduce the number of transport equations and simplify the reaction terms. In each time step, hydrologic/hydraulic variables are solved in the flow module; kinetic variables are then solved in the transport module. This is followed by solving the reactive chemical system node by node to yield concentrations of all species. One example is presented to demonstrate the design

capability of the model.

## 4.2 Introduction

Extensive integration and coupling of hydrological models with water quality models have been performed during the last 20 years (Arheimer and Olsson, 2003). With the advances in the development of computer technology, numerical methods, and a deeper understand of hydrological processes and water quality transport processes, numerous models have been developed to simulate both fluid flow and sediment and water quality in river networks. There are two primary issues. One is the linkage between hydrodynamic models and water quality models and the other is the generality of the water quality models.

Historically, water flow models and water quality models were developed with different methods and thus different spatial grids and temporal size. For example, many of water quality models are based on the finite segments (box model) approach while most water flow models are based on finite difference method or finite element method (Lung, 2001; Thomann and Mueller, 1987). They were not linked using the same spatial and temporal resolutions (Lung and Hwang, 1989). Therefore, temporal and spatial averaging was involved. However, as pointed out by Lung (2001), such an approach has never proved satisfactory. Given that the water quality models are often based on hydrological model through the flow field obtained from hydrological models, most frequently used hydrological models may also have a water quality routine linked to them directly or indirectly (Singh, 1995); however, often those routines are not as comprehensive as more advanced water quality models. Due to the limitation of the routines built into certain

hydrological models, linking of water quality models to hydrological models is still an issue. For instance, EFDC (Hamrick, 1996) and HSPF (Bicknell et al., 2001) are often used by linking to WASP5 (Ambrose et al., 1993) where WASP5 used the flow field data from EFDC or HSPF as input file. The indirect linkage between two models requires significant computer storage (Lung, 2001; Martin and McCutcheon, 1999). Some recently developed integrated models allow hydrodynamic and sediment and water quality simulation, e.g. AWAMP (Covelli et al., 2001), MIKE21 (DHI, 2004), and CCHE3D (<http://www.ncche.olemiss.edu/software/cche3d>). These models have strong water flow and water quality modules, thereby removing the linkage issues in the models. They can be applied for a broad range of water quality simulation issues; they, however, they have the limitation of only being able to simulate some specific bio-chemicals or reactions.

Among the water quality models many mechanistic based models are able to simulate a broad range of water quality parameters, such as WASP and CE-QUAL-ICM (Cercio and Cole, 1995). They can only simulate the specific biochemicals or reactions written in the computer codes. Every time when water quality parameters simulation is needed, one or more new routines are needed to handle these new water quality parameters. The new reaction involved in the new parameter simulation may have to be formulated by *ad hoc* approaches in the add-in routines; they, however, they may have an effect on the current build-in reaction networks in the model. From the mechanistic simulation point of view, the whole reaction network the model should be reformulated so that the effect of new reactions can be taken into account.

It has been pointed out that the reaction-based water quality simulation approach with an

arbitrary number of reactions and biogeochemical species taken into account has the potential to handle a full range of water quality simulations (Steeffel and van Cappellen, 1998; Yeh et al., 2001). A few reaction-based models have been developed to simulate contaminant transport subject to kinetically controlled chemical reactions (Cheng et al., 2000; Yeh et al., 1998). One reaction-based general paradigm for water quality has recently been developed by Zhang (2005). This is adopted as the basis of the reactive water quality module of the newly developed model.

The main objective of this chapter is to present the development of a two-dimensional depth-averaged integrated hydrology/hydraulic and water quality models for land surfaces. The model is comprised of two major modules, the hydrology/hydraulic module is adopted from the well developed current version of WASH123D (Yeh et al., 2005) and the reactive water quality transport module is based on a general paradigm (Zhang, 2005) that is able to simulate sediment and reactive water quality transport based on the reaction-based formulation of biogeochemical reactions.

### 4.3 Theory and mathematical basis

The governing equations of 2-D overland flow and transport simulation can be derived based on the principle of conservation of mass and momentum, similar to the case for 1-D river/stream networks.

#### 4.3.1 Water flow in 2-D overland regime

The continuity equation:

$$\frac{\partial h}{\partial t} + \frac{\partial(uh)}{\partial x} + \frac{\partial(vh)}{\partial y} = S_S + S_R - S_E + S_I \quad (4.1)$$

where  $h$  is the water depth [L];  $u$  is the velocity component in the  $x$ -direction [L/t];  $v$  is the velocity component in the  $y$ -direction [L/t];  $S_S$  is the man-induced source [ $L^3/t/L^2$ ];  $S_R$  is the source due to rainfall [ $L^3/t/L^2$ ];  $S_E$  is the sink due to evapotranspiration [ $L^3/t/L^2$ ]; and  $S_I$  is the source from subsurface media due to exfiltration [L/t]. It should be noted that  $uh = q_x$  is the flux in the  $x$ -direction [ $L^3/t/L^2$ ] and  $vh = q_y$  is the flux in the  $y$ -direction [ $L^3/t/L^2$ ].

The  $x$ -momentum equation:

$$\begin{aligned} \frac{\partial(uh)}{\partial t} + \frac{\partial u(uh)}{\partial x} + \frac{\partial v(uh)}{\partial y} = & -gh \frac{\partial(Z_o + h)}{\partial x} - \frac{gh^2}{2\rho} \frac{\partial \Delta \rho}{\partial x} - \frac{\partial F_{xx}}{\partial x} - \frac{\partial F_{yx}}{\partial y} + \\ & (M_x^S + M_x^R - M_x^E + M_x^I) + \frac{\tau_x^s - \tau_x^b}{\rho} \end{aligned} \quad (4.2)$$

where  $Z_o$  is the bottom elevation of overland [L];  $\Delta \rho = \rho - \rho_o$  is the density deviation [ $M/L^3$ ] from the reference density ( $\rho_o$ ), which is a function of temperature and salinity as well as other chemical concentrations;  $M_x^S$  is the  $x$ -component of momentum-impulse from artificial sources/sinks [ $L^2/t^2$ ];  $M_x^R$  is the  $x$ -component of momentum-impulse gained from rainfall [ $L^2/t^2$ ];  $M_x^E$  is the  $x$ -component of momentum-impulse lost to evapotranspiration [ $L^2/t^2$ ];  $M_x^I$  is the  $x$ -component of momentum-impulse gained from the subsurface media due to exfiltration [ $L^2/t^2$ ];  $F_{xx}$  and  $F_{yx}$  are the water fluxes due to eddy viscosity along the  $x$ -direction [ $L^3/t^2$ ];  $\tau_x^s$  is the component of surface shear stress along the  $x$ -direction over unit horizontal overland area [ $M/L/t^2$ ];  $\tau_x^b$  is the component of bottom shear stress along the  $x$ -direction over unit horizontal overland area [ $M/L/t^2$ ], which can be assumed proportional to the  $x$ -component

flow rate, i.e.,  $\tau_x^b/\rho = \kappa|\mathbf{V}|u$ .

Likewise, y-momentum equation can be derived by replacing the velocity, momentum-impulse, water flux, and surface and bottom shear stress in equation (4.2) by the counterpart for y-direction. Fully dynamic wave, diffusion wave, and kinematic wave approaches are provided with several numerical schemes in WASH123D to simulate 2-D overland flow. See Yeh et al. (2005) for detailed formulae and the associating boundary conditions.

#### 4.3.2 Bed Sediment Transport in 2-D Overland Regime

Sediments are categorized based on their physical and chemical properties. For each category of sediment, we include mobile suspended sediment particles scattered in the water column and immobile bed sediment particles accumulated in the water bed. The distribution of suspended sediment and bed sediment is controlled through hydrological transport as well as erosion and deposition processes.

Continuity equation for bed sediments is given as

$$\frac{\partial M_n}{\partial t} = D_n - R_n, \quad n \in [1, N_s] \quad (4.3)$$

where  $M_n$  is the concentration of the  $n$ -th bed sediment in mass per unit bed area [ $M/L^2$ ],  $D_n$  is the deposition rate of the  $n$ -th sediment in mass per unit bed area per unit time [ $M/L^2/T$ ],  $R_n$  is the erosion rate of the  $n$ -th sediment in mass per unit bed area per unit time [ $M/L^2/T$ ], and  $N_s$  is the total number of sediment size fractions. Concentrations of all bed sediments must be given initially for transient simulations. No boundary condition is needed for bed sediments.

#### 4.3.3 Suspended Sediments

The continuity equation of suspended sediment can be derived based on the conservation law of material mass as ((Yeh et al., 2005)

$$\frac{\partial(hS_n)}{\partial t} + \nabla \cdot (\mathbf{q}S_n) - \nabla \cdot (h\mathbf{K} \cdot \nabla S_n) = M_n^{as} + R_n - D_n, \quad n \in [1, N_s] \quad (4.4)$$

where  $S_n$  is the depth-averaged concentration of the  $n$ -th suspended sediment in the unit of mass per unit column volume  $[M/L^3]$ ,  $q$  is the flux of overland flow  $[L^2/T]$ ,  $K$  is the dispersion coefficient tensor  $[L^2/T]$ , and  $M_{S_n^{as}}$  and  $M_{S_n^{rs}}$  are the mass rate of artificial source and rainfall source of the  $n$ -th suspended sediment  $[M/L^2/T]$ .

The governing equation of suspended sediments is subjective to the initial condition (the initial concentrations of all suspended sediments), and five types of boundary conditions, including: Dirichlet, Variable, Cauchy, Neumann, and river/stream-overland interface boundary conditions (Yeh et al., 2005).

Initial condition

$$S_0 = S(x, y, 0) \text{ in } R \quad (4.5)$$

Dirichlet boundary condition:

Dirichlet boundary conditions are prescribed on the boundary where the suspended sediment concentration is known,

$$S_n = S_{ndb}(x_b, y_b, t) \text{ in } B_d \quad (4.6)$$

where  $x_b$  and  $y_b$  are the coordinates of the boundary node  $[L]$ , and  $S_{ndb}(x_b, y_b, t)$  is a

time-dependent concentration of the  $n$ -th sediment size on the Dirichlet boundary  $B_d$  [M/L<sup>3</sup>]

Variable boundary condition:

Variable boundary conditions are normally specified on the boundary where the flow direction can change with time or on any open boundary. When the flow is directed into the region of the interest ( $\mathbf{n} \cdot \mathbf{q} \leq 0$ ), the mass rate into the region is given as.

$$\mathbf{n} \cdot (\mathbf{q}S_n - h\mathbf{K} \cdot \nabla S_n) = \mathbf{n} \cdot \mathbf{q}S_{nvb}(x_b, y_b, t) \text{ on } B_v \quad (4.7)$$

when the flow is directed out of the region ( $\mathbf{n} \cdot \mathbf{q} \geq 0$ ), the sediment mass assumed carried out of the region of interest via advection is described as

$$-\mathbf{n} \cdot (h\mathbf{K} \cdot \nabla S_n) = 0 \text{ on } B_v \quad (4.8)$$

where  $\mathbf{n}$  is a unit outward direction and  $S_{nvb}(x_b, y_b, t)$  is a time-dependent concentration of the  $n$ -th sediment in the incoming fluid at the boundary [M/L<sup>3</sup>]  $B_v(\mathbf{x}) = 0$ .

Cauchy boundary condition:

Cauchy boundary condition is employed when the total material flow rate is given. Usually, this boundary is an upstream flux boundary.

$$-\mathbf{n} \cdot h\mathbf{K} \cdot \nabla S_n = Q_{S_n nb}(x_b, y_b, t) \text{ on } B_{nb} \quad (4.9)$$

where  $Q_{S_n nb}(x_b, y_b, t)$  is a time-dependent diffusive material flow rate of the  $n$ -th sediment through the Neumann boundary  $B_{nb}$  [M/T/L].

Overland-River/Stream interface boundary condition:

This boundary condition is needed when one-dimensional sediment transport in river/stream networks is coupled with two-dimensional sediment transport in overland regime. We assume that the exchange of sediment mass between river/stream and overland flows is mainly due to advection.

$$\mathbf{n} \cdot (\mathbf{q}S_n - h\mathbf{K} \cdot \nabla S_n) = (\mathbf{n} \cdot \mathbf{q}) \frac{1}{2} \{ [1 + \text{sign}(\mathbf{n} \cdot \mathbf{q})] S_n + [1 - \text{sign}(\mathbf{n} \cdot \mathbf{q})] S_{n1D}(x_b, y_b, t) \} \quad (4.10)$$

where  $S_{n1D}(x_b, y_b, t)$  is the time-dependent concentration of the  $n$ -th sediment at the 1-D node corresponding to the boundary [M/L<sup>3</sup>].

#### 4.3.4 Reactive water quality transport in 2-D overland regime

The biogeochemical species include chemical species in bed sediment phase, suspended sediment phase, immobile phase, and mobile phase, and precipitated particulate, and bed precipitate. The biogeochemical reactions among these species are mostly subject to two types of reactions, fast or equilibrium reactions and slow or kinetic reactions (Rubin, 1983). Fast reactions are sufficiently fast compared to the transport time scale and reversible so that local equilibrium could be assumed, while for slow reactions this assumption does not hold.

Continuity equation for reactive transport:

$$\frac{\partial(h\rho_i C_i)}{\partial t} + \alpha_i L(\rho_i C_i) = hr_i|_N, \quad i \in M \quad (4.11)$$

where  $C_i$  is the concentration of species  $i$ , which is mobile or immobile, in the unit of chemical mass per unit phase mass [M/M],  $\rho_i$  is the density of the phase associated with species  $i$  [M/L<sup>3</sup>],

$\alpha_i$  is 0 for immobile species and 1 for mobile species,  $r_i|_N$  is the production rate of species  $i$  due to all  $N$  reactions in the unit of chemical mass per column volume per time  $[M/L^3/T]$ ,  $M$  is the total number of chemical species which is equal to the summation of the number of mobile chemical species,  $M_m$ , and the number of immobile species,  $M_{im}$ , and the advection-diffusion operator  $L$  is defined as

$$L(\rho_i C_i) = \nabla \cdot (\mathbf{q} \rho_i C_i) - \nabla \cdot [h \mathbf{K} \cdot \nabla (\rho_i C_i)] - (M_{C_i^{as}} + M_{C_i^{rs}} + M_{C_i^{cs}}) \quad (4.12)$$

where  $M_{C_i^{as}}$  is the mass rate of artificial source of species  $i$   $[M/L^2/T]$ ,  $M_{C_i^{rs}}$  is the mass rate of the rainfall source of species  $i$   $[M/L^2/T]$ , and  $M_{C_i^{cs}}$  is mass rate of the source of species  $i$  in the overland from subsurface  $[M/L^2/T]$ .

Initial conditions of all species must be given. Similar to suspended sediment transport, five types of boundary conditions taken into account: Dirichlet, Neumann, Cauchy, Variable, and river/stream-overland interface boundary conditions, similar to suspended sediment.

#### 4.3.5 Diagonalization of 1-D Reactive Transport Governing Equations

In equation (4.11) the determination of  $r_i|_N$  is a primary challenge in the numerical computation of the equation. It can be formulated by an ad hoc method (e.g. (Ambrose et al., 1993) and (Brown and Barnwell, 1987)), and reaction-based formulations (e.g. (Steeffel and van Cappellen, 1998) and (Fang et al., 2003)). Yeh et al. (2001) highlighted that ad-hoc reaction parameters are only applicable to the experimental conditions tested. Reaction-based formulation is used in WASH123D and the fast reactions are decoupled from slow reactions in order to provide an efficient and reliable numerical solution to Eq. (4.11).

In a reaction-based formulation,  $r_i|_N$  is given by the summation of rates of all reactions that the  $i$ -th species participates in,

$$r_i|_N = \frac{\partial(\rho_i C_i)}{\partial t} \Big|_{reaction} = \sum_{k=1}^N [(v_{ik} - \mu_{ik})r_k], \quad i \in M \quad (4.13)$$

where  $v_{ik}$  is the reaction stoichiometry of the  $i$ -th species in the  $k$ -th reaction associated with products,  $\mu_{ik}$  is the reaction stoichiometry of the  $i$ -th species in the  $k$ -th reaction associated with the reactants, and  $r_k$  is the rate of the  $k$ -th reaction.

The mass balance equation for species  $i$  is given by substituting equation (4.13) into (4.11),

$$\frac{\partial(h\rho_i C_i)}{\partial t} + \alpha_i L(\rho_i C_i) = h \sum_{k=1}^N [(v_{ik} - \mu_{ik})r_k], \quad i \in M; \quad \text{or} \quad \mathbf{U} \frac{\partial \mathbf{C}_h}{\partial t} + \boldsymbol{\alpha} L(\mathbf{C}) = h \mathbf{v} \mathbf{r} \quad (4.14)$$

where  $\mathbf{U}$  is a unit matrix,  $\mathbf{C}_h$  is a vector with its components representing  $M$  species concentrations multiply the water depth  $[M/L^2]$ ,  $\boldsymbol{\alpha}$  is a diagonal matrix with  $\alpha_i$  as its diagonal component,  $\mathbf{C}$  is a vector with its components representing  $M$  species concentrations  $[M/L^3]$ ,  $\mathbf{v}$  is the reaction stoichiometry matrix, and  $\mathbf{r}$  is the reaction rate vector with  $N$  reaction rates as its components..

Because numerical solutions to (4.14) still encounters significant challenges and the approach has been proven inadequate (Fang et al., 2003; Yeh et al., 2001), fast reactions must be decoupled from (4.14) and mass conservation must be enforced. The diagonalization of the reactive transport system equation (4.14) is employed. This approach was proposed by Fang et al. (2003) in a reactive batch system.

First, remove the redundant reactions and irrelevant reactions from the reaction network. A “redundant reaction” is defined as a fast reaction that is linearly dependent on other fast reactions, and an “irrelevant reaction” is a kinetic reaction that is linearly dependent on only equilibrium reactions. Consider a reaction system that consists of  $N_e$  fast/equilibrium reactions and  $N_k$  slow/kinetic reactions among  $M$  chemical species. Among  $N_e$  fast/equilibrium reactions are  $N_E$  independent equilibrium reactions and there are  $N_K$  kinetic reactions among the  $N_k$  kinetic reactions that are independent to  $N_E$  equilibrium reaction, in other words, there are  $N_e - N_E$  redundant reactions and  $N_k - N_K$  irrelevant reactions in the system. Finally the reaction network only includes  $N_E$  equilibrium reactions and  $N_K$  kinetic reactions after removing the redundant and irrelevant reactions. Second, decomposition of the system results in decoupling the equilibrium reactions from kinetic reactions. After decomposition by pivoting on the  $N_E$  equilibrium reactions using Gaussian-Jordan decomposition, the system consists two sub-system of equations,  $N_E$  equations for equilibrium variables, and  $N_{KIV} (=M - N_E)$  equations for kinetic variables that include  $N_{KI}$  kinetic variables corresponding to the  $N_{KI}$  kinetic reactions independent of any other kinetic reactions among the  $N_K$  kinetic reactions, and  $N_C$  ( $N_C = M - N_E - N_{KI}$ ) component variables. The system can be written as Eq.(4.15),

$$\begin{bmatrix} \mathbf{A}_{11} & \mathbf{0}_{12} \\ \mathbf{A}_{21} & \mathbf{U}_{22} \end{bmatrix} \begin{Bmatrix} \frac{\partial \mathbf{C}_{h1}}{\partial t} \\ \frac{\partial \mathbf{C}_{h2}}{\partial t} \end{Bmatrix} + \begin{bmatrix} \mathbf{B}_{11} & \mathbf{0}_{12} \\ \mathbf{B}_{21} & \mathbf{a}_{22} \end{bmatrix} \mathbf{L} \left( \begin{Bmatrix} \mathbf{C}_1 \\ \mathbf{C}_2 \end{Bmatrix} \right) = \mathbf{h} \begin{bmatrix} \mathbf{D}_{11} & \mathbf{K}_{12} \\ \mathbf{0}_{21} & \mathbf{K}_{22} \end{bmatrix} \begin{Bmatrix} \mathbf{r}_1 \\ \mathbf{r}_2 \end{Bmatrix} \quad (4.15)$$

where  $\mathbf{A}_{11}$  and  $\mathbf{A}_{21}$  are the submatrices of the reduced  $\mathbf{U}$  matrix with size of  $N_E \times N_E$  and  $N_{KIV} \times N_E$ , respectively (note that  $N_{KIV} = M - N_E = N_{KI} + N_C$ );  $\mathbf{0}_{12}$  and  $\mathbf{U}_{22}$  are the zero- and unit-submatrices, respectively, of the reduced  $\mathbf{U}$  matrix with size of  $N_E \times N_{KIV}$  and  $N_{KIV} \times N_{KIV}$ ,

respectively;  $\mathbf{C}_{h1}$  and  $\mathbf{C}_{h2}$  are the subvectors of the vector  $\mathbf{C}_h$  with sizes of  $N_E$  and  $N_{KIV}$ , respectively;  $\mathbf{B}_{11}$  and  $\mathbf{B}_{21}$  are the submatrices of the reduced  $\alpha$  matrix with sizes of  $N_E \times N_E$  and  $N_{KIV} \times N_E$ , respectively;  $\mathbf{0}_{12}$  and  $\alpha_{22}$  are the zero- and unit- submatrices, respectively, of the reduced  $\alpha$  matrix with size of  $N_E \times N_{KIV}$  and  $N_{KIV} \times N_{KIV}$ , respectively;  $\mathbf{C}_1$  and  $\mathbf{C}_2$  are the subvectors of the vector  $\mathbf{C}$  with sizes of  $N_E$  and  $N_{KIV}$ , respectively;  $\mathbf{D}_{11}$  is the diagonal submatrix of the reduced  $\mathbf{v}$  matrix with size of  $N_E \times N_E$  and  $\mathbf{K}_{12}$  is the submatrix of the reduced  $\mathbf{v}$  matrix with size of  $N_E \times N_{KIV}$ ;  $\mathbf{0}_{21}$  is the zero submatrix of the reduced  $\mathbf{v}$  matrix with size of  $N_{KIV} \times N_E$  and  $\mathbf{K}_{22}$  is the submatrix of the reduced  $\mathbf{v}$  matrix with size of  $N_{KIV} \times N_{KIV}$ ;  $\mathbf{r}_1$  and  $\mathbf{r}_2$  are the subvectors of the vector  $\mathbf{r}$  with sizes of  $N_E$  and  $N_{KIV}$ , respectively.

The system of Equation (4.15) can be further decomposed by pivoting on  $N_{KI}$  independent kinetic reactions.

$$\begin{bmatrix} \mathbf{A}_{11} & \mathbf{A}_{12} & \mathbf{0}_{13} \\ \mathbf{A}_{21} & \mathbf{A}_{22} & \mathbf{0}_{23} \\ \mathbf{A}_{31} & \mathbf{A}_{32} & \mathbf{U}_{33} \end{bmatrix} \begin{Bmatrix} \frac{\partial \mathbf{C}_{h1}}{\partial t} \\ \frac{\partial \mathbf{C}_{h2}}{\partial t} \\ \frac{\partial \mathbf{C}_{h3}}{\partial t} \end{Bmatrix} + \begin{bmatrix} \mathbf{B}_{11} & \mathbf{B}_{12} & \mathbf{0}_{13} \\ \mathbf{B}_{21} & \mathbf{B}_{22} & \mathbf{0}_{23} \\ \mathbf{B}_{31} & \mathbf{B}_{32} & \alpha_{33} \end{bmatrix} \mathbf{L} \begin{Bmatrix} \mathbf{C}_1 \\ \mathbf{C}_2 \\ \mathbf{C}_3 \end{Bmatrix} = \mathbf{h} \begin{bmatrix} \mathbf{D}_{11} & \mathbf{K}_{12} & \mathbf{K}_{13} \\ \mathbf{0}_{21} & \mathbf{D}_{22} & \mathbf{K}_{23} \\ \mathbf{0}_{31} & \mathbf{0}_{32} & \mathbf{0}_{33} \end{bmatrix} \begin{Bmatrix} \mathbf{r}_1 \\ \mathbf{r}_2 \\ \mathbf{r}_3 \end{Bmatrix} \quad (4.16)$$

where  $\mathbf{A}_{11}$  is the submatrix of the reduced  $\mathbf{U}$  matrix with size of  $N_E \times N_E$ ,  $\mathbf{A}_{21}$  is the submatrix of the reduced  $\mathbf{U}$  matrix with size of  $N_{KI} \times N_E$ , and  $\mathbf{A}_{31}$  is the submatrix of the reduced  $\mathbf{U}$  matrix with size of  $N_C \times N_E$ ;  $\mathbf{A}_{12}$  is the submatrix of the reduced  $\mathbf{U}$  matrix with size of  $N_E \times N_{KI}$ ,  $\mathbf{A}_{22}$  is the submatrix of the reduced  $\mathbf{U}$  matrix with size of  $N_{KI} \times N_{KI}$ , and  $\mathbf{A}_{32}$  is the submatrix of the reduced  $\mathbf{U}$  matrix with size of  $N_C \times N_{KI}$ ;  $\mathbf{0}_{13}$  is the zero submatrix of the reduced  $\mathbf{U}$  matrix with size of  $N_E \times N_C$ ,  $\mathbf{0}_{23}$  is the submatrix of the reduced  $\mathbf{U}$  matrix with size of  $N_{KI} \times N_C$ , and  $\mathbf{U}_{33}$  is the

unit submatrix of the reduced  $\mathbf{U}$  matrix with size of  $N_C \times N_C$ ;  $\mathbf{C}_{h1}$ ,  $\mathbf{C}_{h2}$ , and  $\mathbf{C}_{h3}$  are the subvectors of the vector  $\mathbf{C}_h$  with sizes of  $N_E$ ,  $N_{KI}$ , and  $N_C$ , respectively;  $\mathbf{B}_{11}$  is the submatrix of the reduced  $\alpha$  matrix with size of  $N_E \times N_E$ ,  $\mathbf{B}_{21}$  is the submatrix of the reduced  $\alpha$  matrix with size of  $N_{KI} \times N_E$ , and  $\mathbf{B}_{31}$  is the submatrix of the reduced  $\alpha$  matrix with size of  $N_C \times N_E$ ;  $\mathbf{B}_{12}$  is the submatrix of the reduced  $\alpha$  matrix with size of  $N_E \times N_{KI}$ ,  $\mathbf{A}_{22}$  is the submatrix of the reduced  $\alpha$  matrix with size of  $N_{KI} \times N_{KI}$ , and  $\mathbf{B}_{32}$  is the submatrix of the reduced  $\alpha$  matrix with size of  $N_C \times N_{KI}$ ;  $\mathbf{0}_{13}$  is the zero submatrix of the reduced  $\alpha$  matrix with size of  $N_E \times N_C$ ,  $\mathbf{0}_{23}$  is the submatrix of the reduced  $\alpha$  matrix with size of  $N_{KI} \times N_C$ , and  $\alpha_{33}$  is the diagonal submatrix of the reduced  $\alpha$  matrix with size of  $N_C \times N_C$ ;  $\mathbf{C}_1$ ,  $\mathbf{C}_2$ , and  $\mathbf{C}_3$  are the subvectors of the vector  $\mathbf{C}$  with sizes of  $N_E$ ,  $N_{KI}$ , and  $N_C$ , respectively;  $\mathbf{D}_{11}$  is the diagonal submatrix of the reduced  $\mathbf{v}$  matrix with size of  $N_E \times N_E$ ,  $\mathbf{K}_{12}$  is the submatrix of the reduced  $\mathbf{v}$  matrix with size of  $N_E \times N_{KI}$ , and  $\mathbf{K}_{13}$  is the submatrix of the reduced  $\mathbf{v}$  matrix with size of  $N_E \times N_{KD(k)}$ ;  $\mathbf{0}_{21}$  is the zero submatrix of the reduced  $\mathbf{v}$  matrix with size of  $N_{KI} \times N_E$ ,  $\mathbf{D}_{22}$  is the diagonal submatrix of the reduced  $\mathbf{v}$  matrix with size of  $N_{KI} \times N_{KI}$ , and  $\mathbf{K}_{23}$  is the submatrix of the reduced  $\mathbf{v}$  matrix with size of  $N_{KI} \times N_{KD(k)}$ ;  $\mathbf{0}_{13}$  is the zero submatrix of the reduced  $\mathbf{v}$  matrix with size of  $N_C \times N_E$ ,  $\mathbf{0}_{32}$  is the zero submatrix of the reduced  $\mathbf{v}$  matrix with size of  $N_C \times N_{KI}$ , and  $\mathbf{0}_{33}$  is the zero submatrix of the reduced  $\mathbf{v}$  matrix with size of  $N_C \times N_{KD(k)}$ ;  $\mathbf{r}_1$ ,  $\mathbf{r}_2$ , and  $\mathbf{r}_3$  are the subvectors of the vector  $\mathbf{r}$  with sizes of  $N_E$ ,  $N_{KI}$ , and  $N_{KD(k)}$ , respectively.

The two subsets of equations in (4.15) are further defined as follows,

Algebraic Equations for  $N_E$  Equilibrium Reactions

$$\frac{\partial(hE_i)}{\partial t} + L(E_i^m) = hD_{1ii}r_{1i} + h\sum_{j=1}^{N_K} K_{1ij}r_{2j}, \quad i \in N_E \quad (4.17)$$

where

$$L(E_n^m) = \nabla \cdot (\mathbf{q}E_n^m) - \nabla \cdot (h\mathbf{K} \cdot \nabla E_n^m) - (M_{E_n^{as}} + M_{E_n^{rs}} + M_{E_n^{is}}) \quad (4.18)$$

which is replaced with a thermodynamically consistent equation:

$$K_i^e = \frac{\prod_{j \in M} A_j^{\nu_{ji}}}{\prod_{j \in M} A_j^{\mu_{ji}}} \quad (4.19)$$

or  $F_i(C_1, \dots, C_M; p_1, p_2, \dots) = 0$

where

$$E_i = \sum_{j=1}^{N_E} (A_{11})_{ij} (C_{A1})_j, \quad E_i^m = \sum_{j=1}^{N_E} (B_{11})_{ij} C_{1j} \quad (4.20)$$

where  $K_i^e$  is the equilibrium constant of the  $i$ -th fast reaction,  $A_j$  is the activity of the  $j$ -th species,  $F_i(C_1, \dots, C_M; p_1, p_2, \dots)$  is an empirical function of all species and a number of parameters  $p_1, p_2, \dots$  for the  $i$ -th fast reaction.

Transport Equations for  $N_{KIV}$  Kinetic-Variables

$$\frac{\partial(hE_i)}{\partial t} + L(E_i^m) = h\sum_{j=1}^{N_K} K_{2nj}r_{2j}, \quad i \in N_{KIV} = M - N_E \quad (4.21)$$

where  $E_i = \sum_{j=1}^{N_E} (A_{21})_{ij} (C_{A1})_j + (C_{A2})_j$  and  $E_i^m = \sum_{j=1}^{N_E} (B_{21})_{ij} C_{1j} + (\alpha_{22})_{ij} C_{2i}$

where  $E_i$  is called kinetic variable (Fang, et al., 2003) and is subject to only kinetic reactions in the system. For the  $N_C$  component variables among the  $N_{KIV}$  kinetic variables, the right hand side of equation (4.21) is zero.

After diagonalization of the system only  $M-N_E$  kinetic variables needs to be included in the transport computation, which should be less than or equal to the number of  $M$  in Eq.(4.14). And the governing equation (4.14) for reactive chemical transport in 2-D overland regime can be replaced by a set of  $N_E$  algebraic equations (Eq.(4.19) ) and a set of  $M-N_E$  partial differential equations for kinetic variables as written in equation (4.21) by explicitly expressing the transport operator.

$$\frac{\partial(hE_i)}{\partial t} + \nabla \cdot (\mathbf{q}E_i^m) - \nabla \cdot [h\mathbf{K} \cdot \nabla E_i^m] = M_{E_i^{as}} + M_{E_i^{rs}} + M_{E_i^{is}} + hR_i, \quad i \in N_{KIV} \quad (4.22)$$

where  $R_i = \sum_{j=1}^{N_K} K_{2ij}r_{2j}, \quad i \in N_{KIV}$

where  $E_i$  is the concentration of the i-th kinetic-variable [ $M/L^3$ ],  $E^{im}$  is the concentration of mobile part of the i-th kinetic-variable [ $M/L^3$ ],  $M_{E_i^{as}}$  is the artificial source of the i-th kinetic-variable [ $M/L/T$ ],  $M_{E_i^{rs}}$  is the rainfall source of the i-th kinetic-variable [ $M/L/T$ ],  $M_{E_i^{os1}}$  and  $M_{E_i^{os2}}$  are overland sources of the i-th kinetic-variable from river banks 1 and 2, respectively [ $M/L/T$ ],  $M_{E_i^{is}}$  is the mass rate of the source of the i-th kinetic-variable in river/stream from subsurface [ $M/L/T$ ],  $R_i$  is the production rate of i-th kinetic-variable due to biogeochemical reactions [ $M/L^3/T$ ], and  $N_{KIV}$  is the number of kinetic variables.

The initial concentration of each species including immobile species (bed precipitates, particulate sorbed onto bed sediment, and dissolved chemical in the immobile water phase), and mobile species (dissolved chemical in mobile water phase, suspended precipitates, and particulate sorbed onto suspended sediment), should be obtained either by field measurement or by simulating the steady state of the system. No boundary conditions are needed for immobile

species, while four types of boundary conditions are taken into account for mobile species, Dirichlet, Neumann, Cauchy, and Variable boundary conditions (Yeh et al., 2006), which are similar to the boundary conditions for suspended sediments transport presented in section 4.2.2.

#### 4.4 Numerical approaches

##### 4.4.1 Finite Difference Method to Bed Sediment Transport

The continuity equation for 2-D bed sediment transport, Eq.(4.3), is approximated as

$$\frac{M_n^{n+1} - M_n^n}{\Delta t} \approx W_1(D_n^{n+1} - R_n^{n+1}) + W_2(D_n^n - R_n^n) \quad (4.23)$$

##### 4.4.2 Numerical approaches for Suspended Sediment Transport

Five spatially discretization approaches are provided, which are 1) FEM on the conservative form of equation, 2) FEM on the advective form of equation, 3) modified Lagrangian-Eulerian approach, 4) LE for the interior nodes + FEM conservative for the upstream boundary nodes; and 5) LE for the interior nodes + FEM on advective form for the upstream boundary nodes. These five numerical scheme will be discussed in detail in the next section.

##### 4.4.3 Strategies for the coupling of transport and biogeochemical reactions

Three strategies are often used to do with the coupling of transport and reactions, fully implicit scheme, mixed predictor-corrector/operator-splitting scheme, and operator-splitting scheme. The differences among the three approaches are how the kinetically complexed species are solved between two subsystems (Yeh, 2000).

The governing equation for kinetic variables, Eq.(4.21), can be rewritten as

$$h \frac{(E_n)^{n+1} - (E_n)^n}{\Delta t} + \frac{\partial h}{\partial t} E_n + L(E_n^m) = hR_{E_n} \quad (4.24)$$

Fully implicit approach

According to Fully-implicit scheme, Eq.(4.24) can be separated into two equations as follows

$$h \frac{(E_n)^{n+1/2} - (E_n)^n}{\Delta t} + \frac{\partial h}{\partial t} E_n + L(E_n^m) = hR_{E_n} \quad (4.25)$$

$$\frac{(E_n)^{n+1} - (E_n)^{n+1/2}}{\Delta t} = 0 \quad (4.26)$$

where the superscripts  $n$ ,  $n+1/2$ , and  $n+1$  represent the old, intermediate, and new time step, respectively, and terms without superscript is the corresponding average values calculated with time weighting factors.

In fully implicit scheme,  $E^{n+1/2}$  is solved through Equation (4.25) first, and then  $E^{n+1}$  is solved through Equation (4.26) together with algebraic equations for equilibrium reactions using BIOGEOCHEM model (Fang et al., 2003) so as to obtain the species concentrations. Iteration between these two steps is needed because the new reaction terms  $RA_n^{n+1}$  and the equation coefficients in equation (4.25) need to be updated by the calculation results of (4.26). To improve the standard SIA method, the nonlinear reaction terms are approximated by the Newton-Raphson linearization.

Mixed Predictor-corrector/Operator-splitting scheme

According to the mixed Predictor-correct/Operator-Splitting, Eq. (4.24) can be separated into

two equations as follows

$$h \frac{(E_n^m)^{n+1/2} - (E_n^m)^n}{\Delta t} + \frac{\partial h}{\partial t} E_n^m + L(E_n^m) = h R_{E_n}^n - h \frac{\partial(\ell n h)}{\partial t} (E_n^{im})^n \quad (4.27)$$

$$\frac{E_n^{n+1} - [(E_n^m)^{n+1/2} + (E_n^{im})^n]}{\Delta t} = R_{E_n}^{n+1} - R_{E_n}^n - \frac{\partial(\ell n h)}{\partial t} (E_n^{im})^{n+1} + \frac{\partial(\ell n h)}{\partial t} (E_n^{im})^n \quad (4.28)$$

Eq. (4.27) is solved first to obtain  $(E_n^m)^{n+1/2}$ , then Eq. (4.28) together with the algebraic equations for equilibrium reactions, Eq.(4.19) is solved with BIOGEOCHEM (Fang et al., 2003) to obtain the individual species concentration.

#### Operator-Splitting Scheme

According to the operator-splitting scheme, Eq. (4.24) can be separated into two equations as follows

$$h \frac{(E_n^m)^{n+1/2} - (E_n^m)^n}{\Delta t} + \frac{\partial h}{\partial t} E_n^m + L(E_n^m) = 0 \quad (4.29)$$

$$\frac{(E_n^m)^{n+1} - [(E_n^m)^{n+1/2} + (E_n^{im})^n]}{\Delta t} = h R_{E_n}^{n+1} - \frac{\partial(\ell n h)}{\partial t} (E_n^{im})^{n+1} \quad (4.30)$$

#### 4.4.4 Discretization schemes

##### FEM in Conservative Form of 2-D Transport Governing Equations

According to different coupling strategies, the discretization of the kinetic variable transport equation gives different matrix equations. For the implicit coupling, the kinetic variable transport equation, Eq. (4.25), can be written explicitly as

$$h \frac{(E_n)^{n+1/2} - (E_n)^n}{\Delta t} + \frac{\partial h}{\partial t} E_n + \nabla \cdot (\mathbf{q} E_n^m) - \nabla \cdot (h \mathbf{K} \cdot \nabla E_n^m) = M_{E_n^{as}} + M_{E_n^{rs}} + M_{E_n^{is}} + h R_{E_n} \quad (4.31)$$

Introducing two terms,  $L_{HS}$  and  $R_{HS}$ , which are calculated by the following procedure, to handle the source/sink terms. First, assign

$$R_{HS} = 0 \quad \text{and} \quad L_{HS} = 0 \quad (4.32)$$

then update the terms consistently as follows

$$M_{E_n^{rs}} = \begin{cases} S_R * E_n^{rs}, & \text{if } S_R > 0 \Rightarrow R_{HSn} = R_{HSn} + M_{E_n^{rs}} \\ S_R * E_n^m, & \text{if } S_R \leq 0 \Rightarrow L_{HSn} = L_{HSn} - S_R \end{cases} \quad (4.33)$$

$$M_{E_n^{as}} = \begin{cases} S_S * E_n^{as}, & \text{if } S_S > 0 \Rightarrow R_{HSn} = R_{HSn} + M_{E_n^{as}}, \\ S_S * E_n^m, & \text{if } S_S \leq 0 \Rightarrow L_{HSn} = L_{HSn} - S_S \end{cases} \quad (4.34)$$

$$M_{E_n^{is}} = \begin{cases} S_I * E_n^{is}, & \text{if } S_I > 0 \Rightarrow R_{HSn} = R_{HSn} + M_{E_n^{is}} \\ S_I * E_n^m, & \text{if } S_I \leq 0 \Rightarrow L_{HSn} = L_{HSn} - S_I \end{cases} \quad (4.35)$$

Replacing the source/sink terms in Eq. (4.31), it can be simplified as

$$h \frac{(E_n)^{n+1/2} - (E_n)^n}{\Delta t} + \frac{\partial h}{\partial t} E_n + \nabla \cdot (\mathbf{q} E_n^m) - \nabla \cdot (h \mathbf{K} \cdot \nabla E_n^m) + L_{HS} E_n^m = R_{HS} + h R_{E_n} \quad (4.36)$$

Express  $E_n^m$  in terms of  $(E_n^m / E_n) E_n^m$  to make  $E_n$ 's as primary dependent variables,

$$\begin{aligned} & h \frac{(E_n)^{n+1/2} - (E_n)^n}{\Delta t} + \nabla \cdot \left( \mathbf{q} \frac{E_n^m}{E_n} E_n \right) - \nabla \cdot \left( h \mathbf{K} \cdot \frac{E_n^m}{E_n} \nabla E_n \right) \\ & - \nabla \cdot \left[ h \mathbf{K} \cdot \left( \nabla \frac{E_n^m}{E_n} \right) E_n \right] + \left( L_{HS} \frac{E_n^m}{E_n} + \frac{\partial h}{\partial t} \right) E_n = R_{HS} + h R_{E_n} \end{aligned} \quad (4.37)$$

Applying Galerkin or Petrov-Galerkin FEM method to Eq. (4.37) with appropriate mathematic manipulation, we can obtain the following matrix equation,

$$[CMATRIX1] \left\{ \frac{dE_n}{dt} \right\} + ([Q1] + [Q2] + [Q3] + [Q4]) \{E_n\} = \{SS\} + \{B\} \quad (4.38)$$

where

$$CMATRIX1_{ij} = \int_R N_i h N_j dR \quad (4.39)$$

$$Q1_{ij} = - \int_R \nabla W_i \cdot \mathbf{q} \frac{E_n^m}{E_n} N_j dR \quad (4.40)$$

$$Q2_{ij} = \int_R \nabla W_i \cdot \left[ h \mathbf{K} \cdot \left( \nabla \frac{E_n^m}{E_n} \right) N_j \right] dR \quad (4.41)$$

$$Q3_{ij} = \int_R \nabla N_i \cdot \left( h \mathbf{K} \cdot \frac{E_n^m}{E_n} \nabla N_j \right) dR \quad (4.42)$$

$$Q4_{ij} = \int_R N_i \left( L_{HS} \frac{E_n^m}{E_n} + \frac{\partial h}{\partial t} \right) N_j dR \quad (4.43)$$

$$SS_i = \int_R N_i \left( R_{HS} + h R_{E_n} \right) dR \quad (4.44)$$

$$B_i = - \int_B \mathbf{n} \cdot W_i \mathbf{q} \frac{E_n^m}{E_n} E_n dB + \int_B \mathbf{n} \cdot \left( N_i h \mathbf{K} \cdot \frac{E_n^m}{E_n} \nabla E_n \right) dB + \int_B \mathbf{n} \cdot \left[ W_i h \mathbf{K} \cdot \left( \nabla \frac{E_n^m}{E_n} \right) E_n \right] dB \quad (4.45)$$

in which,  $N_i$  and  $N_j$  are the FEM base function at the  $i$ -th and  $j$ -th node, respectively;  $W_i$  is the weighting function at the  $i$ -th node with the same order as  $N$  or one order higher when Petrov-Galerkin method is used. The boundary term  $B$  can be calculated based on the boundary

conditions similarly to those defined for suspended sediment in section 4.2.3.

For the mixed predictor-corrector/operator-splitting strategy, the special discretization of the kinetic variable transport equation can be formulated in a similar procedure as that for implicit strategy. The only difference is that the primary dependent variable in this case is  $E_n^m$ , rather than  $E_n$ . So the discretization can be performed by simply replacing the term  $E_n^m / E_n$  with 1, so that any differential terms of  $E_n^m / E_n$  will vanish. The load vector should be calculated by

$$SS_i = \int_R N_i \left( R_{HS} + h R_{E_n}^n - \frac{\partial h}{\partial t} (E_n^m)^n \right) dR \quad (4.46)$$

Whereas for the case of operator-splitting strategy, the spatial discretization is the same as for the mixed predictor-corrector/operator-splitting strategy except that the load vector should be calculated by the following equation

$$SS_i = \sum_{e=1}^{M_e} \int_{R_e} N_i^e R_{HS} dR \quad (4.47)$$

#### FEM in Advective Form of 2-D Transport Governing Equations

For implicit coupling strategy, substituting the continuity equation for flow into the kinetic variable transport equation, Eq. (4.25), and calculating term  $L_{HS}$  and  $R_{HS}$  the same as those in last section beginning with

$$R_{HS} = 0 \quad \text{and} \quad L_{HS} = S_S + S_R + S_I - \partial h / \partial t \quad (4.48)$$

we obtain

$$h \frac{\partial E_n}{\partial t} + \frac{\partial h}{\partial t} E_n + \mathbf{q} \cdot \nabla E_n^m - \nabla \cdot (h \mathbf{K} \cdot \nabla E_n^m) + L_{HS} E_n^m = R_{HS} + h R_{E_n} \quad (4.49)$$

Expressing  $E_n^m$  in terms of  $(E_n^m / E_n) E_n$  to make  $E_n$ 's as primary dependent variables, Eq.(4.49)

can be rewritten as

$$\begin{aligned} & h \frac{\partial E_n}{\partial t} + \mathbf{q} \cdot \nabla \left( \frac{E_n^m}{E_n} E_n \right) - \nabla \cdot \left( h \mathbf{K} \cdot \frac{E_n^m}{E_n} \nabla E_n \right) \\ & - \nabla \cdot \left[ h \mathbf{K} \cdot \left( \nabla \frac{E_n^m}{E_n} \right) E_n \right] + \left( L_{HS} \frac{E_n^m}{E_n} + \frac{\partial h}{\partial t} \right) E_n = R_{HS} + h R_{E_n} \end{aligned} \quad (4.50)$$

Applying Galerkin or Petrov-Galerkin FEM method to Eq.(4.37) with appropriate mathematic manipulation, we can obtain the following matrix equation,

$$[CMATRIX1] \left\{ \frac{dE_n}{dt} \right\} + ([Q1] + [Q2] + [Q3] + [Q4] + [Q5]) \{E_n\} = \{SS\} + \{B\} \quad (4.51)$$

Where  $[CMATRIX1]$ ,  $[Q3]$ ,  $[Q4]$ ,  $[Q5]$ , and  $\{SS\}$  are defined the same as Eq.(4.39), Eq.(4.41) through (4.44), respectively,

$$Q1_{ij} = \int_R W_i \mathbf{q} \cdot \frac{E_n^m}{E_n} \nabla N_j dR \quad (4.52)$$

$$Q2_{ij} = \int_R W_i \mathbf{q} \cdot \left( \nabla \frac{E_n^m}{E_n} \right) N_j dR \quad (4.53)$$

$$B_i = \int_B \mathbf{n} \cdot \left( N_i h \mathbf{K} \cdot \frac{E_n^m}{E_n} \nabla E_n \right) dB + \int_B \mathbf{n} \cdot \left[ W_i h \mathbf{K} \cdot \left( \nabla \frac{E_n^m}{E_n} \right) E_n \right] dB \quad (4.54)$$

The boundary term B can be determine based on the five types of boundary conditions similar to those described in section 4.2.1 for suspended sediments. Eq.(4.51) is then solved by time-weighting FDM for temporal discretization.

For mixed predictor-corrector/operator-splitting strategy, the kinetic variable transport equation can be discretized in the same manner as the implicit strategy by replacing the term of  $E_n^m / E_n$  with 1 so that all the differentials of term  $E_n^m / E_n$  will be zero and replacing the primary variable  $E_n$  with  $E_n^m$ . The load vector  $\{SS\}$  should be calculated by

$$SS_i = \int_R N_i \left( R_{HS} + hR_{E_n} - \frac{\partial h}{\partial t} (E_n^{im})^n \right) dR \quad (4.55)$$

Whereas for the case of operator-splitting method, the discretization follows the same procedure as that for mixed predictor-corrector/operator-splitting strategy except for the load vector term which should be calculated by

$$SS_i = \int_R N_i R_{HS} dR \quad (4.56)$$

### Modified Lagrangian-Eulerian Approach

For the implicit strategy, the kinetic-variable transport equation can be rewritten as follows by expressing  $E_n^m$  in terms of  $E_n^m / E_n * E_n$  to make  $E_n$ 's as primary dependent variables,

$$h \frac{\partial E_n}{\partial t} + \frac{\partial h}{\partial t} E_n + \mathbf{q} \cdot \nabla E_n - \nabla \cdot (h\mathbf{K} \cdot \nabla E_n) + L_{HS} E_n = \mathbf{q} \cdot \nabla E_n^{im} - \nabla \cdot (h\mathbf{K} \cdot \nabla E_n^{im}) + R_{HS} + hR_{E_n} \quad (4.57)$$

where the terms  $L_{HS}$  and  $R_{HS}$  are calculated continuously by the same procedure as (4.33)

through (4.35) beginning with

$$R_{HS} = 0 \quad \text{and} \quad L_{HS} = (S_S + S_R + S_I - \partial h / \partial t) E_n^m / E_n \quad (4.58)$$

Define

$$h \mathbf{v}_{true} = \mathbf{q} \quad (4.59)$$

So that Eq.(4.57) can be written in the Lagrangian and Eulerian forms as follows,

In Lagrangian step

$$h \frac{dE_n}{d\tau} = h \frac{\partial E_n}{\partial t} + \mathbf{q} \cdot \nabla E_n = 0 \quad \Rightarrow \quad \frac{dE_n}{d\tau} = \frac{\partial E_n}{\partial t} + \mathbf{v}_{true} \cdot \nabla E_n = 0 \quad (4.60)$$

In Eulerian step

$$h \frac{dE_n}{d\tau} - \nabla \cdot (h \mathbf{K} \cdot \nabla E_n) + \left( L_{HS} + \frac{\partial h}{\partial t} \right) E_n = \mathbf{q} \cdot \nabla E_n^{im} - \nabla \cdot (h \mathbf{K} \cdot \nabla E_n^{im}) + R_{HS} + h R_{E_n} \quad (4.61)$$

or

$$\frac{dE_n}{d\tau} - D + K E_n = T + R_L \quad (4.62)$$

where

$$K = \left( L_{HS} + \frac{\partial h}{\partial t} \right) / h, \quad R_L = (R_{HS} + h R_{E_n}) / h \quad (4.63)$$

$$D = \frac{1}{h} \nabla \cdot (h \mathbf{K} \cdot \nabla E_n) \quad (4.64)$$

$$T = \frac{1}{h} \left[ \mathbf{q} \cdot \nabla E_n^{im} - \nabla \cdot (h \mathbf{K} \cdot \nabla E_n^{im}) \right] \quad (4.65)$$

Apply FEM to Eq.(4.64), so that D can be approximated by

$$\{D\} = \{D1\} + \{QB1\} \quad (4.66)$$

where

$$\{D1\} = -[QE]\{E_n\} \quad (4.67)$$

$$QE_{ij} = \int_R \nabla N_i \cdot (h\mathbf{K} \cdot \nabla N_j) dR / A1_{ii} \quad (4.68)$$

$$QB1_i = \int_B \mathbf{n} N_i \cdot (h\mathbf{K} \cdot \nabla E_n) dB / A1_{ii} \quad (4.69)$$

in which [A1] is the mass lumped diagonal matrix  $A1_{ij} = \int_R N_i h N_j dR$ .

Similarly, use FEM to approximate the term T, so that

$$\{T\} = \{T1\} + \{QB2\} \quad (4.70)$$

Where

$$\{T1\} = [QT]\{E_n^{im}\} \quad (4.71)$$

$$QT_{ij} = \left( \int_R \nabla N_i \cdot (h\mathbf{K} \cdot \nabla N_j) dR + \int_R N_i \mathbf{q} \cdot \nabla N_j dR \right) / A1_{ii} \quad (4.72)$$

$$QB2_i = - \int_B \mathbf{n} \cdot N_i (h\mathbf{K} \cdot \nabla E_n^{im}) dB / A1_{ii} \quad (4.73)$$

Thus, Eq.(4.62) can be written in matrix format as follows

$$\frac{dE_n}{d\tau} - D1 + KE_n = T1 + R_L + B \quad (4.74)$$

where  $\{B\} = \{QB1\} + \{QB2\}$ , which can be calculated by according to the formulation of boundary conditions described in section 4.2.1. Eq.(4.74) is then solved by time-weighted FDM temporally. It should be noted that for upstream flux boundary nodes, Eq.(4.74) cannot be applied since  $\Delta\tau$  equals zero.  $\Delta\tau$  equals zero. Thus, we formulate the upstream boundary node by explicitly applying the FEM to the boundary conditions. For instance, at the upstream variable boundary

$$\int_B N_i n \cdot (qE_n^m - hK \cdot \nabla E_n^m) dB = \int_B N_i n \cdot qE_n^m(x_b, y_b, t) dB \quad (4.75)$$

The following matrix equation can be assembled for the boundary nodes

$$[QF]\{E_n^m\} = [QB]\{B\} \quad (4.76)$$

where

$$QF_{ij} = \int_B (N_i n \cdot \mathbf{q} N_j - N_i n \cdot h\mathbf{K} \cdot \nabla N_j) dB \quad (4.77)$$

$$QB_{ij} = \int_B N_i n \cdot \mathbf{q} N_j dB \quad (4.78)$$

$$B_i = E_n^m(x_b, y_b, t) \quad (4.79)$$

For the case of predictor-corrector/operator-splitting strategy, the discretization of the kinetic variable transport equation follows the same procedure as for the implicit strategy.

## Mixed LE and FEM schemes

Because the LE method cannot perform at the upstream boundary nodes, two mixed LE and FEM schemes are provided to overcome the conventional LE scheme's inaccuracy at upstream boundary nodes. The basic consideration is to treat the upstream boundary nodes differently from the interior nodes by FEM method. The first one is to apply the LE method for all interior nodes and downstream boundary nodes while using FEM in conservative form of the equation on the upstream nodes. In this case, the discretized matrix equation for the interior nodes and downstream nodes can be obtained by following the same formulation for the modified LE approach with FEM in conservative form of transport equation is used for the upstream boundary nodes. The second one is applying the LE method to all interior nodes and downstream nodes while using FEM in advective form of the equation on the upstream boundary nodes. In this case, the discretized matrix equation for interior nodes and downstream boundary nodes is obtained by LE method, while the equations for upstream boundary nodes is obtained by the procedure for FEM on the advective form.

### 4.5 Model verification

The model verification basically is comprised of three major steps listed in order.

(1) Verify the flow module stand alone: In this step the flow module alone is run and the results are compared with those obtained from WASH123D version 1.5, with exact the same simulation conditions and numerical options. The results are expected to be identical if the flow module is correct.

(2) Verify the reactive chemical transport module: In this step, the reactive transport module is run alone with the flow field read in. The flow field is obtained from the first step. The results are compared with those generated using a general water quality paradigm (Zhang, 2005) where the same conditions are specified and the same flow field is input. Since this paradigm is adopted and incorporated into the current version of WASH123D, we expect no difference in solution from the comparison.

(3) Verify the fully coupled model: In this step, the flow module and reactive transport module are run concurrently and the flow field and chemical species concentrations are obtained simultaneously, with the same flow and transport boundary and initial conditions and numerical approaches taken. The simulated flow results should be the same as the ones from the first step, and the simulated reactive water quality is also expected to be nearly identical to the ones in step two if the same time step is used.

#### 4.5.1 Example 1

This hypothetical example is to demonstrate the capability of the model in simulating water flow and sediment and reactive chemical transport involving in 20 chemical reactions in a wetland. The domain of interest is a wetland dimensioned  $5000 \text{ m} \times 1,000 \text{ m}$ , which was discretized into 125 square elements sized  $200 \text{ m} \times 200 \text{ m}$  each. Manning's roughness is assumed to be 0.05. For flow simulation, the incoming flux boundary condition is applied to the upstream boundary and the depth-depended flux condition is applied to the downstream boundary. Initially the water depth is assumed to be 0.2m while the velocity is assumed to be zero. A half day simulation is performed using diffusion wave model with a fixed time step of 50 seconds. A relative error of  $10^{-4}$  is used to determine the convergence of the computation.

Figure 4.1 and Figure 4.2 show the simulated water depth and velocity at time= half day by WASH123D version 1.5 and the new model, respectively. The new model yields exactly the same results as WASH123D version 1.5 by examining the numerical results.



Figure 4.1 Simulated depth at t = half day

Upper: WASH123D version 1.5 Lower: WASH123D version 3.0

In the sediment and reactive transport simulation, one size of cohesive sediment and 14 chemical species, including 3 dissolved chemicals in mobile water phase (CMW1, CMW2, and CMW3); 3 dissolved chemicals in immobile water phase (CIMW1, CIMW2, and CIMW3); 3 particulate chemicals sorbed onto suspended sediment (CS1, CS2, and CS3); 3 particulate chemicals sorbed onto bed sediment (CB1, CB2, and CB3); 1 suspension precipitate (SP3); and 1 bed precipitate (BP3), are considered in the system. The settling speed of the sediment is assumed to be  $1.2 \times 10^{-6}$  m/s, the critical shear stress for deposition is  $4.15 \text{ g/m}^2\text{s}^2$ , the critical shear stress for erosion is

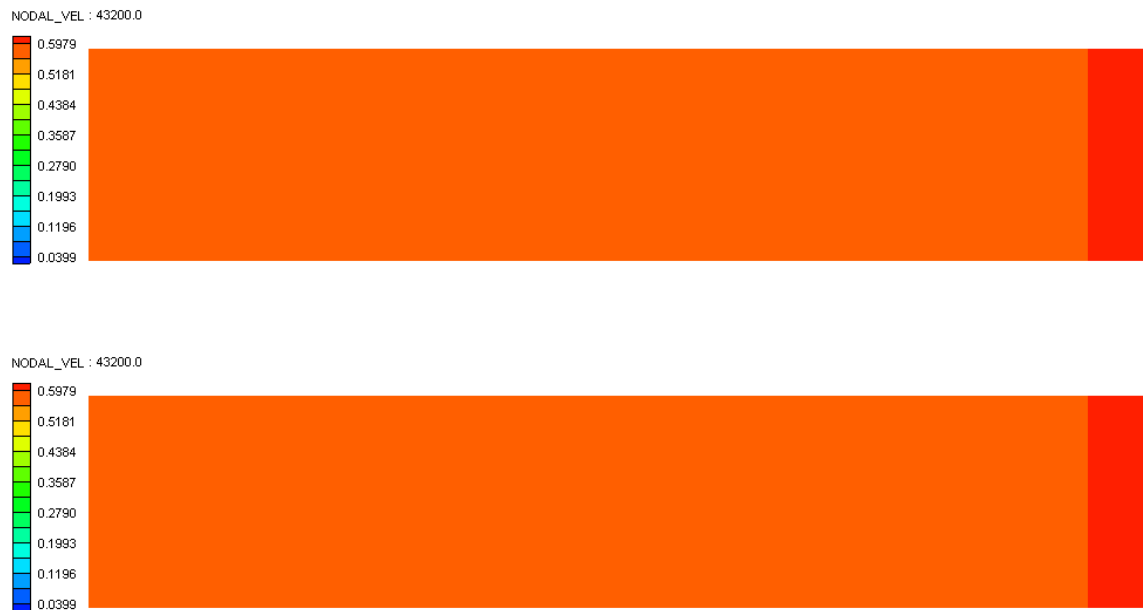


Figure 4.2 Simulated depth at t = half day

Upper: WASH123D version 1.5 Lower: WASH123D version 3.0

4.08 g/m<sup>2</sup>, and the erodibility is assumed to be 0.1 g/m<sup>2</sup>/s. These species are involved in 20 reactions, as shown in Table 5.1, including aqueous complexation reactions, adsorption/desorption reactions, ion-exchange reactions, precipitation/dissolution reactions, volatilization reactions, diffusion reactions, and sedimentation reactions taking place between different chemical phases. Initially, only bed sediment, BS, with a concentration of 50 g/m<sup>2</sup>, exists in the domain of interest. The in-flow variable boundary conditions are applied to the upstream boundary sides, where all dissolved chemicals have a constant incoming concentration of 1 g/m<sup>3</sup> and all other mobile species and suspended sediment, SS, have zero incoming concentration. Out flow variable boundary conditions are applied to the downstream boundary

sides. The longitudinal dispersivity is 10.0 m. A half day simulation is performed with fixed time step size of 50 seconds. The temperature in the domain ranges from 15 °C to 25 °C with a higher temperature in the edge of domain and lower temperature in the center of domain. Both sediment and reactive chemical transport simulation use FEM in conservative form of the transport equation and the coupling between them is dealt with the mixed predictor-corrector and operator-splitting scheme. A relative error of  $10^{-4}$  is used to determine the convergence of computation.

Figure 4.3 and Figure 4.4 plot the concentration distribution of CMW1 and CIMW1 by the paradigm and the new model, respectively, at the end of simulation. The two figures indicate the good agreement between the general paradigm and the new model. The third step of verifying the model is to run the flow and transport module simultaneously and the numerical results are the same those from the paradigm using flow field as input. The results are show presented here since they are the same as Figure 4.3 and Figure 4.4.

Table 4.1 Chemical Reactions Considered in Example 1

Reaction type	Reaction and rate parameter	No.
Aqueous complexation reaction in mobile water phase	CMW1 + CMW2 $\leftrightarrow$ CMW3 ( $k_{eq} = 0.4 \text{ m}^3/\text{g}$ )	R <sub>1</sub>
Adsorption/desorption or ion-exchange reaction between mobile water and suspended sediment phases	CMW1+SS $\leftrightarrow$ CS1 + SS CMW2+SS $\leftrightarrow$ CS2 + SS CMW3+SS $\leftrightarrow$ CS3 + SS ( $k_f = 0.0001 \text{ m}^3/\text{g SS /s}$ , $k_b = 0.0 \text{ s}^{-1}$ )	R <sub>2</sub> R <sub>3</sub> R <sub>4</sub>
Adsorption/desorption or ion-exchange reaction between mobile water and bed sediment phases	CMW1+BS $\leftrightarrow$ CB1 + BS CMW2+BS $\leftrightarrow$ CB2+ BS CMW3+BS $\leftrightarrow$ CB3 + BS ( $k_f = 0.00001 \text{ m}^2/\text{g BS /s}$ , $k_b = 0.0/\text{h m}^{-1}\text{s}^{-1}$ )	R <sub>5</sub> R <sub>6</sub> R <sub>7</sub>
Sedimentation of particulate chemical between suspended and bed sediment phases	CS1 $\leftrightarrow$ CB1 ( $k_f = \text{Depo}/\text{h g SS}/\text{m}^3/\text{s}$ , $k_b = \text{Eros}/\text{h g BS}/\text{m}^3/\text{s}$ )	R <sub>8</sub>
	CS2 $\leftrightarrow$ CB2 ( $k_f = \text{Depo}/\text{h g SS}/\text{m}^3/\text{s}$ , $k_b = \text{Eros}/\text{h g BS}/\text{m}^3/\text{s}$ )	R <sub>9</sub>
	CS3 $\leftrightarrow$ CB3 ( $k_f = \text{Depo}/\text{h g SS}/\text{m}^3/\text{s}$ , $k_b = \text{Eros}/\text{h g BS}/\text{m}^3/\text{s}$ )	R <sub>10</sub>
Diffusion of dissolved chemical between mobile and immobile water phases	CMW1 $\leftrightarrow$ CIMW1 CMW2 $\leftrightarrow$ CIMW2 CMW3 $\leftrightarrow$ CIMW3 ( $k_f = 0.0001\theta^{T-15^\circ\text{C}} \text{ s}^{-1}$ , $k_b = 0.0h_b\theta_b/h\theta^{T-15^\circ\text{C}} \text{ s}^{-1}$ , $\theta = 1.2$ )	R <sub>11</sub> R <sub>12</sub> R <sub>13</sub>
Aqueous complexation reaction in immobile water phase	CIMW1+ CIMW2 $\leftrightarrow$ CIMW3 ( $k_f = 0.002h_b\theta_b/\text{h m}^3/\text{g /s}$ , $k_b = 0.005h_b\theta_b/\text{h s}^{-1}$ )	R <sub>14</sub>
Adsorption/desorption or ion-exchange reaction between immobile water and bed sediment phases	CIMW1+BS $\leftrightarrow$ CB1 + BS CIMW2+BS $\leftrightarrow$ CB2 + BS CIMW3+BS $\leftrightarrow$ CB3 + BS ( $k_f = 0.00001h_b\theta_b/\text{h m}^2/\text{g BS/s}$ , $k_b = 0.0/\text{h /m/s}$ )	R <sub>15</sub> R <sub>16</sub> R <sub>17</sub>
Volatilization reaction of dissolved chemical from mobile water phase	CMW2 $\leftrightarrow$ P ( $k_f = 0.00002 /\text{s}$ , $k_b = 0.02 \text{ g}/\text{m}^3/\text{ATM/s}$ ) ( $P=0.0025\text{ATM}$ )	R <sub>18</sub>
Precipitation/dissolution reaction between mobile water and suspension precipitate phases	CMW3 $\leftrightarrow$ SP3 ( $k_f = 0.0001 /\text{s}$ , $k_b = 0.0000001 /\text{s}$ )	R <sub>19</sub>
Precipitation/dissolution reaction between immobile water and bed precipitate phases	CIMW3 $\leftrightarrow$ BP3 ( $k_f = 0.0001 h_b\theta_b/\text{h s}^{-1}$ , $k_b = 0.0000001 h_b\theta_b/\text{h s}^{-1}$ )	R <sub>20</sub>

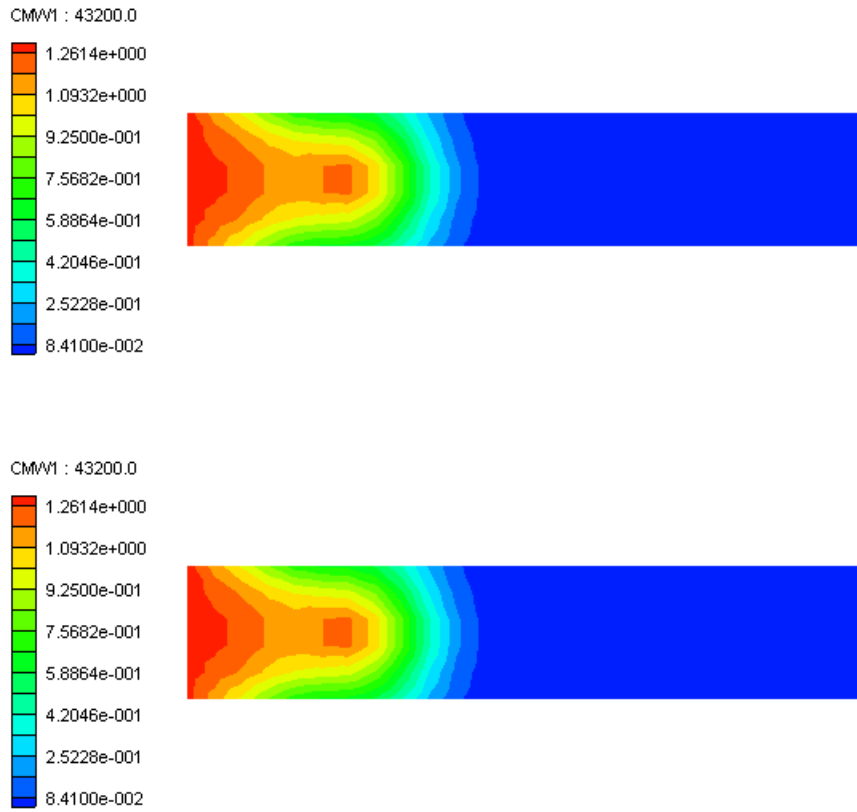


Figure 4.3 Concentration distribution of CMW1  
 Upper: WASH123D version 1.5 Lower: WASH123D version 3.0

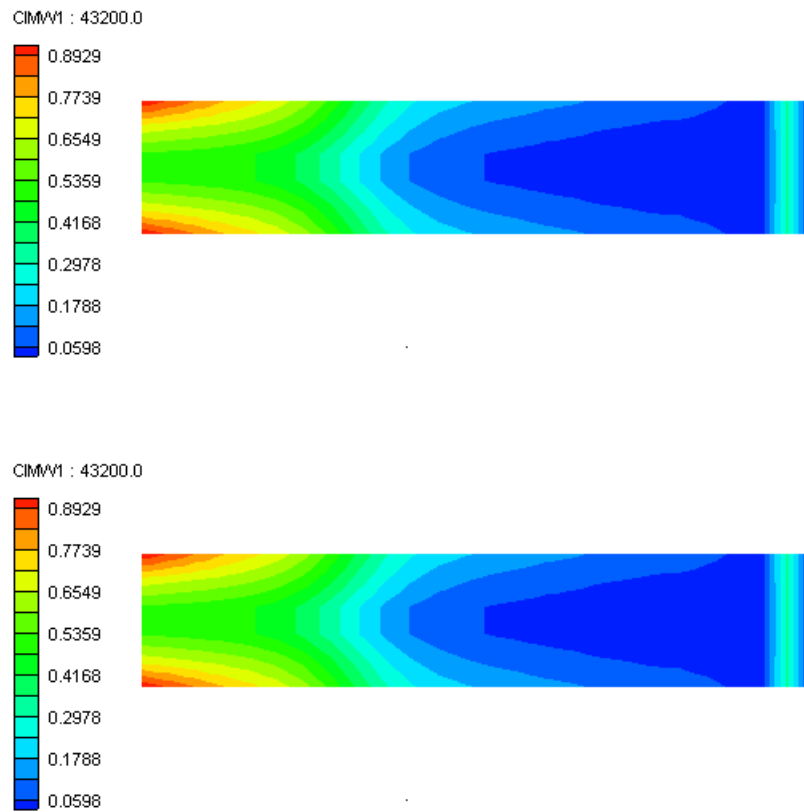


Figure 4.4 Concentration distribution of CIMW1  
Upper: WASH123D version 1.5 Lower: WASH123D version 3.0

#### 4.5.2 Example 2

This example shows the application of the model to simulate a two dimensional problem of flow and sediment and reactive water quality transport in an estuary. It is used to verify the correctness of the new model bay comparing its simulation flow and water quality results with the corresponding results by WASH123D version 1.5 and the general paradigm, respectively. Figure 4.5 shows the two dimensional study domain was discretized with 462 elements and 275 nodes. The tide cycles every 12 hours. For the flow simulation, the Dirichlet boundary condition was applied to the ocean boundary side and the closed boundary condition was applied to the rest of the boundary (Figure 4.5). The initial velocity was assumed zero and the initial water stage was assumed to be at the mean sea level. The system was subject to 10 point sources of  $1 \text{ m}^3/\text{s}$ . A 10-day simulation using dynamic wave model was performed with a fixed time step of 20 seconds. The maximum relative error of water depth less than  $10^{-4}$  was used to determine the convergence.

Figure 4.6 shows the water depth at various times in one tidal cycle by WASH123D version 1.5 and the new integrated model. Figure 4.7 shows the simulated flow velocity at different time in one tide cycle by the two models. It was seen that the new model generated exactly the same simulation water depth and velocity as does WASH123D version 1.5. The examining of output file of the water flow output from the two models confirmed the correctness of the water flow output files.

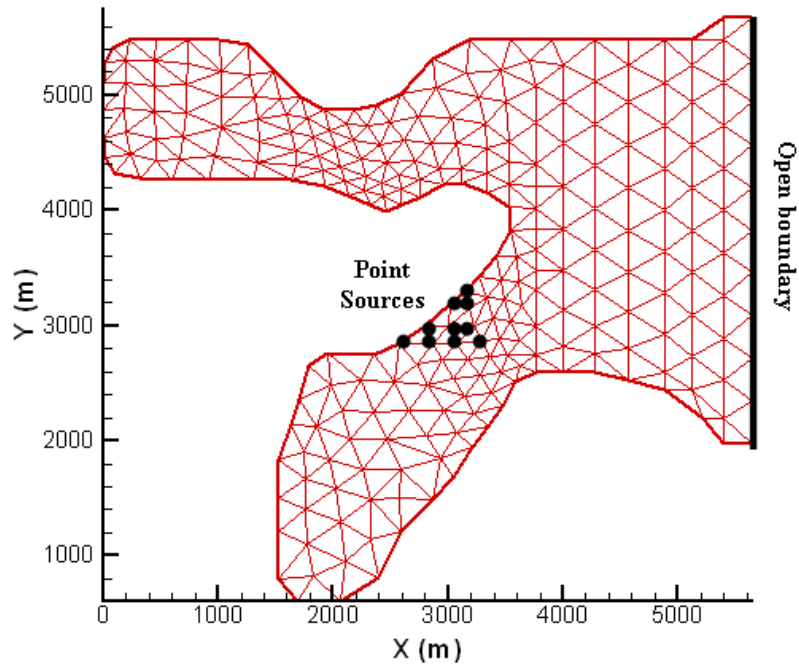


Figure 4.5 Discretization, open boundary, and point sources.

Figure 4.6 shows the water depth at various times in one tidal cycle by WASH123D version 1.5 and the new integrated model. Figure 4.7 shows the simulated flow velocity at different time in one tide cycle by the two models. It was seen that the new model gave exactly the same simulation water depth and velocity as does WASH123D version 1.5. The examining of output file of the water flow output from the two models confirmed the correctness of the water velocity output file.

The biogeochemical reactions in transport simulation are extracted from the WASP5 model (Ambrose et al. 1993). In the reaction system, a total of 22 species involves 32 kinetic reactions and 6 equilibrium reactions, as shown in Table 4.2 and Table 4.3, respectively. The reaction

coefficient and the rate parameters associating with the reaction system are given in Table 4.5 and Table 4.6 respectively.

In order to test the transport module of the integrated model alone, the flow field obtained from the flow-only simulation was used as input data to the transport module and the paradigm (Zhang 2005). We assume the water temperature is 15°C throughout the region. Initial concentration of the 22 species is listed in Table 4.4. Variable boundary conditions were specified at the open boundary side; the concentration of each species with incoming flow is given in Table 4.4. The dispersion coefficient was assumed 5.2 m<sup>2</sup>/s. A total of 10-day simulation was performed with a fixed time step size of 600 seconds. The modified Lagrangian-Eulerian approach is employed to discretize the transport equation and the operator-splitting scheme is used for the coupling of water quality transport and the reaction term. The allowed maximum relative error of concentration was set to 10<sup>-4</sup> to determine the convergence.

Figure 4.8 and Figure 4.9 show the concentration contours of NO<sub>3</sub> and PHYT respectively from the simulation by the new model and by the paradigm developed by Zhang (2005). The contours for the two species generated by both models are the same. In fact, the numerical results from the two models are identical according to the output data file. The match of the results indicates the correctness of the transport module alone in the integrated model.

The final step of verification of the coupled model requires simulating water flow and reactive transport concurrently. The same conditions and numerical methods were utilized. A 10-day simulation was performed with a fixed time step of 20 seconds for flow simulation and a time step size of 600 seconds for transport simulation. In other words, we perform one transport

computation in every 30 flow time steps. The output file showed identical results to those in flow-only and transport-only simulation. The flow field and water quality profiles were not presented herein since they would be identical to Figure 4.6 through Figure 4.9.

The PHYT concentration was initially high as seen from Figure 4.9; however, it reduces over time at majority of locations except around the source of  $\text{NO}_3$  and in the upper inland estuary. This is due to the fact that tidal flow in and out of the region helps with the dispersion of the phytoplankton. The  $\text{NO}_3$  concentration is higher for the upper estuary than the lower region because the velocity in upper region is lower. Higher velocities in the lower estuary help lower  $\text{NO}_3$  levels except at locations near the source. Therefore advection plays an important role in the distribution of the chemical species for such problems. PHYT growth increases in the presence  $\text{NO}_3$  and ammonia as seen from the reaction scheme in Table 4.2. Therefore PHYT concentration is high in the vicinity of  $\text{NO}_3$  source.

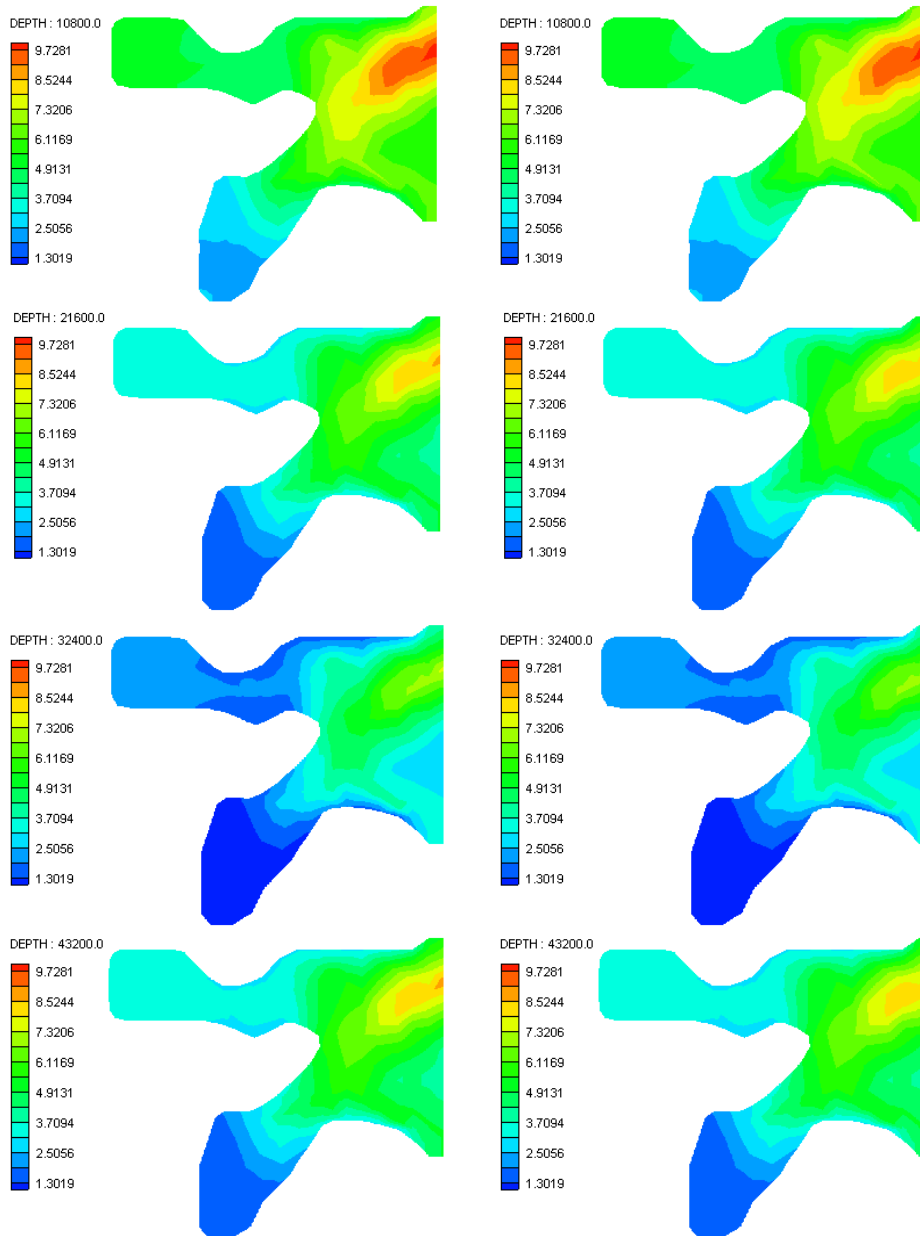


Figure 4.6 Simulated water depth  
 Left: WASH123D version 1.5 Right: new model  
 From top: 0.25T, 0.5T, 0.75T, 1.0T (1T = 12hr).

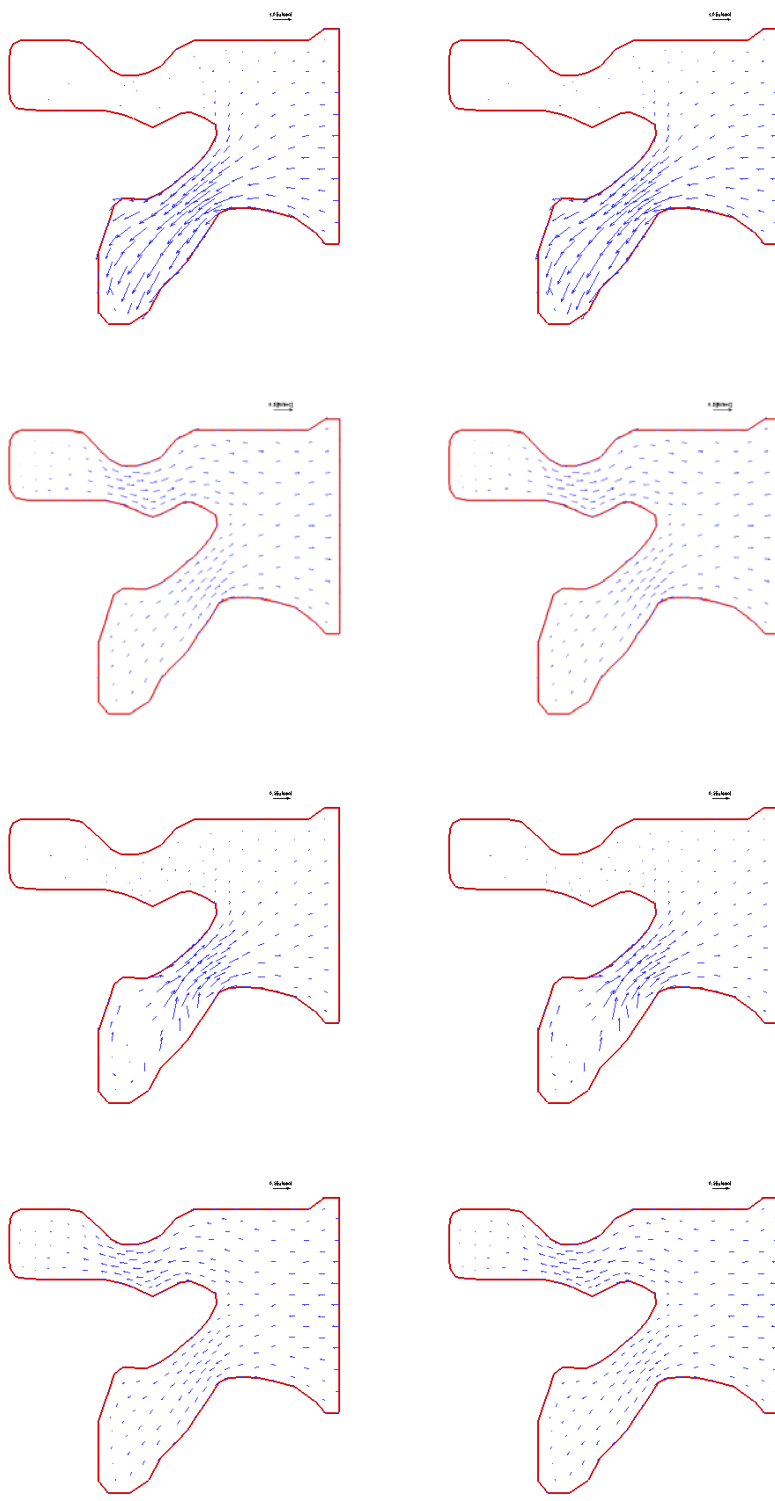


Figure 4.7 . Simulated velocity profile  
 Left: WASH123D version 1.5    Right: new model  
 From top: 0.25T, 0.5T, 0.75T, 1.0T (1T = 12hr).

Table 4.2 The 32 kinetic chemical Reactions in the system

No.	Mechanism	Reaction	Reaction Rate
K1	PHYT growth	$a_{nc}NH_3 + a_{pc}OPO_4 + CO_2 + H_2O \rightarrow PHYT + \frac{32}{12}O_2$	$R_1 = G_p C_7$
K2	PHYT growth related nitrate reduction	$a_{nc}NO_3^- \rightarrow a_{nc}NH_3 + \frac{48}{12}O_2$	$R_2 = (1 - P_{NH_3})G_p C_7$
K3	PHYT death-endogenous respiration	$PHYT + \frac{32}{12}O_2 \rightarrow CO_2 + H_2O + a_{nc}ON + a_{pc}OP$	$R_3 = k_{ir}\Theta_{ir}^{T-20}C_7$
K4	PHYT death-parasitization	$PHYT \rightarrow a_{nc}CH_2O + a_{nc}ON + a_{pc}OP$	$R_4 = k_{id}C_7$
K5	PHYT death-herbivorous grazing	$PHYT \rightarrow a_{nc}CH_2O + a_{nc}ON + a_{pc}OP$	$R_5 = k_{ig}ZC_7$
K6	PHYT death-promoted oxidation of ON	$a_{nc}ON \rightarrow a_{nc}NH_3$	$R_6 = (1 - f_{on})(k_{ir}\Theta_{ir}^{T-20}C_7 + k_{id}C_7 + k_{ig}ZC_7)$
K7	PHYT death-promoted oxidation of OP	$a_{pc}OP \rightarrow a_{pc}OPO_4$	$R_7 = (1 - f_{op})(k_{ir}\Theta_{ir}^{T-20}C_7 + k_{id}C_7 + k_{ig}ZC_7)$
K8	Benthic PHYT decomposition	$PHYT_{(b)} \rightarrow a_{nc}CH_2O_{(b)} + a_{nc}ON_{(b)} + a_{pc}OP_{(b)}$	$R_8 = k_{pzd}\Theta_{pzd}^{T-20}C_8$
K9	PHYT <sub>(b)</sub> decomposition promoted oxidation of ON <sub>(b)</sub>	$a_{nc}ON_{(b)} \rightarrow a_{nc}NH_{3(b)}$	$R_9 = (1 - f_{on(bed)})k_{pzd}\Theta_{pzd}^{T-20}C_8 \cdot h_b P/A$
K10	PHYT <sub>(b)</sub> decomposition Promoted oxidation of OP <sub>(b)</sub>	$a_{pc}OP_{(b)} \rightarrow a_{pc}OPO_{4(b)}$	$R_{10} = (1 - f_{op(bed)})k_{pzd}\Theta_{pzd}^{T-20}C_8 \cdot h_b P/A$
K11	Phytoplankton settling	$PHYT \rightarrow PHYT_{(b)}$	$R_{11} = \frac{V_{s3}}{h_b}C_7 \cdot h_b P/A$
K12	Re-aeration	$O_{2(g)} \rightarrow O_2$	$R_{12} = k_2\Theta_a^{(T-20)}(C_8 - C_{13})$
K13	Oxygen diffusion	$O_2 \rightarrow O_{2(b)}$	$R_{13} = \frac{E_{DIF}}{h_b}(C_{13} - C_{14}) \cdot h_b P/A$
K14	Carbonaceous oxidation	$CH_2O + O_2 \rightarrow CO_2 + H_2O$	$R_{14} = k_3\Theta_3^{(T-20)}\left(\frac{C_{13}}{K_{BOD} + C_{13}}\right)(C_9 + C_{10})$
K15	Benthic carbonaceous oxidation	$CH_2O_{(b)} + O_{2(b)} \rightarrow CO_2 + H_2O$	$R_{15} = k_{D8}\Theta_{D8}^{T-20}(C_{11} + C_{12}) \cdot h_b P/A$
K16	Carbonaceous settling	$CH_2O_{(p)} \rightarrow CH_2O_{(bp)}$	$R_{16} = \frac{V_{s3}}{h_b}C_{10} \cdot h_b P/A$
K17	Carbonaceous re-suspension	$CH_2O_{(bp)} \rightarrow CH_2O_{(p)}$	$R_{17} = \frac{V_{R3}}{h_b}C_{12} \cdot h_b P/A$
K18	Carbonaceous diffusion	$CH_2O \rightarrow CH_2O_{(b)}$	$R_{18} = \frac{E_{DIF}}{h_b}(C_9 - C_{11}) \cdot h_b P/A$
K19	Nitrogen mineralization	$ON \rightarrow NH_3$	$R_{19} = k_{71}\Theta_{71}^{(T-20)}\left(\frac{C_7}{K_{mpe} + C_7}\right)(C_{15} + C_{16})$
K20	Nitrification	$NH_3 + \frac{64}{14}O_2 \rightarrow NO_3^- + H_2O + H^+$	$R_{20} = k_{12}\Theta_{12}^{(T-20)}\left(\frac{C_{13}}{K_{NIT} + C_{13}}\right)C_1$
K21	De-nitrification	$\frac{5}{4}CH_2O + \frac{14}{32}NO_3^- + H^+ \rightarrow \frac{5}{4}CO_2 + \frac{1}{2}N_2 + \frac{7}{4}H_2O$	$R_{21} = k_{2D}\Theta_{2D}^{(T-20)}\left(\frac{K_{NO_3}}{K_{NO_3} + C_{13}}\right)C_3 \cdot \frac{32}{14}$
K22	Benthic nitrogen mineralization	$ON_{(b)} \rightarrow NH_{3(b)}$	$R_{22} = k_{OND}\Theta_{OND}^{T-20}C_{17} \cdot h_b P/A$
K23	Benthic de-nitrification	$\frac{5}{4}CH_2O_{(b)} + \frac{14}{32}NO_3^-_{(b)} + H^+ \rightarrow \frac{5}{4}CO_2 + \frac{1}{2}N_2 + \frac{7}{4}H_2O$	$R_{23} = k_{2D}\Theta_{2D}^{(T-20)}C_4 \cdot \frac{32}{14} \cdot h_b P/A$
K24	Ammonia flux	$NH_{3(b)} \rightarrow NH_3$	$R_{24} = \frac{E_{DIF}}{h_b}(C_2 - C_1) \cdot h_b P/A$
K25	Nitrate flux	$NO_{3(b)} \rightarrow NO_3$	$R_{25} = \frac{E_{DIF}}{h_b}(C_4 - C_3) \cdot h_b P/A$
K26	Organic nitrogen settling	$ON_{(p)} \rightarrow ON_{(bp)}$	$R_{26} = \frac{V_{s3}}{h_b}C_{16} \cdot h_b P/A$
K27	Organic nitrogen flux	$ON_{(b)} \rightarrow ON$	$R_{27} = \frac{E_{DIF}}{h_b}(C_{17} - C_{15}) \cdot h_b P/A$
K28	Phosphorous mineralization	$OP \rightarrow OPO_4$	$R_{28} = k_{83}\Theta_{83}^{(T-20)}\left(\frac{C_7}{K_{mpe} + C_7}\right)(C_{19} + C_{20})$
K29	Benthic phosphorous mineralization	$OP_{(b)} \rightarrow OPO_{4(b)}$	$R_{29} = k_{OPD}\Theta_{OPD}^{T-20}C_{21} \cdot h_b P/A$
K30	Phosphorous flux	$OPO_{4(b)} \rightarrow OPO_4$	$R_{30} = \frac{E_{DIF}}{h_b}(C_6 - C_5) \cdot h_b P/A$
K31	Organic phosphorous setting	$OP_{(p)} \rightarrow OP_{(bp)}$	$R_{31} = \frac{V_{s3}}{h_b}C_{20} \cdot h_b P/A$
K32	Organic phosphorous flux	$OP_{(b)} \rightarrow OP$	$R_{32} = \frac{E_{DIF}}{h_b}(C_{21} - C_{19}) \cdot h_b P/A$

Table 4.3 The 6 equilibrium chemical reactions in the system

No	Mechanism	Reaction	Reaction rate
E1	Carbonaceous sorption	$\text{CH}_2\text{O} \rightarrow \text{CH}_2\text{O}_{(p)}$	$f_{D5} = \frac{C_9}{C_9 + C_{10}}$
E2	Organic nitrogen sorption	$\text{ON} \rightarrow \text{ON}_{(p)}$	$f_{D7} = \frac{C_{15}}{C_{15} + C_{16}}$
E3	Organic phosphorous sorption	$\text{OP} \rightarrow \text{OP}_{(p)}$	$f_{D8} = \frac{C_{19}}{C_{19} + C_{20}}$
E4	Benthic carbonaceous sorption	$\text{CH}_2\text{O}_{(b)} \rightarrow \text{CH}_2\text{O}_{(bp)}$	$f_{D5(\text{bed})} = \frac{C_{11}}{C_{11} + C_{12}}$
E5	Benthic organic nitrogen sorption	$\text{ON}_{(b)} \rightarrow \text{ON}_{(bp)}$	$f_{D7(\text{bed})} = \frac{C_{17}}{C_{17} + C_{18}}$
E6	Benthic organic phosphorous sorption	$\text{OP}_{(b)} \rightarrow \text{OP}_{(bp)}$	$f_{D8(\text{bed})} = \frac{C_{21}}{C_{21} + C_{22}}$

Table 4.4 Initial and boundary conditions for the reactive water quality simulation

No.	Species	Notation	Initial	Boundary	$\rho_i$
1	NH <sub>3</sub>	C <sub>1</sub>	1 mg N/kg	0.1 mg N/L	$\rho_w$
2	NO <sub>3</sub>	C <sub>3</sub>	1 mg N/kg	0.1 mg N/L	$\rho_w$
3	OPO <sub>4</sub>	C <sub>5</sub>	0.1 mg P/kg	0.01 mg P/L	$\rho_w$
4	PHYT	C <sub>7</sub>	2 mg C/kg	0.2 mg C/L	$\rho_w$
5	CH <sub>2</sub> O	C <sub>9</sub>	10 mg O <sub>2</sub> /kg	1.0 mg O <sub>2</sub> /L	$\rho_w$
6	O <sub>2</sub>	C <sub>13</sub>	2 mg O <sub>2</sub> /kg	0.2 mg O <sub>2</sub> /L	$\rho_w$
7	ON	C <sub>15</sub>	2 mg N/kg	0.2 mg N/L	$\rho_w$
8	OP	C <sub>19</sub>	0.35 mg P/kg	0.035 mg P/L	$\rho_w$
9	CH <sub>2</sub> O <sub>(p)</sub>	C <sub>10</sub>	0.2 mg O <sub>2</sub> /mg	1.0 mg O <sub>2</sub> /L	SS
10	ON <sub>(p)</sub>	C <sub>16</sub>	0.0 mg N/mg	0 mg N/L	SS
11	OP <sub>(p)</sub>	C <sub>20</sub>	0.003 mg P/mg	0.015 mg P/L	SS
12	NH <sub>3(b)</sub>	C <sub>2</sub>	1 mg N/kg	-	$h_b\rho_{wb}\theta_b/h$
13	NO <sub>3(b)</sub>	C <sub>4</sub>	1 mg N/kg	-	$h_b\rho_{wb}\theta_b/h$
14	OPO <sub>4(b)</sub>	C <sub>6</sub>	0.1 mg P/kg	-	$h_b\rho_{wb}\theta_b/h$
15	PHYT <sub>(b)</sub>	C <sub>8</sub>	2 mg C/kg	-	$h_b\rho_{wb}\theta_b/h$
16	CH <sub>2</sub> O <sub>(b)</sub>	C <sub>11</sub>	10 mg O <sub>2</sub> /kg	-	$h_b\rho_{wb}\theta_b/h$
17	O <sub>2(b)</sub>	C <sub>14</sub>	2 mg O <sub>2</sub> /kg	-	$h_b\rho_{wb}\theta_b/h$
18	ON <sub>(b)</sub>	C <sub>17</sub>	2 mg N/kg	-	$h_b\rho_{wb}\theta_b/h$
19	OP <sub>(b)</sub>	C <sub>21</sub>	0.35 mg P/kg	-	$h_b\rho_{wb}\theta_b/h$
20	CH <sub>2</sub> O <sub>(bp)</sub>	C <sub>12</sub>	0.002 mg O <sub>2</sub> /mg	-	BS/h
21	ON <sub>(bp)</sub>	C <sub>18</sub>	0.0 mg N/mg	-	BS/h
22	OP <sub>(bp)</sub>	C <sub>22</sub>	0.00003 mg P/mg	-	BS/h

Table 4.5 Reaction Coefficient

Description	Variable	Value	Unit
Phytoplankton nitrogen-carbon ratio	$a_{nc}$	0.25	mgN/mgC
Phytoplankton phosphorus-carbon ratio	$a_{pc}$	0.025	mgP/mgC
Phytoplankton oxygen-carbon ratio	$a_{oc}$	2.67	mgO <sub>2</sub> /mgC

Table 4.6 The reaction rate parameters

Description	Variable	Value	Unit
Phytoplankton growth rate	$G_{p1}$	$k_{iC}X_{RT}X_{RI}X_{RN}$	day <sup>-1</sup>
Maximum phytoplankton growth rate	$k_{iC}$	2.0	day <sup>-1</sup>
Temperature adjustment factor for phytoplankton growth	$X_{RT}$	$\Theta_{1C}^{T-20}$	-
Temperature coefficient for phytoplankton growth	$\Theta_{1C}$	1.068	-
Light adjustment coefficient for phytoplankton growth	$X_{RI}$	$\min \{e^{f[e^{-(I_s/I_e)^{k_{iC}}]} - e^{-I_s/I_e}]/(K_e D), 1.0\}$	-
Light extinction coefficient	$K_e$	2	m <sup>-1</sup>
Fraction of day that is daylight	$f$	0.5	-
Average daily surface solar radiation	$I_a$	400	Langley/day
Saturating light intensity of phytoplankton	$I_s$	540	Langley/day
Nutrient limitation factor for phytoplankton growth	$X_{RN}$	$\min (DIN/(K_{mN} + DIN), DIP/(K_{mP} + DIP))$	-
Concentration of the dissolved inorganic nitrogen	DIN	$C_1 + C_3$	mg N/L
Half-saturation constant for nitrogen	$K_{mN}$	0.025	mg N/L
Dissolved inorganic phosphorus	DIP	$f_{D3}C_5$	mg P/L
Fraction of dissolved inorganic phosphorus	$f_{D3}$	0.85	-
Half-saturation constant for phosphorus	$K_{mP}$	0.001	mg P/L
Preference for ammonia uptake term	$P_{NH3}$	$[C_1 C_3 / (K_{mN} + C_1) + C_1 K_{mN} / (C_1 + C_3)] / (K_{mN} + C_3)$	-
Phytoplankton respiration rate constant	$k_{1r}$	0.125	day <sup>-1</sup>
Temperature coefficient for Phytoplankton respiration	$\Theta_{1r}$	1.045	-
Phytoplankton death rate constant	$k_{1d}$	0.02	day <sup>-1</sup>
Phytoplankton Grazing Rate Constant	$k_{1g}$	0	L/mgC
Zooplankton Population	$Z$	0	mgC/L
Fraction of dead and respired PHYT recycled to ON	$f_{on}$	0.5	-
Fraction of dead and respired PHYT recycled to OP	$f_{op}$	0.5	-
Benthic phytoplankton decomposition rate constant	$k_{pzd}$	0.02	day <sup>-1</sup>
Temperature coefficient for benthic PHYT decomposition	$\Theta_{pzd}$	1.08	-
Benthic fraction of decomposed PHYT recycled to ON	$f_{on(bed)}$	0.5	-
Benthic fraction of PHYT recycled to the OP pool	$f_{op(bed)}$	0.5	-
Phytoplankton Settling Velocity	$V_{s4}$	0.1	m/day
Re-aeration rate constant	$k_2$	$\min [\text{Max}(k_q, k_w), 10.0]$	-
Flow-induced re-aeration rate coefficient	$k_q$	$5.049v^{0.97}h^{-1.67}$	-
Wind-induced re-aeration rate coefficient	$k_w$	0	-

Table 4.5 The reaction rate parameters (Continued)

Description	Variable	Value	Unit
Re-aeration rate temperature coefficient	$\Theta_a$	1.028	-
Dissolve oxygen saturation	Cs	$e^{\frac{-139.34+1.5757 \cdot 10^4 T_c^{-1} - 6.6423 \cdot 10^7 T_c^{-2} + 1.2438 \cdot 10^{10} T_c^{-3} + 8.6219 \cdot 10^9 T_c^{-4}}{-0.55335(0.01929-19.428 T_c^{-1} - 3868.3 T_c^{-2})}}$	-
Oxygenation rate constant	$k_d$	0.185	day <sup>-1</sup>
Oxygenation rate Temperature coefficient	$\Theta_d$	1.047	-
Half saturation constant for oxygen limitation	$K_{BOD}$	0.5	mgO <sub>2</sub> /L
Benthic Oxygenation rate constant	$k_{DS}$	0.0004	day <sup>-1</sup>
Oxygenation rate Temperature coefficient	$\Theta_{DS}$	1.08	-
Organic matter settling velocity	$V_{S3}$	0.1	m/day
Organic matter re-suspension velocity	$V_{R3}$	0.01	m/day
Fraction of dissolved Carbonaceous	$f_{D5}$	0.5	-
Fraction of dissolved benthic Carbonaceous	$f_{D5(b)}$	0.5	-
Diffusive exchange coefficient is	$E_{DIF}$	0.0002	m <sup>2</sup> /day
Organic nitrogen mineralization rate constant	$k_{71}$	0.075	day <sup>-1</sup>
Organic nitrogen mineralization Temperature coefficient	$\Theta_{71}$	1.08	-
Half saturation constant for PHYT limitation of P recycle	$K_{mPc}$	1.0	mgC/L
Nitrification rate constant	$k_{12}$	0.105	day <sup>-1</sup>
Nitrification rate temperature coefficient	$\Theta_{12}$	1.08	
Half saturation for oxygen limitation of Nitrification	$K_{NIT}$	2.0	mgO <sub>2</sub> /L
De-nitrification rate constant	$K_{2D}$	0.09	day <sup>-1</sup>
De-nitrification rate temperature coefficient	$\Theta_{2D}$	1.045	-
Half saturation constant for oxygen of De-nitrification	$K_{NO3}$	0.1	mgO <sub>2</sub> /L
Benthic Organic nitrogen mineralization rate constant	$k_{OND}$	0.0004	day <sup>-1</sup>
Mineralization rate Temperature coefficient	$\Theta_{OND}$	1.08	-
Fraction of dissolved Organic Nitrogen	$f_{D7}$	1.0	-
Fraction of dissolved benthic Organic Nitrogen	$f_{D7(b)}$	1.0	-
Dissolved OP mineralization rate constant	$k_{83}$	0.22	day <sup>-1</sup>
Dissolved OP mineralization temperature coefficient	$\Theta_{83}$	1.08	-
Half saturation constant for PHYT limitation of P recycle	$K_{mPc}$	1.0	mgC/L
Benthic dissolved OP mineralization rate constant	$k_{OPD}$	0.0004	day <sup>-1</sup>
Benthic dissolved OP mineralization temperature coefficient	$\Theta_{OPD}$	1.08	-

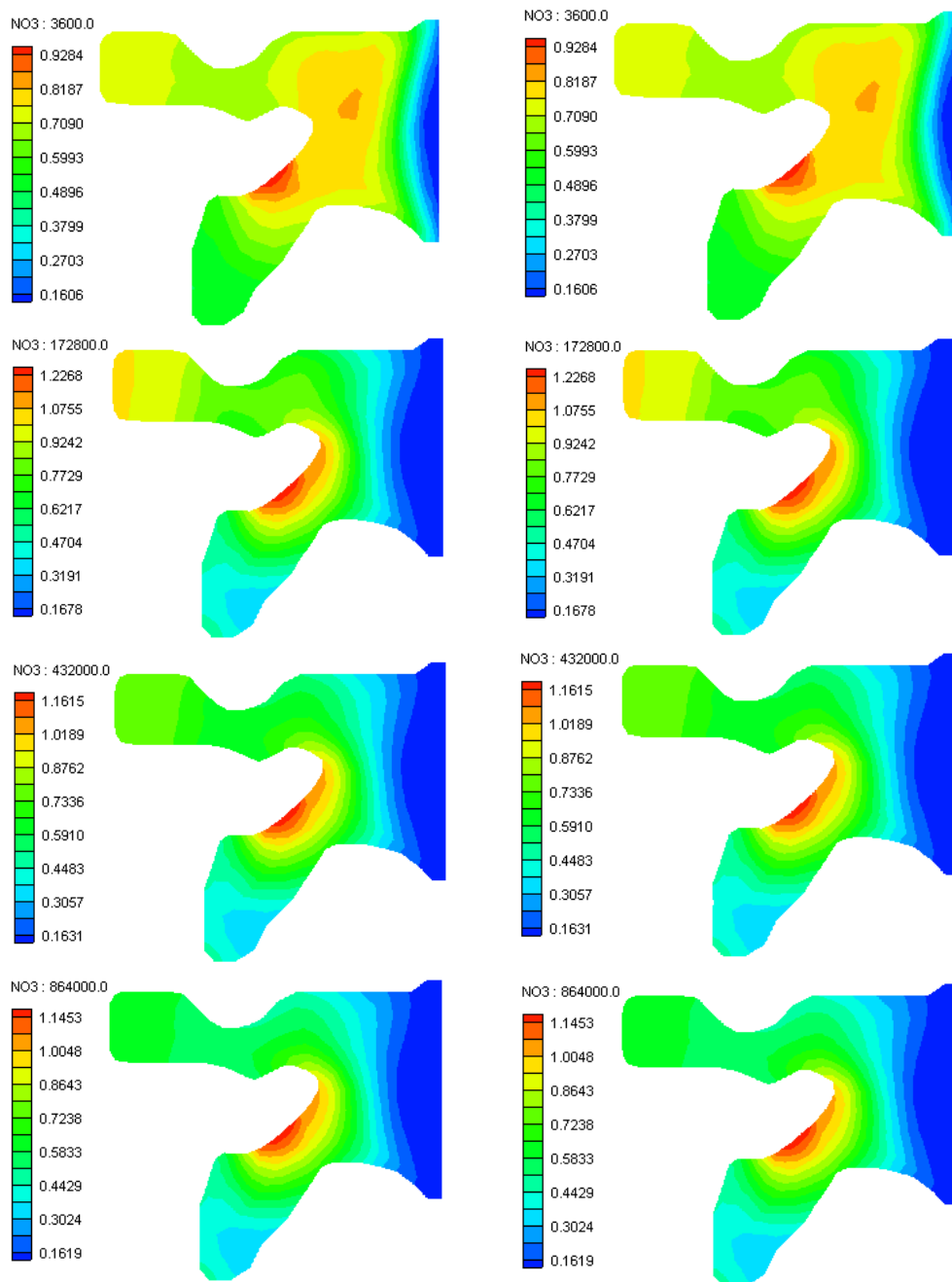


Figure 4.8 Simulated NO<sub>3</sub> concentration profile  
 Left: WASH123D version 1.5 Right: new model  
 From top: 1 hr, 2 day, 5 day, 10 day

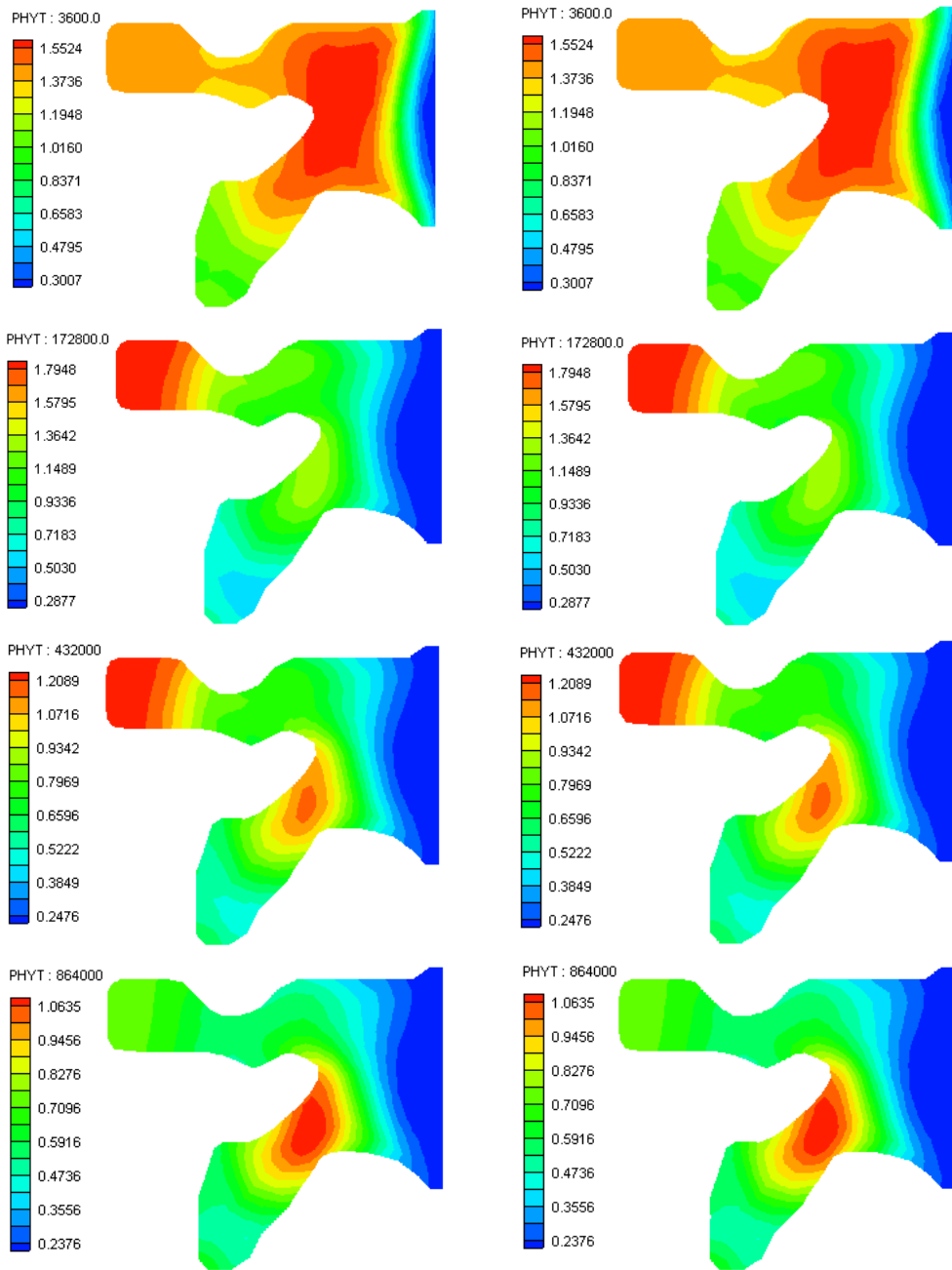


Figure 4.9 Simulated concentration profile of PHYT  
 Left: WASH123D version 1.5 Right: new model  
 From top: 1hr, 2 day, 5 day, 10 day

## 4.6 Conclusion

This chapter presents the development of a numerical model for water flow and sediment and reactive water quality simulation in land surface by incorporating a general water quality simulation paradigm into the current version of WASH123D model. The model is one of three major components of an integrated hydrology/hydraulic water quality model for watershed scale simulations.

The coupling of water flow and water quality simulations provides the model with a full range of simulation capability and saves computer storage compared with the commonly used indirectly linked models. The coupling of water quality transport with an arbitrary number of mixed equilibrium and kinetic reactions makes the model general and flexible enough to simulation water quality problems subject to any number of chemical reactions.

Through the diagonalization of the reactive transport equation via Gauss-Jordan column reduction of the chemical reaction network, equilibrium reactions are decoupled from the kinetic reactions. Species reactive transport equations are transformed into two sets: reactive transport equations of kinetic-variables and algebraic equations of equilibrium variables. Kinetic variable is adopted as the primary dependent variable in solving the transport equation rather than individual species to reduce the number of transport equations and simplify the reaction terms. Three coupling strategies, fully implicit scheme, mixed predictor-corrector/operator-splitting scheme, and operator-splitting scheme, are included in the model to deal with the coupling of transport and biogeochemical reactions at different levels of efficiency and accuracy. Fiver spatial discretization approaches are utilized to solve the advection-dispersion transport equation

describing the kinetic variable transport.

In each time step, hydrologic/hydraulic variables are solved in the flow module; kinetic variables are then solved in the transport module. This is followed by solving the reactive chemical system node by node to yield concentrations of all species. Two examples are employed to verify the design capability of the model.

#### 4.7 References

Ambrose, R.B., Wool, T.A. and Martin, J.L., 1993. The water quality analysis simulation program, WASP5 Part A: model documentation Environmental Research Laboratory, US Environmental Protection Agency, Athens, GA.

Arheimer, B. and Olsson, J., 2003. Integration and Coupling of Hydrological Models with Water Quality Models: Applications in Europe, Swedish Meteorological and Hydrological Institute (SMHI).

Bicknell, B.R., Imhoff, J.C., Kittle, J.L., Jobs Jr., T.H. and Donigian Jr., A.S., 2001. HYDROLOGICAL SIMULATION PROGRAM - FORTRAN, Version 12, User's manual, AQUA TERRA Consultants.

Brown, L.C. and Barnwell, T.O., 1987. The enhanced stream water quality models QUAL2E and QUAL2E-UNCAS: Documentation and user Manual. EPA/600/3-87/007.

Cerco, C.F. and Cole, T., 1995. User's Guide to the CE-QUAL-ICM Three-dimensional eutrophication model, release version 1.0. Technical Report EL-95-15, US Army Corps of Engineers Water Experiment Station, Vicksburg, MS.

- Cheng, H.P., Yeh, G.T. and Cheng, J.R., 2000. A numerical model simulating reactive transport in shallow water domains: model development and demonstrative applications. *Advances in Environmental Research*, 4: 187-209.
- Covelli, P., Marsili-Libelli, S. and Pacini, G., 2001. SWAMP: A Two-dimensional Hydrodynamic and Quality Modeling Platform for Shallow Waters. *Numerical Methods for Partial Differential Equations*, 18(5): 663-687.
- DHI Software. 2004. Coastal and Inland Waters in 2D. <http://www.dhisoftware.com/MIKE21/>
- Fang, Y.L., Yeh, G.T. and Burgos, W.D., 2003. A Generic Paradigm to Model Reaction-Based Biogeochemical Processes in Batch Systems. *Water Resources Research*, 33(4): 1083-1118.
- Hamrick, J.M., 1996. A user's manual for the environmental fluid dynamics computer code (EFDC), The College of William and Mary, Virginia Institute of Marine Science, Gloucester Point, VA.
- Lung, W.S. and Hwang, C.C., 1989. Integrating hydrodynamic and water quality models for Patuxent Estuary. In: ASCE (Editor), *Estuarine and Coastal Engineering*. ASCE, New York, NY, pp. 420-429.
- Lung, W.S., 2001. *Water quality modeling for wasteload allocations and TMDLs*. John Wiley & Sons, Inc, New York.
- Martin, J.L. and McCutcheon, S.C., 1999. *Hydrodynamics and transport for water quality modeling*. CRC Press Inc., Boca Raton, Florida.
- Rubin, J., 1983. Transport of reacting solutes in porous media: relation between mathematical nature of problem formulation and chemical nature of reactions. *Water Resources*

- Research, 38(11): 253-260.
- Singh, V.P., 1995. Computer Models of Watershed Hydrology. Water Resources Publications, Littleton, Colorado.
- Steeffel, C.I. and van Cappellen, P., 1998. Preface: reactive transport modeling of natural systems. *Journal of Hydrology*, 209: 1-7.
- Thomann, R.V. and Mueller, J.A., 1987. Principle of surface water quality modeling and control. Harper & Row, New York.
- Yeh, G. T., 2000. Computational subsurface hydrology: reactions, Transport, and Fate. Kluwer Academic Publishers, Boston.
- Yeh, G. T., H. P. Cheng, and J. R. Cheng. (1998). BEST: a numerical model of simulating Bay/Estuary hydrodynamics and Sediment/Contaminant Transport. The Pennsylvania State University, University Park, PA.
- Yeh, G.-T., Burgosb, W.D. and Zacharac, J.M., 2001. Modeling and measuring biogeochemical reactions: system consistency, data needs, and rate formulations. *Advances in Environmental Research*, 5: 219-237.
- Yeh, G.T., Cheng, H.P., Cheng, J.R. and Jerry, H.L., 1998. A Numerical Model to Simulate Water Flow and Contaminant and Sediment Transport in Watershed Systems of 1-D Stream-River Network, 2-D Overland Regime, and 3-D Subsurface Media (WASH123D: Version 1.0). Technial Report CHL-98-19, Waterways Experiment Station, U. S. Army Corps of Engineers, Vicksburg, MS 39180-6199.
- Yeh, G.-T., Huang, G, Cheng, H.-P., Zhang, F., Lin, H.-C., Edris, E. and Richards, D., 2006. A first-principle, physics-based watershed model: WASH123D. In: V.P. Singh and D.K.

- Frevert (Editors), *Watershed Models*. CRC Press, Boca Raton, FL.
- Yeh, G.-T., Huang, G., Zhang, F., Cheng, H.P. and Lin, H.-C., 2005. WASH123D: A numerical model of flow, thermal transport, and salinity, sediment, and water quality transport in WAterSHed systems of 1-D stream-river network, 2-D overland regime, and 3-D subsurface media, Office of Research and Development, Orlando, FL.
- Zhang, F., 2005. A new paradigm of modeling watershed water quality, Ph.D Dissertation. Depart of Civil, Environmental, & Construction Engineering, University of Central Florida, Orlando, FL.
- Zhang, F., G. T. Yeh, J. C. Parker, and P. M. Jardine, 2008. A reaction-based river/stream water quality model: Model development and numerical schemes. *Journal of Hydrology*, 348(3-4), 496-509.
- Zhang, F., Yeh, G.T., Parker, J.C., Brooks, S.C., Pace, M.N., Kim, Y.J., Jardine, P.M. and Watson, D.B., 2007. A reaction-based paradigm to model reactive chemical transport in groundwater with general kinetic and equilibrium reactions. *Journal of Contaminant Hydrology*, 92(1-2): 10-32.

## CHAPTER 5 AN INTEGRATED HYDROLOGY/HYDRAULIC AND WATER QUALITY MODEL FOR SUBSURFACE WATER SYSTEMS

### 5.1 Abstract

This chapter presents the design of a first principle, physics-based subsurface model that integrates hydrology/hydraulics and reactive water quality transport. The model is capable of simulating separated and integrated fluid flow, as well as reactive water quality transport in subsurface media.

The modified Richards equation is applied as the governing equation for subsurface flow simulation. The reaction-based advection-dispersion equation is used as the governing equation for water quality transport. The capability of reaction-based algorithm for biogeochemical reaction rate formulation allows the model to simulate an arbitrary number of biogeochemical species involved in any mixed equilibrium and kinetic reaction, and thus gives the model much flexibility and generality. Three strategies: fully implicit scheme, mixed predictor-corrector and operator-splitting scheme, and operator-splitting scheme, are included in the model to deal with the coupling of transport and reaction along with five numerical approaches in the model for spatial discretization.

In the transport simulations, fast/equilibrium reactions are decoupled from slow/kinetic reactions by the decomposition of reaction networks; this enables robust numerical integrations of the governing equation. Kinetic variables are adopted as primary dependent variables rather than

biogeochemical species to reduce the number of transport equations and simplify the reaction terms. In each time step, hydrologic/hydraulic variables are solved in the flow module; kinetic variables are then solved in the transport module. This is followed by solving the reactive chemical system node by node to yield concentrations of all species. One application example is presented to verify the correctness of the model and to demonstrate its design capability.

## 5.2 Introduction

Groundwater flow and contaminant transport models have been used as an essential tool for simulating the subsurface environment. To date many models have been developed. It has been recognized that consideration of equilibrium chemistry, kinetic chemistry, and geohydrologic transport and the interaction between fluid flow and reactive transport is necessary to reflect the complexity of many real systems (Yeh et al., 2009). However, most models cannot simulate density-dependent flow, while some take into account density-dependent flow and solute transport, e.g. SEAWAT (Guo and Langevin, 2002), SUTRA (VOSS, 1984), FEMWATER (Lin et al., 1997), HST3D (Jr. Kipp, 1997), MODFLOW/MT3DMS (Prommer et al., 2003), and FEFLOW (Trefry and Muffels, 2007). Most of them, however, only simulate single or multi solute without taking the biogeochemical reactions into account. A few models are capable of simulating both flow and reactive transport in a mechanistic way, e.g. PHWAT (Mao et al., 2006; Parkhurst and Appelo, 1999), but can only simulate the equilibrium biogeochemical reactions. On the other hand, many models have been developed mainly for reactive transport simulation with various capabilities (Keum and Hahn, 2003). Many couple transport with equilibrium geochemistry (Cheng, 1995; Parkhurst and Appelo, 1999; Yeh and Tripathi, 1991), while some

models couple transport with kinetic biogeochemistry (Cheng and Yeh, 1994; Lichtner, 1996; Steefel and Yabusaki, 1996; Szecsody et al., 1998; Wood et al., 1994). More recently, many models have been developed with coupling of transport and mixed equilibrium/kinetic reactions (Salvage et al., 1996; Yeh et al., 1996; Yeh et al., 2001b). Most of these models can only simulate a limited reaction network. Fang et al. (2003) proposed a reaction-based batch model, BIOGEOCHEM, capable of handling any number of mixed equilibrium and kinetic reactions. Several models have been coupled BIOGEOCHEM with transport successfully (Yeh et al., 2009; Yeh et al., 2004; Zhang et al., 2007). These models are very flexible and provide a promising generality.

This chapter presents the development of a mechanistic-based numerical model for simulation of coupled fluid flow and reactive geochemical transport, including both fast and slow reactions, in variably saturated media.

### 5.3 Theory and mathematical basis

#### 5.3.1 Water flow in subsurface system

The governing equation for subsurface density dependent flow in variably saturated porous media is given as Eq.(5.1) (Yeh, 2000),

$$\frac{\rho}{\rho_o} F \frac{\partial h}{\partial t} = \nabla \cdot \left[ \mathbf{K} \cdot \left( \nabla h + \frac{\rho}{\rho_o} \nabla z \right) \right] + \frac{\rho^*}{\rho_o} q \quad (5.1)$$

where  $\rho$  is the density of the subsurface water;  $\rho_o$  is the reference density of water;  $h$  is the referenced pressure head [L];  $t$  is the time [T];  $\mathbf{K}$  is the hydraulic conductivity tensor [L/T];  $z$  is

the potential head [L];  $\rho^*$  is the density of source water;  $q$  is the source and/or sink [ $L^3/L^3/T$ ]; and  $F$  is the water capacity [1/L].

Five types of boundary conditions are taken into account including Dirichlet, Neumann, Cauchy, River, and variable boundary conditions. See Yeh et al. (2005) for details on each of these boundary conditions..

### 5.3.2 Reactive Chemical Transport In Subsurface Systems

Continuity equation for kinetic-variables:

$$\frac{\partial(\theta\rho_i C_i)}{\partial t} + \alpha_i L(\rho_i C_i) = \theta r_i \Big|_N, \quad i \in M \quad (5.2)$$

where

$$L(\rho_i C_i) = \nabla \cdot (\mathbf{V} \rho_i C_i) - \nabla \cdot [\theta \mathbf{D} \cdot \nabla (\rho_i C_i)] - M_{C_i}^{as} \quad (5.3)$$

where  $\theta$  is the moisture content [ $L^3$  solution/ $L^3$  matrix];  $C_i$  is the concentration of the  $i$ -th dissolved species in the unit of chemical mass per unit water mass [M/M],  $\rho_i$  is the density of water [i.e.,  $C_i = C_w$ ] [ $M/L^3$ ],  $\mathbf{V}$  is the Darcy velocity [L/T],  $\mathbf{D}$  is the dispersion coefficient tensor [ $L^2/T$ ],  $r_i \Big|_N$  is the production rate of species  $i$  due to all  $N$  reactions in the unit of chemical mass per volume of water per time [ $M/L^3/T$ ],  $M_{C_i}^{as}$  is the artificial source of  $C_i$  in unit of chemical mass per unit of medium volume [ $M/L^3/T$ ], and  $M$  is the number of chemical species

The initial condition of each chemical species must be specified for transient simulations. No boundary conditions are needed for immobile species. Six types of boundary conditions are taken into account for: Dirichlet boundary condition, Neumann boundary condition, Cauchy boundary

condition, Variable boundary condition, River/stream-subsurface interface boundary condition, and Overland-subsurface interface boundary condition.

Dirichlet boundary condition:

This condition is applied when the species concentration is prescribed as a function of time on the boundaries:

$$C_i(\mathbf{x}, t) = C_{i_{db}}(\mathbf{x}, t) \text{ on } B_d(\mathbf{x}) = 0 \quad (5.4)$$

where  $C_{i_{db}}(\mathbf{x}, t)$  is the concentration of the  $i$ -th species on the Dirichlet boundary,  $B_d(\mathbf{x}) = 0$ , [M/M]

Variable boundary condition:

This boundary condition is employed when the flow direction would change with time during simulations. Two cases are considered, regarding to the flow direction on the boundary.

< Case 1 > Flow is coming in from outside

$$\mathbf{n} \cdot [\mathbf{V}\rho_i C_i - \theta \mathbf{D} \cdot \nabla(\rho_i C_i)] = (\mathbf{n} \cdot \mathbf{V})\rho_i C_{i_{vb}}(\mathbf{x}, t) \text{ on } B_v(\mathbf{x}) = 0 \quad (5.5)$$

< Case 2 > Flow is going out from inside:

$$-\mathbf{n} \cdot [\theta \mathbf{D} \cdot \nabla(\rho_i C_i)] = 0 \text{ on } B_v(\mathbf{x}) = 0 \quad (5.6)$$

where  $C_{i_{vb}}(\mathbf{x}, t)$  is a time-dependent concentration of the  $i$ -th species [M/M] on the variable boundary,  $B_v(\mathbf{x}) = 0$ , which is associated with the incoming flow.

Cauchy boundary condition:

This boundary condition is employed when the total salt-flow rate is given at pervious boundaries. Usually, this boundary is a flow-in boundary. The conditions are expressed as

$$\mathbf{n} \cdot [\mathbf{V} \rho_i C_i - \theta \mathbf{D} \cdot \nabla(\rho_i C_i)] = Q_{C_i,cb}(\mathbf{x}, t) \quad \text{on} \quad B_c(\mathbf{x}) = 0 \quad (5.7)$$

where  $Q_{C_i,cb}(\mathbf{x}, t)$  is total chemical flux of the  $i$ -th species [M/L<sup>2</sup>/t] through the Cauchy boundary,  $B_c(\mathbf{x}) = 0$ , which takes a positive value if it is going out of the region and a negative value if it is coming into the region

Neumann boundary condition:

This boundary condition is used when the dispersive salt-flow rate is known at the boundary. It can be written as

$$-\mathbf{n} \cdot (\theta \mathbf{D} \cdot \nabla(\rho_i C_i)) = Q_{C_i,nb}(\mathbf{x}, t) \quad \text{on} \quad B_n(\mathbf{x}) = 0 \quad (5.8)$$

where  $Q_{C_i,nb}(\mathbf{x}, t)$  is the chemical flux of the  $i$ -th species through the Neumann boundary,  $B_n(\mathbf{x}) = 0$ , [M/L<sup>2</sup>/t]

Subsurface-river interface boundary condition:

$$\mathbf{n} \cdot [\mathbf{V} \rho_i C_i - \theta \mathbf{D} \cdot \nabla(\rho_i C_i)] = (\mathbf{n} \cdot \mathbf{V}) \frac{1}{2} \{ [1 + \text{sign}(\mathbf{n} \cdot \mathbf{V})] \rho_i C_i + [1 - \text{sign}(\mathbf{n} \cdot \mathbf{V})] \rho_i C_{i1D}(x_b, y_b, z_b, t) \} \quad (5.9)$$

where  $C_{i1D}(x_b, y_b, z_b, t)$  is the time-dependent concentration of the  $i$ -th species at the 1-D node corresponding to the subsurface-river/stream interfacial boundary points [M/M]

Subsurface-overland interface boundary condition:

$$\mathbf{n} \cdot [\mathbf{V}\rho_i C_i - \theta \mathbf{D} \cdot \nabla(\rho_i C_i)] = (\mathbf{n} \cdot \mathbf{V}) \frac{1}{2} \left\{ [1 + \text{sign}(\mathbf{n} \cdot \mathbf{V})] \rho_i C_i + [1 - \text{sign}(\mathbf{n} \cdot \mathbf{V})] \rho_i C_{i2D}(x_b, y_b, z_b, t) \right\}$$

where  $C_{i2D}(x_b, y_b, z_b, t)$  is the time-dependent concentration of the  $i$ -th species at the 2-D node corresponding to the subsurface-overland interfacial boundary point [M/M]

### 5.3.3 Diagonalization of Species Transport Equations

In equation (5.2) the determination of  $r_i | N$  is a primary challenge in the numerical computation of the equation. It can be formulated by an ad hoc method (e.g. (Ambrose et al., 1993) and (Brown and Barnwell, 1987)), and reaction-based formulations (e.g. (Steeffel and van Cappellen, 1998) and (Fang et al., 2003)). Yeh et al. (2001a) highlighted that ad-hoc reaction parameters are only applicable to the experimental conditions tested. Reaction-based formulation is used in WASH123D and the fast reactions are decoupled from slow reactions in order to provide an efficient and reliable numerical solution to Eq.(5.2).

In a reaction-based formulation,  $r_i | N$  is given by the summation of rates of all reactions that the  $i$ -th species participates in,

$$r_i | N = \frac{\partial(\rho_i C_i)}{\partial t} \Big|_{reaction} = \sum_{k=1}^N [(v_{ik} - \mu_{ik}) r_k], \quad i \in M \quad (5.10)$$

where  $v_{ik}$  is the reaction stoichiometry of the  $i$ -th species in the  $k$ -th reaction associated with products,  $\mu_{ik}$  is the reaction stoichiometry of the  $i$ -th species in the  $k$ -th reaction associated with the reactants, and  $r_k$  is the rate of the  $k$ -th reaction.

The mass balance equation for species  $i$  is given by substituting Eq.(5.10) into Eq.(5.2),

$$\frac{\partial(\theta\rho_i C_i)}{\partial t} + \alpha_i L(\rho_i C_i) = \theta \sum_{k=1}^N [(v_{ik} - \mu_{ik})r_k], \quad i \in M; \quad \text{or} \quad \mathbf{U} \frac{\partial \mathbf{C}_\theta}{\partial t} + \boldsymbol{\alpha} L(\mathbf{C}) = \theta \mathbf{v} \mathbf{r} \quad (5.11)$$

where  $\mathbf{U}$  is a unit matrix,  $\mathbf{C}_\theta$  is a vector with its components representing  $M$  species concentrations multiplied by the moisture content  $[\text{M}/\text{L}^3]$ ,  $\boldsymbol{\alpha}$  is a diagonal matrix with  $\alpha_i$  as its diagonal component,  $\mathbf{C}$  is a vector with its components representing  $M$  species concentrations  $[\text{M}/\text{L}^3]$ ,  $\mathbf{v}$  is the reaction stoichiometry matrix, and  $\mathbf{r}$  is the reaction rate vector with  $N$  reaction rates as its components.

Because numerical solutions to (5.11) still encounters significant challenges and the approach has been proven inadequate (Fang et al., 2003; Yeh et al., 2001a), fast reactions must be decoupled from (5.11) and mass conservation must be enforced. The diagonalization of the reactive transport system equation (5.11) is employed. This approach was used by Fang et al. (2003) in a reactive batch system.

First, remove the redundant reactions and irrelevant reactions from the reaction network. A “redundant reaction” is defined as a fast reaction that is linearly dependent on other fast reactions, and an “irrelevant reaction” is a kinetic reaction that is linearly dependent on only equilibrium reactions. Consider a reaction system that consists of  $N_E$  fast/equilibrium reactions and  $N_K$  slow/kinetic reactions among  $M$  chemical species. Among  $N_E$  fast/equilibrium reactions are  $N_E$  independent equilibrium reactions and there are  $N_K$  kinetic reactions among the  $N_K$  kinetic reactions that are independent to  $N_E$  equilibrium reaction, in other words, there are  $N_E - N_E$  redundant reactions and  $N_K - N_K$  irrelevant reactions in the system. Finally the reaction network only includes  $N_E$  equilibrium reactions and  $N_K$  kinetic reactions after removing the redundant

and irrelevant reactions. Second, decomposition of the system results in decoupling the equilibrium reactions from kinetic reactions. After decomposition by pivoting on the  $N_E$  equilibrium reactions using Gaussian-Jordan decomposition, the system consists two sub-system of equations,  $N_E$  equations for equilibrium variables, and  $N_{KIV}(=M-N_E)$  equations for kinetic variables that include  $N_{KI}$  kinetic variables corresponding to the  $N_{KI}$  kinetic reactions independent of any other kinetic reactions among the  $N_K$  kinetic reactions, and  $N_C$  ( $N_C=M-N_E-N_{KI}$ ) component variables. The system can be written as equation(3.16),

$$\begin{bmatrix} \mathbf{A}_{11} & \mathbf{0}_{12} \\ \mathbf{A}_{21} & \mathbf{U}_{22} \end{bmatrix} \begin{Bmatrix} \frac{\partial \mathbf{C}_{\theta 1}}{\partial t} \\ \frac{\partial \mathbf{C}_{\theta 2}}{\partial t} \end{Bmatrix} + \begin{bmatrix} \mathbf{B}_{11} & \mathbf{0}_{12} \\ \mathbf{B}_{21} & \mathbf{a}_{22} \end{bmatrix} \mathbf{L} \left( \begin{Bmatrix} \mathbf{C}_1 \\ \mathbf{C}_2 \end{Bmatrix} \right) = \theta \begin{bmatrix} \mathbf{D}_{11} & \mathbf{K}_{12} \\ \mathbf{0}_{21} & \mathbf{K}_{22} \end{bmatrix} \begin{Bmatrix} \mathbf{r}_1 \\ \mathbf{r}_2 \end{Bmatrix} \quad (5.12)$$

where  $\mathbf{A}_{11}$  and  $\mathbf{A}_{21}$  are the submatrices of the reduced  $\mathbf{U}$  matrix with size of  $N_E \times N_E$  and  $N_{KIV} \times N_E$ , respectively (note that  $N_{KIV} = M - N_E = N_{KI} + N_C$ );  $\mathbf{0}_{12}$  and  $\mathbf{U}_{22}$  are the zero- and unit-submatrices, respectively, of the reduced  $\mathbf{U}$  matrix with size of  $N_E \times N_{KIV}$  and  $N_{KIV} \times N_{KIV}$ , respectively;  $\mathbf{C}_{\theta 1}$  and  $\mathbf{C}_{\theta 2}$  are the subvectors of the vector  $\mathbf{C}_\theta$  with sizes of  $N_E$  and  $N_{KIV}$ , respectively;  $\mathbf{B}_{11}$  and  $\mathbf{B}_{21}$  are the submatrices of the reduced  $\alpha$  matrix with sizes of  $N_E \times N_E$  and  $N_{KIV} \times N_E$ , respectively;  $\mathbf{0}_{12}$  and  $\mathbf{a}_{22}$  are the zero- and unit- submatrices of the reduced  $\alpha$  matrix with size of  $N_E \times N_{KIV}$  and  $N_{KIV} \times N_{KIV}$ , respectively;  $\mathbf{C}_1$  and  $\mathbf{C}_2$  are the subvectors of the vector  $\mathbf{C}$  with sizes of  $N_E$  and  $N_{KIV}$ , respectively;  $\mathbf{D}_{11}$  is the diagonal submatrix of the reduced  $\mathbf{v}$  matrix with size of  $N_E \times N_E$  and  $\mathbf{K}_{12}$  is the submatrix of the reduced  $\mathbf{v}$  matrix with size of  $N_E \times N_{KIV}$ ;  $\mathbf{0}_{21}$  is the zero submatrix of the reduced  $\mathbf{v}$  matrix with size of  $N_{KIV} \times N_E$  and  $\mathbf{K}_{22}$  is the submatrix of the reduced  $\mathbf{v}$  matrix with size of  $N_{KIV} \times N_{KIV}$ ;  $\mathbf{r}_1$  and  $\mathbf{r}_2$  are the subvectors of the vector  $\mathbf{r}$  with sizes of  $N_E$  and  $N_{KIV}$ , respectively.

The system of Eq.(5.12) can be further decomposed by pivoting on  $N_{KI}$  independent kinetic reactions.

$$\begin{bmatrix} \mathbf{A}_{11} & \mathbf{A}_{12} & \mathbf{0}_{13} \\ \mathbf{A}_{21} & \mathbf{A}_{22} & \mathbf{0}_{23} \\ \mathbf{A}_{31} & \mathbf{A}_{32} & \mathbf{U}_{33} \end{bmatrix} \begin{Bmatrix} \frac{\partial \mathbf{C}_{\theta 1}}{\partial t} \\ \frac{\partial \mathbf{C}_{\theta 2}}{\partial t} \\ \frac{\partial \mathbf{C}_{\theta 3}}{\partial t} \end{Bmatrix} + \begin{bmatrix} \mathbf{B}_{11} & \mathbf{B}_{12} & \mathbf{0}_{13} \\ \mathbf{B}_{21} & \mathbf{B}_{22} & \mathbf{0}_{23} \\ \mathbf{B}_{31} & \mathbf{B}_{32} & \mathbf{\alpha}_{33} \end{bmatrix} \mathbf{L} \begin{Bmatrix} \mathbf{C}_1 \\ \mathbf{C}_2 \\ \mathbf{C}_3 \end{Bmatrix} = \theta \begin{bmatrix} \mathbf{D}_{11} & \mathbf{K}_{12} & \mathbf{K}_{13} \\ \mathbf{0}_{21} & \mathbf{D}_{22} & \mathbf{K}_{23} \\ \mathbf{0}_{31} & \mathbf{0}_{32} & \mathbf{0}_{33} \end{bmatrix} \begin{Bmatrix} \mathbf{r}_1 \\ \mathbf{r}_2 \\ \mathbf{r}_3 \end{Bmatrix} \quad (5.13)$$

where  $\mathbf{A}_{11}$  is the submatrix of the reduced  $\mathbf{U}$  matrix with size of  $N_E \times N_E$ ,  $\mathbf{A}_{21}$  is the submatrix of the reduced  $\mathbf{U}$  matrix with size of  $N_{KI} \times N_E$ , and  $\mathbf{A}_{31}$  is the submatrix of the reduced  $\mathbf{U}$  matrix with size of  $N_C \times N_E$ ;  $\mathbf{A}_{12}$  is the zero submatrix of the reduced  $\mathbf{U}$  matrix with size of  $N_E \times N_{KI}$ ,  $\mathbf{A}_{22}$  is the submatrix of the reduced  $\mathbf{U}$  matrix with size of  $N_{KI} \times N_{KI}$ , and  $\mathbf{A}_{32}$  is the submatrix of the reduced  $\mathbf{U}$  matrix with size of  $N_C \times N_{KI}$ ;  $\mathbf{0}_{13}$  is the zero submatrix of the reduced  $\mathbf{U}$  matrix with size of  $N_E \times N_C$ ,  $\mathbf{0}_{23}$  is the submatrix of the reduced  $\mathbf{U}$  matrix with size of  $N_{KI} \times N_C$ , and  $\mathbf{U}_{33}$  is the unit submatrix of the reduced  $\mathbf{U}$  matrix with size of  $N_C \times N_C$ ;  $\mathbf{C}_{h1}$ ,  $\mathbf{C}_{h2}$ , and  $\mathbf{C}_{h3}$  are the subvectors of the vector  $\mathbf{C}_h$  with sizes of  $N_E$ ,  $N_{KI}$ , and  $N_C$ , respectively;  $\mathbf{B}_{11}$  is the submatrix of the reduced  $\mathbf{\alpha}$  matrix with size of  $N_E \times N_E$ ,  $\mathbf{B}_{21}$  is the submatrix of the reduced  $\mathbf{\alpha}$  matrix with size of  $N_{KI} \times N_E$ , and  $\mathbf{B}_{31}$  is the submatrix of the reduced  $\mathbf{\alpha}$  matrix with size of  $N_C \times N_E$ ;  $\mathbf{B}_{12}$  is the zero submatrix of the reduced  $\mathbf{\alpha}$  matrix with size of  $N_E \times N_{KI}$ ,  $\mathbf{A}_{22}$  is the submatrix of the reduced  $\mathbf{\alpha}$  matrix with size of  $N_{KI} \times N_{KI}$ , and  $\mathbf{B}_{32}$  is the submatrix of the reduced  $\mathbf{\alpha}$  matrix with size of  $N_C \times N_{KI}$ ;  $\mathbf{0}_{13}$  is the zero submatrix of the reduced  $\mathbf{\alpha}$  matrix with size of  $N_E \times N_C$ ,  $\mathbf{0}_{23}$  is the submatrix of the reduced  $\mathbf{\alpha}$  matrix with size of  $N_{KI} \times N_C$ , and  $\mathbf{\alpha}_{33}$  is the diagonal submatrix of the reduced  $\mathbf{\alpha}$  matrix with size of  $N_C \times N_C$ ;  $\mathbf{C}_1$ ,  $\mathbf{C}_2$ , and  $\mathbf{C}_3$  are the subvectors of the vector  $\mathbf{C}$  with

sizes of  $N_E$ ,  $N_{KI}$ , and  $N_C$ , respectively;  $\mathbf{D}_{11}$  is the diagonal submatrix of the reduced  $\mathbf{v}$  matrix with size of  $N_E \times N_E$ ,  $\mathbf{K}_{12}$  is the submatrix of the reduced  $\mathbf{v}$  matrix with size of  $N_E \times N_{KI}$ , and  $\mathbf{K}_{13}$  is the submatrix of the reduced  $\mathbf{v}$  matrix with size of  $N_E \times N_{KD(k)}$ ;  $\mathbf{0}_{21}$  is the zero submatrix of the reduced  $\mathbf{v}$  matrix with size of  $N_{KI} \times N_E$ ,  $\mathbf{D}_{22}$  is the diagonal submatrix of the reduced  $\mathbf{v}$  matrix with size of  $N_{KI} \times N_{KI}$ , and  $\mathbf{K}_{23}$  is the submatrix of the reduced  $\mathbf{v}$  matrix with size of  $N_{KI} \times N_{KD(k)}$ ;  $\mathbf{0}_{13}$  is the zero submatrix of the reduced  $\mathbf{v}$  matrix with size of  $N_C \times N_E$ ,  $\mathbf{0}_{32}$  is the zero submatrix of the reduced  $\mathbf{v}$  matrix with size of  $N_C \times N_{KI}$ , and  $\mathbf{0}_{33}$  is the zero submatrix of the reduced  $\mathbf{v}$  matrix with size of  $N_C \times N_{KD(k)}$ ;  $\mathbf{r}_1$ ,  $\mathbf{r}_2$ , and  $\mathbf{r}_3$  are the subvectors of the vector  $\mathbf{r}$  with sizes of  $N_E$ ,  $N_{KI}$ , and  $N_{KD(k)}$ , respectively.

The two subsets of equations in (5.12) are further defined as follows,

Algebraic Equations for NE Equilibrium Reactions

$$\frac{\partial(\theta E_i)}{\partial t} + L(E_i^m) = \theta D_{1ii} r_{1i} + \theta \sum_{j=1}^{N_K} K_{1ij} r_{2j}, \quad i \in N_E \quad (5.14)$$

where

$$L(\rho_i C_i) = \nabla \cdot (\mathbf{V} \rho_i C_i) - \nabla \cdot [\theta \mathbf{D} \cdot \nabla (\rho_i C_i)] - M_{C_i}^{as} \quad (5.15)$$

Eq. (3.18) is replaced with a thermodynamically consistent equation

$$K_i^e = \prod_{j \in M} A_j^{\nu_j} / \prod_{j \in M} A_j^{\mu_j} \quad (5.16)$$

or  $F_i(C_1, \dots, C_M; p_1, p_2, \dots) = 0$

where

$$E_i = \sum_{j=1}^{N_E} (A_{11})_{ij} (C_{A1})_j, \quad E_i^m = \sum_{j=1}^{N_E} (B_{11})_{ij} C_{1j} \quad (5.17)$$

where  $K_i^e$  is the equilibrium constant of the  $i$ -th fast reaction,  $A_j$  is the activity of the  $j$ -th species,  $F_i(C_1, \dots, C_M; p_1, p_2, \dots)$  is an empirical function of all species and a number of parameters  $p_1, p_2, \dots$  for the  $i$ -th fast reaction.  $E_i$  was called an equilibrium-variable

Transport Equations for  $N_{KIV}$  Kinetic-Variables

$$\frac{\partial(\theta E_i)}{\partial t} + L(E_i^m) = \theta \sum_{j=1}^{N_K} K_{2nj} r_{2j}, \quad i \in N_{KIV} = M - N_E \quad (5.18)$$

where  $E_i = \sum_{j=1}^{N_E} A_{2ij} C_{1j} + C_{2i}$  and  $E_i^m = \sum_{j=1}^{N_E} B_{2ij} C_{1j} + \alpha_{1i} C_{2i}$

where  $E_i$  is called kinetic variable (Fang, et al., 2003) and is subject to only kinetic reactions in the system. For the  $N_C$  component variables among the  $N_{KIV}$  kinetic variables, the right hand side of Eq.(5.18) is zero.

After diagonalization of the system only  $M-N_E$  kinetic variables needs to be included in the transport computation, which should be less than or equal to the number of  $M$  in Eq.(5.11). And the governing equation for reactive chemical transport in 2-D overland regime can be replaced by a set of  $N_E$  algebraic equations (Eq.(5.16) ) and a set of  $M-N_E$  partial differential equations for kinetic variables as written in Eq.(5.18) by explicitly expressing the transport operator.

$$\frac{\partial(\theta E_i)}{\partial t} + \nabla \cdot (\mathbf{V} E_i^m) - \nabla \cdot [(\theta \mathbf{D} \cdot \nabla E_i^m)] = M_{E_i^{as}} + \theta R_i, \quad i \in N_{KIV} \quad (5.19)$$

where  $E_i$  is the concentration of the  $i$ -th kinetic-variable  $[M/L^3]$ ,  $E_i^{im}$  is the concentration of mobile part of the  $i$ -th kinetic-variable  $[M/L^3]$ ,  $M_{E_i^{as}}$  is the artificial source of the  $i$ -th

kinetic-variable  $[M/L/T]$ ,  $M_{E_i}^{rs}$  is the rainfall source of the  $i$ -th kinetic-variable  $[M/L/T]$ ,  $M_{E_i}^{os1}$  and  $M_{E_i}^{os2}$  are overland sources of the  $i$ -th kinetic-variable from river banks 1 and 2, respectively  $[M/L/T]$ ,  $M_{E_i}^{is}$  is the mass rate of the source of the  $i$ -th kinetic-variable in river/stream from subsurface  $[M/L/T]$ ,  $R_i$  is the production rate of  $i$ -th kinetic-variable due to biogeochemical reactions  $[M/L^3/T]$ , and  $N_{KIV}$  is the number of kinetic variables.

The initial concentration of each species including immobile species (bed precipitates, particulate sorbed onto bed sediment, and dissolved chemical in the immobile water phase), and mobile species (dissolved chemical in mobile water phase, suspended precipitates, and particulate sorbed onto suspended sediment), should be obtained either by field measurement or by simulating the steady state of the system. No boundary conditions are needed for immobile species, while four types of boundary conditions are taken into account for mobile species, Dirichlet, Neumann, Cauchy, and Variable boundary conditions (Yeh et al., 2006), as described in section .5.2.2.

## 5.4 Numerical approaches

### 5.4.1 Strategies for the coupling transport and biogeochemical reactions

#### Fully Implicit Method

According to the fully implicit scheme, the governing equation for kinetic variable transport, Eq.(5.19) can be separated into two equations

$$\theta \frac{E_n^{n+1/2} - E_n^n}{\Delta t} + \frac{\partial \theta}{\partial t} E_n + \nabla \cdot (\mathbf{V} E_n^m) - \nabla \cdot (\theta \mathbf{D} \cdot \nabla E_n^m) = M_{E_n^{as}} + \theta R_{E_n}, \quad i \in N_{KIV} \quad (5.20)$$

$$\frac{E_n^{n+1} - E_n^{n+1/2}}{\Delta t} = 0 \quad (5.21)$$

First, we express  $E_n^m$  in terms of  $(E_n^m/E_n) \cdot E_n$  or  $(E_n - E_n^{im})$  to make  $E_n$ 's as primary dependent variables, so that  $E_n^{n+1/2}$  can be solved through Eq.(5.20). It is noted that the approach of expressing  $E_n^m$  in terms of  $(E_n^m/E_n) \cdot E_n$  improves model accuracy but is less robust than the approach of expressing  $E_n^m$  in terms of  $(E_n - E_n^{im})$  (Yeh et al., 2004). Only the first option, i.e. expressing  $E_n^m$  in terms of  $(E_n^m/E_n) \cdot E_n$  to make  $E_n$  as primary dependent variable, is presented herein. The detailed mathematical representation of the second option can be found elsewhere (Yeh et al., 2005). Second, we solve Eq.(5.21) together with algebraic equations for equilibrium reactions using BIOGEOCHEM (Fang et al., 2003) to obtain all individual species concentrations. Iteration between these two steps is needed because the new reaction terms  $RA_n^{n+1}$  and the equation coefficients in Eq.(5.20) need to be updated by the calculation results of Eq.(5.21). The nonlinear reaction terms are approximated by the Newton-Raphson method

#### Mixed Predictor-Corrector and Operator-Splitting Method

According to the mixed predictor-corrector/operator-splitting scheme, Eq.(5.19) can be separated into two equations as follows

$$\begin{aligned} \theta \frac{(E_n^m)^{n+1/2} - (E_n^m)^n}{\Delta t} + \frac{\partial \theta}{\partial t} E_n^m + \nabla \cdot (\mathbf{V} E_n^m) - \nabla \cdot (\theta \mathbf{D} \cdot \nabla E_n^m) \\ = M_{E_n^{as}} + \theta R_{E_n} - \frac{\partial \theta}{\partial t} (E_n^{im})^n \end{aligned} \quad (5.22)$$

$$\frac{E_n^{n+1} - [(E_n^m)^{n+1/2} + (E_n^{im})^{n+1/2}]}{\Delta t} = \theta R_{E_n}^{n+1} - \theta R_{E_n}^n - \frac{\partial \ln \theta}{\partial t} (E_n^{im})^{n+1} + \frac{\partial \ln \theta}{\partial t} (E_n^{im})^n \quad (5.23)$$

First, solve Eq.(5.22) to obtain  $(E_n^m)^{n+1/2}$ . Second, solve Eq.(5.23) together with algebraic equations for equilibrium reactions using BIOGEOCHM scheme (Fang et al., 2003) to obtain the individual species concentration.

### Operator-Splitting scheme

According to the operator-splitting approach, Eq.(5.19), can be separated into two equations as

$$\theta \frac{(E_n^m)^{n+1/2} - (E_n^m)^n}{\Delta t} + \nabla \cdot (\mathbf{V} E_n^m) - \nabla \cdot (\theta \mathbf{D} \cdot \nabla E_n^m) + \frac{\partial \theta}{\partial t} = M_{E_n^{as}} \quad (5.24)$$

$$\frac{E_n^{n+1} - [(E_n^m)^{n+1/2} + (E_n^{im})^n]}{\Delta t} = \theta R_{E_n}^{n+1} - \frac{\partial \ln \theta}{\partial t} (E_n^{im})^{n+1} \quad (5.25)$$

First, solve Eq.(5.24) and get  $(E_n^m)^{n+1/2}$ . Second, solve Eq.(5.25) together with algebraic equations representing equilibrium reactions using BIOGEOCHM scheme (Fang et al., 2003) to obtain the individual species concentration.

### 5.4.2 Discretization schemes

FEM on the conservative form of equation

Assign two terms  $R_{HS}$  and  $L_{HS}$  as follows to handle the source term in Eq.(5.19)

$$\begin{aligned} \text{If } q \leq 0, \quad M_{E_n^{as}} &= q E_n^m, \quad L_{HS} = -q, \quad R_{HS} = 0 \\ \text{Else } q > 0, \quad M_{E_n^{as}} &= q E_n^{as}, \quad L_{HS} = 0, \quad R_{HS} = M_{E_n^{as}} \end{aligned} \quad (5.26)$$

and express  $E_n^m$  in terms of  $(E_n^m / E_n) E_n^m$ , the governing equation for kinetic variable transport

can be rewritten as

$$\begin{aligned} & \theta \frac{\partial E_n}{\partial t} + \nabla \cdot \left( \mathbf{v} \frac{E_n^m}{E_n} E_n \right) - \nabla \cdot \left( \theta \mathbf{D} \cdot \frac{E_n^m}{E_n} \nabla E_n \right) \\ & - \nabla \cdot \left[ \theta \mathbf{D} \cdot \left( \nabla \frac{E_n^m}{E_n} \right) E_n \right] + \left( L_{HS} \frac{E_n^m}{E_n} + \frac{\partial \theta}{\partial t} \right) E_n = R_{HS} + \theta R_{E_n} \end{aligned} \quad (5.27)$$

Using Galerkin or Petrov-Galerkin FEM for the spatial discretization of Eq.(5.27), it can be written in matrix form as

$$[Q1] \left\{ \frac{\partial E_n}{\partial t} \right\} + [Q2] \{ E_n \} + [Q3] \{ E_n \} = \{ RLS \} + \{ B \} \quad (5.28)$$

where

$$Q1_{ij} = \int_R N_i \theta N_j dR \quad (5.29)$$

$$Q2_{ij} = - \int_R \nabla W_i \cdot \mathbf{v} \frac{E_n^m}{E_n} N_j dR + \int_R \nabla W_i \cdot \left[ \theta \mathbf{D} \cdot \left( \nabla \frac{E_n^m}{E_n} \right) N_j \right] dR \quad (5.30)$$

$$Q3_{ij} = \int_R \nabla N_i \cdot \left( \theta \mathbf{D} \cdot \frac{E_n^m}{E_n} \nabla N_j \right) dR + \int_R N_i \left( L_{HS} \frac{E_n^m}{E_n} + \frac{\partial \theta}{\partial t} \right) N_j dR \quad (5.31)$$

$$RLS_i = \int_R N_i (R_{HS} + \theta R_{E_n}) dR \quad (5.32)$$

$$B_i = - \int_B \mathbf{n} \cdot W_i \mathbf{v} E_n^m dB + \int_B \mathbf{n} \cdot \left( N_i \theta \mathbf{D} \cdot \nabla E_n^m \right) dB \quad (5.33)$$

For interior node  $i$ , the boundary term  $B_i$  is zero, while for boundary node  $i=b$ ,  $B_i$  is calculated according to the specified boundary condition as described in section 5.2.2.

For the mixed predictor-corrector/operator-splitting strategy, the special discretization of the kinetic variable transport equation can be formulated in the same way with that for implicit strategy while replacing term  $E_n^m / E_n$  by 1, so that any differential terms with respect to  $E_n^m / E_n$  will vanish. The load vector should be calculated by

$$RLS_i = \int_R N_i \left( R_{HS} + \theta R_{E_n} - \frac{\partial h}{\partial t} (E_n^m)^n \right) dR \quad (5.34)$$

Whereas for the case of operator-splitting strategy, the spatial discretization is the same as for the mixed predictor-corrector/operator-splitting strategy except that the load vector should be calculated by the following equation

$$SS_i = \sum_{e=1}^{M_e} \int_{R_e} N_i R_{HS} dR \quad (5.35)$$

FEM on the advective form of equation

Write the governing equation for kinetic variable transport, Eq.(5.20) in advective form by expanding the advection term,

$$\begin{aligned} \theta \frac{E_n^{n+1/2} - E_n^n}{\Delta t} + \frac{\partial \theta}{\partial t} E_n + \mathbf{V} \cdot \nabla E_n^m - \nabla \cdot (\theta \mathbf{D} \cdot \nabla E_n^m) + (\nabla \cdot \mathbf{V}) E_n^m \\ = M_{E_n^{as}} + \theta R_{E_n}, \quad n \in [1, M - N_E] \end{aligned} \quad (5.36)$$

Assign two terms  $R_{HS}$  and  $L_{HS}$  as follows

$$\begin{aligned} \text{If } q \leq 0, \quad M_{E_n^{as}} = q E_n^m, \quad L_{HS} = \left( -\mathbf{V} \cdot \ell n \left( \frac{\rho}{\rho_o} \right) - F \frac{\partial h}{\partial t} \right), \quad RHS = 0 \\ \text{Else } q > 0, \quad M_{E_n^{as}} = M_{E_n^{as}}, \quad L_{HS} = \left( q - \mathbf{V} \cdot \ell n \left( \frac{\rho}{\rho_o} \right) - F \frac{\partial h}{\partial t} \right), \quad RHS = M_{E_n^{as}} \end{aligned} \quad (5.37)$$

so that Eq.(5.36) can be simplified as

$$\theta \frac{E_n^{n+1/2} - E_n^n}{\Delta t} + \frac{\partial \theta}{\partial t} E_n + \mathbf{V} \cdot \nabla E_n^m - \nabla \cdot (\theta \mathbf{D} \cdot \nabla E_n^m) + L_{HS} E_n^m = R_{HS} + \theta R_{E_n} \quad (5.38)$$

Expressing  $E_n^m$  in terms of  $(E_n^m / E_n) E_n$  to make  $E_n$ 's as primary dependent variables, Eq.(5.38)

can be modified as

$$\begin{aligned} & \theta \frac{\partial E_n}{\partial t} + \mathbf{V} \cdot \nabla \left( \frac{E_n^m}{E_n} E_n \right) - \nabla \cdot \left( \theta \mathbf{D} \cdot \frac{E_n^m}{E_n} \nabla E_n \right) \\ & - \nabla \cdot \left[ \theta \mathbf{D} \cdot \left( \nabla \frac{E_n^m}{E_n} \right) E_n \right] + \left( L_{HS} \frac{E_n^m}{E_n} + \frac{\partial \theta}{\partial t} \right) E_n = R_{HS} + \theta R_{E_n} \end{aligned} \quad (5.39)$$

Apply Galerkin or Petrov-Galerkin FEM to discretize Eq.(5.39) in spatial, and we can obtain the following matrix equation

$$[Q1] \left\{ \frac{\partial E_n}{\partial t} \right\} + [Q2] \{ E_n \} + [Q3] \{ E_n \} = \{ RLS \} + \{ B \} \quad (5.40)$$

where [Q1], [Q3], and {RLS} are given in the same form as those in Eq.(5.29), (5.31), and (5.32), respectively, while [Q2] and {B} are given as

$$\begin{aligned} Q2_{ij} = & \int_R W_i \mathbf{V} \cdot \left( \nabla \frac{E_n^m}{E_n} \right) N_j dR \\ & + \int_R W_i \mathbf{V} \cdot \frac{E_n^m}{E_n} \nabla N_j dR + \int_R \nabla W_i \cdot \left[ \theta \mathbf{D} \cdot \left( \nabla \frac{E_n^m}{E_n} \right) N_j \right] dR \end{aligned} \quad (5.41)$$

$$B_i = \int_B \mathbf{n} \cdot \left( N_i \theta \mathbf{D} \cdot \nabla E_n^m \right) dB \quad (5.42)$$

For interior node i, the boundary term  $B_i$  is zero; for boundary node  $i=b$ ,  $B_i$  is calculated according to the specified boundary conditions as described in section 5.2.2.

For the mixed predictor-corrector/operator-splitting strategy, the special discretization of the kinetic variable transport equation can be formulated in the same manner as that for implicit strategy while replacing term  $E_n^m / E_n$  with 1, so that any differential terms with respect to  $E_n^m / E_n$  will vanish. The load vector should be calculated by

$$RLS_i = \int_R N_i \left( R_{HS} + \theta R_{E_n} - \frac{\partial h}{\partial t} (E_n^m)^n \right) dR \quad (5.43)$$

Whereas for the case of operator-splitting strategy, the spatial discretization is the same as for the mixed predictor-corrector/operator-splitting strategy except that the load vector should be calculated by the following equation

$$SS_i = \sum_{e=1}^{M_e} \int_{R_e} N_i R_{HS} dR \quad (5.44)$$

Modified LE method to the equation

Rewrite Eq. (5.39) as

$$\begin{aligned} & \theta \frac{\partial E_n}{\partial t} + \frac{\partial \theta}{\partial t} E_n + \left[ \mathbf{V} \frac{E_n^m}{E_n} - \theta \mathbf{D} \cdot \left( \nabla \frac{E_n^m}{E_n} \right) \right] \cdot \nabla (E_n) - \nabla \cdot \left( \theta \mathbf{D} \cdot \frac{E_n^m}{E_n} \nabla E_n \right) \\ & \left\{ \mathbf{V} \cdot \nabla \left( \frac{E_n^m}{E_n} \right) - \nabla \cdot \left[ \theta \mathbf{D} \cdot \left( \nabla \frac{E_n^m}{E_n} \right) \right] + L_{HS} \frac{E_n^m}{E_n} \right\} E_n = R_{HS} + \theta R_{E_n} \end{aligned} \quad (5.45)$$

Assign the particle tracking velocity  $\mathbf{V}_{track}$  as follows

$$\mathbf{V}_{track} = \frac{1}{\theta} \left[ \mathbf{V} \frac{E_n^m}{E_n} - \theta \mathbf{D} \cdot \left( \nabla \frac{E_n^m}{E_n} \right) \right] \quad (5.46)$$

Eq.(5.45) can be written in Lagrangian-Eulerian form as

In Lagrangian step

$$\frac{DE_n}{D\tau} = \frac{\partial E_n}{\partial t} + \mathbf{V}_{track} \cdot \nabla E_n = 0 \quad (5.47)$$

In Eulerian step

$$\frac{DE_n}{D\tau} - D + KE_n = R_L \quad (5.48)$$

where

$$\theta D = \nabla \cdot \left( \theta \mathbf{D} \frac{E_n^m}{E_n} \cdot \nabla E_n \right) \quad (5.49)$$

$$K = \frac{1}{\theta} \left\{ \mathbf{V} \cdot \nabla \left( \frac{E_n^m}{E_n} \right) - \nabla \cdot \left[ \theta \mathbf{D} \cdot \left( \nabla \frac{E_n^m}{E_n} \right) \right] + \left( \frac{\partial \theta}{\partial t} + L_{HS} \frac{E_n^m}{E_n} \right) \right\} \quad (5.50)$$

$$R_L = \frac{1}{\theta} (R_{HS} + \theta R_{E_n}) \quad (5.51)$$

Apply Galerkin FEM to Eq.(5.49) and approximate D and  $E_n$  by linear combination of the base function, we obtain

$$\{D\} = -[QD]\{E_n\} + \{B\} \quad (5.52)$$

where

$$QD_{ij} = \int_R \nabla N_i \cdot \left( \theta \mathbf{D} \frac{E_n^m}{E_n} \cdot \nabla N_j \right) dR / QA_{ii} \quad (5.53)$$

$$B_i = \int_B \mathbf{n} \cdot N_i (\theta \mathbf{D} \cdot \nabla E_n^m) dB / QA_{ii} - \int_B \mathbf{n} \cdot N_i (\theta \mathbf{D} \cdot \nabla \frac{E_n^m}{E_n} E_n) dB / QA_{ii} \quad (5.54)$$

where in Eq.(5.53) and (5.54),  $QA_{ii}$  is a diagonal matrix after mass lumping from

$$QA_{ij} = \int_R N_i \theta N_j dR \quad (5.55)$$

The kinetic variable  $E_n^{n+1/2}$  can be approximated from the following equation

$$\left( \frac{[U]}{\Delta \tau} + W_1 [QD^{n+1}] + W_1 [K^{n+1}] \right) \{ E_n^{n+1/2} \} = \frac{[U]}{\Delta \tau} \{ E_n^* \} - W_2 \left( [K] \{ E_n^m \} \right)^* + W_2 \{ D \}^* + W_1 \{ R_L^{n+1} \} + W_2 \{ R_L^* \} + W_1 \{ B^{n+1} \} \quad (5.56)$$

where  $[U]$  is the unit matrix,  $\Delta \tau$  is the tracking time,  $W_1$  and  $W_2$  are time weighting factors, matrices and vectors with  $^{n+1}$  and  $^{n+1/2}$  are evaluated over the region at the new time step  $n+1$ . Matrices and vectors with superscript  $*$  correspond to the  $n$ -th time step values interpolated at the location where a node is tracked through particle tracking in Lagrangian step.

For interior nodes  $i$ ,  $B_i$  is zero, for boundary nodes  $i = b$ ,  $B_i$  is calculated according to the specified boundary conditions as described in section 5.2.2.

At upstream flux boundary nodes, equation (5.56) cannot be applied because  $\Delta \tau$  equals zero. Thus, we propose a modified LE approach in which the matrix equation for upstream boundary nodes is obtained by explicitly applying the finite element method to the boundary conditions. For example, at the upstream variable boundary

$$\int_B N_i \mathbf{n} \cdot (\mathbf{V} E_n^m - \theta \mathbf{D} \cdot \nabla E_n^m) dB = \int_B N_i \mathbf{n} \cdot \mathbf{V} E_n^m (x_b, y_b, z_b, t) dB \quad (5.57)$$

So that the following matrix equation can be assembled at the boundary nodes

$$[QF]\{E_n^m\} = [QB]\{B\} \quad (5.58)$$

where

$$QF_{ij} = \int_B (N_i \mathbf{n} \cdot \mathbf{V} N_j - N_i \mathbf{n} \cdot \theta \mathbf{D} \cdot \nabla N_j) dB \quad (5.59)$$

$$QB_{ij} = \int_B N_i \mathbf{n} \cdot \mathbf{V} N_j dB \quad (5.60)$$

$$B_j = E_n^m(x_b, y_b, z_b, t) \quad (5.61)$$

where  $E_n^m(x_b, y_b, z_b, t)$  is the value of  $E_n^m(x_b, y_b, z_b, t)$  evaluated at point  $j$ .

For the case of predictor-corrector/operator-splitting strategy, the discretization of the kinetic variable transport equation follows the same procedure as for the implicit strategy. It should be noted that in predictor-corrector/operator-splitting scheme, the primary dependent variable is  $E_n^m$ . So replace the term  $E_n^m / E_n$  with 1 and replace  $E_n^{im}$  with zero in the derivation. For the spatial discretization for the kinetic variable transport equation under operator-splitting scheme follow the same procedure as that for the case of mixed predictor-corrector/operator-splitting scheme except that the load vector term should be calculated by

$$R_L = \frac{R_{HS}}{\theta} \quad (5.62)$$

Mixed LE and FEM schemes

Two mixed LE and FEM schemes are provided to overcome the conventional LE scheme's

inaccuracy at upstream boundary nodes. The basic consideration is to treat the upstream boundary nodes differently from the interior nodes by FEM method. The first one is applying LE method for all interior nodes and downstream boundary nodes while using FEM in conservative form of the equation to the upstream nodes. In this case, the discretized matrix equation for interior nodes and downstream nodes can be obtained by following the same formulation in section 5.3.2.3 while for the upstream boundary nodes, the procedure in section 5.3.2.1. The second one is applying the LE method to all interior nodes and downstream nodes while using FEM in advective form of the equation on the upstream boundary nodes. In this case, the discretized matrix equation for interior nodes and downstream boundary nodes is obtained by LE method as described in section 5.3.2.3, while for downstream boundary nodes, the equation is obtained by the procedure for FEM on advective form as discussed in section 5.3.2.2.

## 5.5 Model verification

In this section, a hypothetical example is illustrated to verify the new model and demonstrate its capability to deal with the complex geochemistry within a three-dimensional subsurface domain. The domain of interested is dimensioned as 800 m×500 m×400 m, as shown in Figure 5.1, it was discretized with uniform hexahedral elements sized 80 m×50 m×40 m.

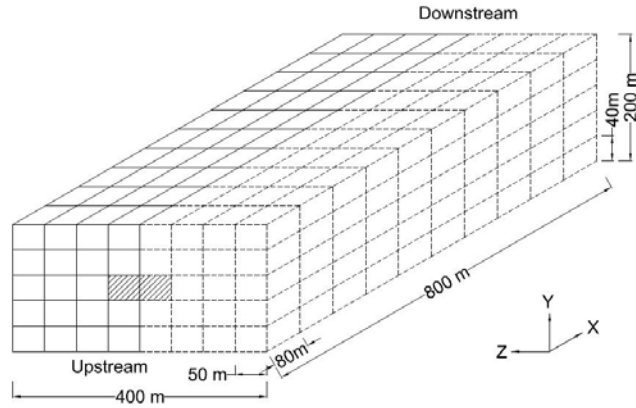


Figure 5.1 Simulation domain and discretization

For flow simulation, Dirichlet boundary condition was imposed on the upstream boundary ( $x=0$  m) with a total head of 190 m and to the downstream boundary ( $x=600$  m) with a total head of 180 m. Variable boundary condition was applied to the top boundary ( $z=200$  m) with a flux of 0.0015 m/d. The effective porosity was assumed to be constant at 0.3 constantly during the entire simulation. The saturated hydraulic conductivity is  $K_{xx}= 1.0$ ,  $K_{yy}=1.0$ , and  $K_{zz} = 0.1$  m/d. The unsaturated hydraulic properties were described as follows

$$\theta = 0.1 + (0.3 - 0.1) / (1 + 4h^2) \quad (5.63)$$

$$K_r = \left[ 0.1 + (0.3 - 0.1) / (1 + 4h^2) \right] / 0.3 \quad (5.64)$$

Where,  $\theta$  is the moisture content and  $K_r$  is the relative conductivity. According to this relationship, the moisture content varied between 0.1 and 0.3 and Darcy velocity varied between 0.0014 and 0.021 m/day. A 100-year simulation was performed with a fixed time step of 1 day after steady state was reached.

For reactive water quality simulation, the reactions and the species ((Brooks, 2001; Langmuir,

1997; Lindsay, 1979; Waite, 1994; Zhang, 2005) involved are described in Table 5.1, where species A in reaction 40 was a hypothetical undergoing a kinetic reduction/oxidation reaction. The aqueous and adsorbed Uranium concentrations were assumed to be zero initially, while the initial concentration of  $\text{Fe}(\text{OH})_3$  was assumed to be 0.0523 mol/L and the pH was 4.6 throughout the region. There was no flux at the bottom ( $z = 0\text{ m}$ ), the front ( $y = 0\text{ m}$ ), and the back ( $y = 400\text{ m}$ ) boundary; at the downstream boundary flow-out variable boundary condition was applied while flow-in variable boundary condition was employed for the top ( $z = 200\text{ m}$ ) and the upstream boundary ( $x = 0\text{ m}$ ) with zero concentration for all species except for the two shaded boundary faces, as shown in Figure 5.0, where the inflow contained  $\text{UO}_2^{2+}$  of  $1.15 \times 10^{-5}$  mol/L,  $\text{NO}_3^-$  of 0.05 mol/L, and a nonreactive tracer of  $1.15 \times 10^{-5}$  mol/L. The longitudinal and transverse dispersivity were assumed to be 60 m and 6 m, respectively. The molecular diffusion coefficient was assumed to be zero.

Following the verification procedure, the flow only was simulated with WASH123D version 1.5 and the newly developed version 3.0 first; the simulated velocity and pressure head at year 1 and year 100 are presented in Figure 5.2 through Figure 5.5, respectively. After checking the numerical output, we found the results from two models are shown to be identical. The results are shown in Figure 5.2 through Figure 5.5 for pressure head and velocity at year 1 and year 100, respectively. Since all conditions for flow simulation remained the constant throughout the simulation period, the flow variation along the time was very small. Therefore, the flow could be assumed to be steady state.

Second, the flow information obtained from the first step was used as input to the paradigm and

the newly developed model; then transport only are simulated with the paradigm and new model, the simulated concentration of tracer, aqueous Uranium, and absorbed Uranium at year 100 are presented in Figure 5.6 through Figure 5.8, respectively. The results obtained were identical.

Finally, the simulation of both flow and transport was performed simultaneously by using the fully coupled new model, and the output shows that the velocity and pressure head are the same as those obtained by WASH123D version 1.5 in the first step and the concentration distribution of tracer, aqueous Uranium, and absorbed Uranium are the same as those by the paradigm. After comparing the simulation results in all three steps, we conclude that both modules perform identically to their counterpart of WASH123D version 1.5, and the paradigm, respectively. This verifies the correctness of the integration of the models.

Table 5.1 Reactions in the example

No.	Reactions and Parameters
(1)	$\text{Fe}(\text{OH})_3 + 3\text{H}^+ = \text{Fe}^{3+} + 3\text{H}_2\text{O} \quad \log K = 2.7$
(2)	$\text{UO}_2^{2+} + \text{H}_2\text{O} = \text{UO}_2\text{OH}^+ + \text{H}^+ \quad \log K = -5.2$
(3)	$\text{UO}_2^{2+} + 2\text{H}_2\text{O} = \text{UO}_2(\text{OH})_{2(\text{aq})} + 2\text{H}^+ \quad \log K = -10.3$
(4)	$\text{UO}_2^{2+} + 3\text{H}_2\text{O} = \text{UO}_2(\text{OH})_3^- + 3\text{H}^+ \quad \log K = -19.2$
(5)	$\text{UO}_2^{2+} + 4\text{H}_2\text{O} = \text{UO}_2(\text{OH})_4^{2-} + 4\text{H}^+ \quad \log K = -33.0$
(6)	$2\text{UO}_2^{2+} + \text{H}_2\text{O} = (\text{UO}_2)_2\text{OH}^{3+} + \text{H}^+ \quad \log K = -2.7$
(7)	$2\text{UO}_2^{2+} + 2\text{H}_2\text{O} = (\text{UO}_2)_2(\text{OH})_2^{2+} + 2\text{H}^+ \quad \log K = -5.62$
(8)	$3\text{UO}_2^{2+} + 4\text{H}_2\text{O} = (\text{UO}_2)_3(\text{OH})_4^{2+} + 4\text{H}^+ \quad \log K = -11.9$
(9)	$3\text{UO}_2^{2+} + 5\text{H}_2\text{O} = (\text{UO}_2)_3(\text{OH})_5^+ + 5\text{H}^+ \quad \log K = -15.5$
(10)	$3\text{UO}_2^{2+} + 7\text{H}_2\text{O} = (\text{UO}_2)_3(\text{OH})_7^- + 7\text{H}^+ \quad \log K = -31.0$
(11)	$\text{UO}_2^{2+} + \text{CO}_3^{2-} = \text{UO}_2\text{CO}_{3(\text{aq})} \quad \log K = 9.68$
(12)	$\text{UO}_2^{2+} + 2\text{CO}_3^{2-} = \text{UO}_2(\text{CO}_3)_2^{2-} \quad \log K = 16.94$
(13)	$\text{UO}_2^{2+} + 3\text{CO}_3^{2-} = \text{UO}_2(\text{CO}_3)_3^{4-} \quad \log K = 21.6$
(14)	$3\text{UO}_2^{2+} + 6\text{CO}_3^{2-} = (\text{UO}_2)_3(\text{CO}_3)_6^{6-} \quad \log K = 54.0$
(15)	$2\text{UO}_2^{2+} + 4\text{H}_2\text{O} + \text{CO}_{2(\text{g})} = (\text{UO}_2)_2\text{CO}_3(\text{OH})_3^- + 5\text{H}^+ \quad \log K = -19.01$
(16)	$> \text{Fe}_s\text{OH} + \text{H}^+ + \text{CO} \Rightarrow \text{Fe}_s\text{OH}_2^+ \quad \log K = 6.51$
(17)	$> \text{Fe}_s\text{OH} \Rightarrow \text{Fe}_s\text{O}^- + \text{H}^+ + \text{CO} \quad \log K = -9.13$
(18)	$> \text{Fe}_s\text{OH} + \text{H}_2\text{CO}_3 \Rightarrow \text{Fe}_s\text{CO}_3\text{H} + \text{H}_2\text{O} \quad \log K = 2.90$
(19)	$> \text{Fe}_s\text{OH} + \text{H}_2\text{CO}_3 \Rightarrow \text{Fe}_s\text{CO}_3^- + \text{H}_2\text{O} + \text{H}^+ + \text{CO} \quad \log K = -5.09$
(20)	$> \text{Fe}_s(\text{OH})_2 + \text{UO}_2^{2+} + \text{H}_2\text{CO}_3 = (> \text{Fe}_s\text{O}_2)\text{UO}_2\text{CO}_3^{2-} + 4\text{H}^+ + 2\text{CO} \quad \log K = -13.0$
(21)	$> \text{Fe}_w(\text{OH})_2 + \text{UO}_2^{2+} + \text{H}_2\text{CO}_3 = (> \text{Fe}_w\text{O}_2)\text{UO}_2\text{CO}_3^{2-} + 4\text{H}^+ + 2\text{CO} \quad \log K = -17.10$
(22)	$\text{FeOH}^{2+} + \text{H}^+ = \text{Fe}^{3+} + \text{H}_2\text{O} \quad \log K = 2.19$
(23)	$\text{Fe}(\text{OH})_2^+ + 2\text{H}^+ = \text{Fe}^{3+} + 2\text{H}_2\text{O} \quad \log K = 5.67$
(24)	$\text{Fe}(\text{OH})_3^0 + 3\text{H}^+ = \text{Fe}^{3+} + 3\text{H}_2\text{O} \quad \log K = 12.56$
(25)	$\text{Fe}(\text{OH})_4^- + 4\text{H}^+ = \text{Fe}^{3+} + 4\text{H}_2\text{O} \quad \log K = 21.6$
(26)	$\text{H}_2\text{O} + \text{CO}_{2(\text{g})} = \text{H}_2\text{CO}_3^0 \quad \log K = -1.47$
(27)	$\text{H}_2\text{CO}_3^0 = \text{H}^+ + \text{HCO}_3^- \quad \log K = -6.35$
(28)	$\text{HCO}_3^- = \text{H}^+ + \text{CO}_3^{2-} \quad \log K = -10.33$
(29)	$> \text{Fe}_w\text{OH} + \text{H}^+ + \text{CO} \Rightarrow \text{Fe}_w\text{OH}_2^+ \quad \log K = 6.51$
(30)	$> \text{Fe}_w\text{OH} \Rightarrow \text{Fe}_w\text{O}^- + \text{H}^+ + \text{CO} \quad \log K = -9.13$
(31)	$> \text{Fe}_w\text{OH} + \text{H}_2\text{CO}_3 \Rightarrow \text{Fe}_w\text{CO}_3\text{H} + \text{H}_2\text{O} \quad \log K = 2.90$
(32)	$> \text{Fe}_w\text{OH} + \text{H}_2\text{CO}_3 \Rightarrow \text{Fe}_w\text{CO}_3^- + \text{H}_2\text{O} + \text{H}^+ + \text{CO} \quad \log K = -5.09$
(33)	$0 \cdot \text{Fe}(\text{OH})_3 = 0 \cdot [ > \text{Fe}_s\text{OH}_2^+ + > \text{Fe}_s\text{O}^- + > \text{Fe}_s\text{CO}_3\text{H} + > \text{Fe}_s\text{CO}_3^- + (> \text{Fe}_s\text{O}_2)\text{UO}_2 + (> \text{Fe}_s\text{O}_2)\text{UO}_2\text{CO}_3^{2-} ] +$
(34)	$0 \cdot \text{Fe}(\text{OH})_3 = 0 \cdot [ > \text{Fe}_w\text{OH}_2^+ + > \text{Fe}_w\text{O}^- + > \text{Fe}_w\text{CO}_3\text{H} + > \text{Fe}_w\text{CO}_3^- + (> \text{Fe}_w\text{O}_2)\text{UO}_2 + (> \text{Fe}_w\text{O}_2)\text{UO}_2\text{CO}_3^{2-} ] +$
(35)	$0 \cdot \text{Fe}(\text{OH})_3 = 0 \cdot [ > \text{Fe}_s\text{OH}_2^+ + > \text{Fe}_s\text{O}^- + > \text{Fe}_s\text{CO}_3\text{H} + > \text{Fe}_s\text{CO}_3^- + (> \text{Fe}_s\text{O}_2)\text{UO}_2 + (> \text{Fe}_s\text{O}_2)\text{UO}_2\text{CO}_3^{2-} ] +$ $> \text{Fe}_s\text{OH}, 0.0018C_{\text{Fe}(\text{OH})_3} = C_{>\text{Fe}_s\text{OH}} + C_{>\text{Fe}_s\text{OH}_2^+} + C_{>\text{Fe}_s\text{O}^-} + C_{>\text{Fe}_s\text{CO}_3\text{H}} + C_{>\text{Fe}_s\text{CO}_3^-} + 2(C_{(>\text{Fe}_s\text{O}_2)\text{UO}_2} + C_{(>\text{Fe}_s\text{O}_2)\text{UO}_2\text{CO}_3^{2-}})$
(36)	$0 \cdot \text{Fe}(\text{OH})_3 = 0 \cdot [ > \text{Fe}_w\text{OH}_2^+ + > \text{Fe}_w\text{O}^- + > \text{Fe}_w\text{CO}_3\text{H} + > \text{Fe}_w\text{CO}_3^- + (> \text{Fe}_w\text{O}_2)\text{UO}_2 + (> \text{Fe}_w\text{O}_2)\text{UO}_2\text{CO}_3^{2-} ] +$ $> \text{Fe}_w\text{OH}, 0.8732C_{\text{Fe}(\text{OH})_3} = C_{>\text{Fe}_w\text{OH}} + C_{>\text{Fe}_w\text{OH}_2^+} + C_{>\text{Fe}_w\text{O}^-} + C_{>\text{Fe}_w\text{CO}_3\text{H}} + C_{>\text{Fe}_w\text{CO}_3^-} + 2(C_{(>\text{Fe}_w\text{O}_2)\text{UO}_2} + C_{(>\text{Fe}_w\text{O}_2)\text{UO}_2\text{CO}_3^{2-}})$
(37)	$\text{UO}_2^{2+} + \text{NO}_3^- = \text{UO}_2\text{NO}_3^+ \quad \log K = -0.300$
(38)	$> \text{Fe}_s(\text{OH})_2 + \text{UO}_2^{2+} = (> \text{Fe}_s\text{O}_2)\text{UO}_2 + 2\text{H}^+ \quad \log K_f = 3.04, \log K_b = -10.1$
(39)	$> \text{Fe}_w(\text{OH})_2 + \text{UO}_2^{2+} = (> \text{Fe}_w\text{O}_2)\text{UO}_2 + 2\text{H}^+ \quad \log K_f = -0.494, \log K_b = 4.5$
(40)	$\text{UO}_2^{2+} = A \quad \log K_f = -10.0, \log K_b = -5.0$

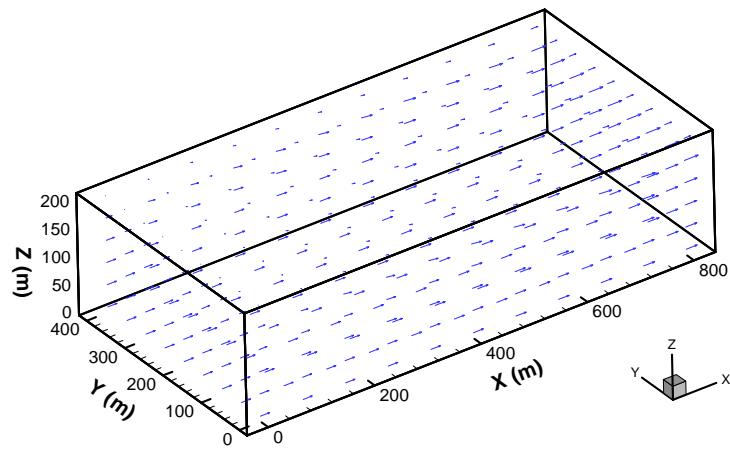
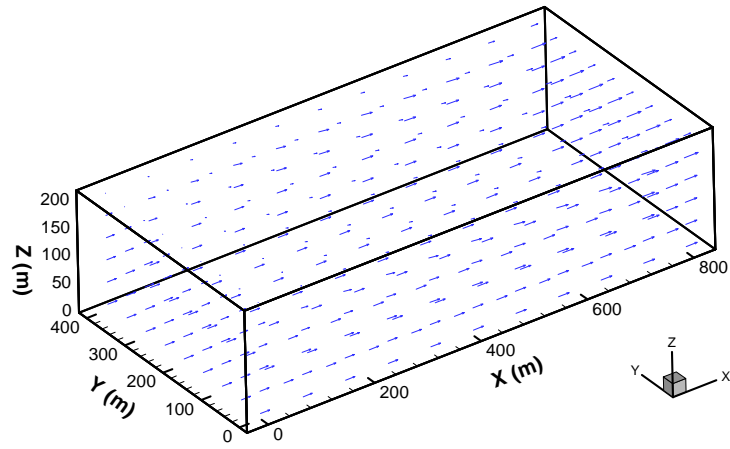


Figure 5.2 Velocity simulated by two the two models at year 1  
 Upper: WASH123D version 1.5 Lower: WASH123D version 3.0

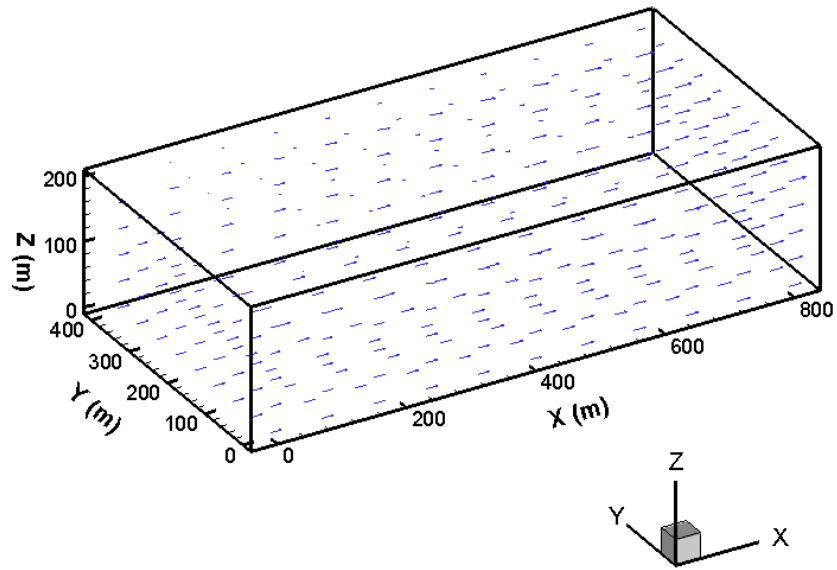
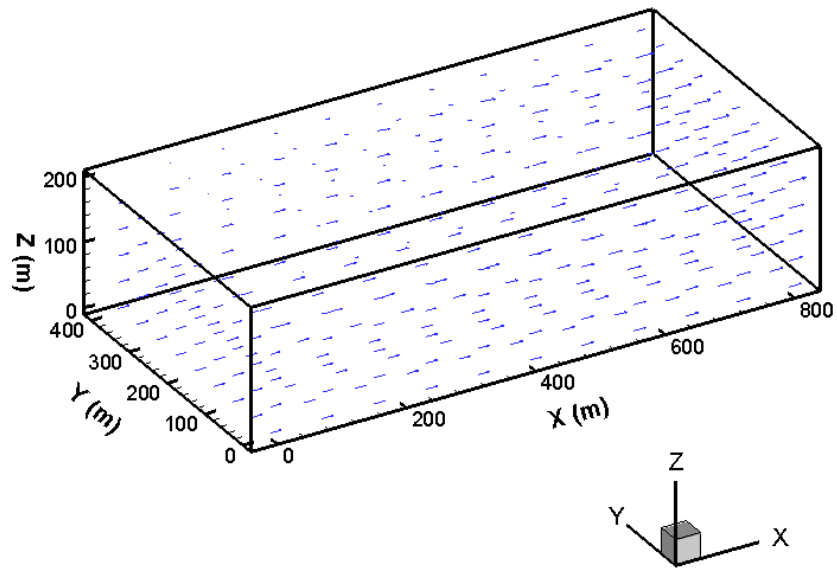


Figure 5.3 Simulated velocity at year 100  
 Upper: WASH123D version1.5 Lower: WASH123D version 3.0

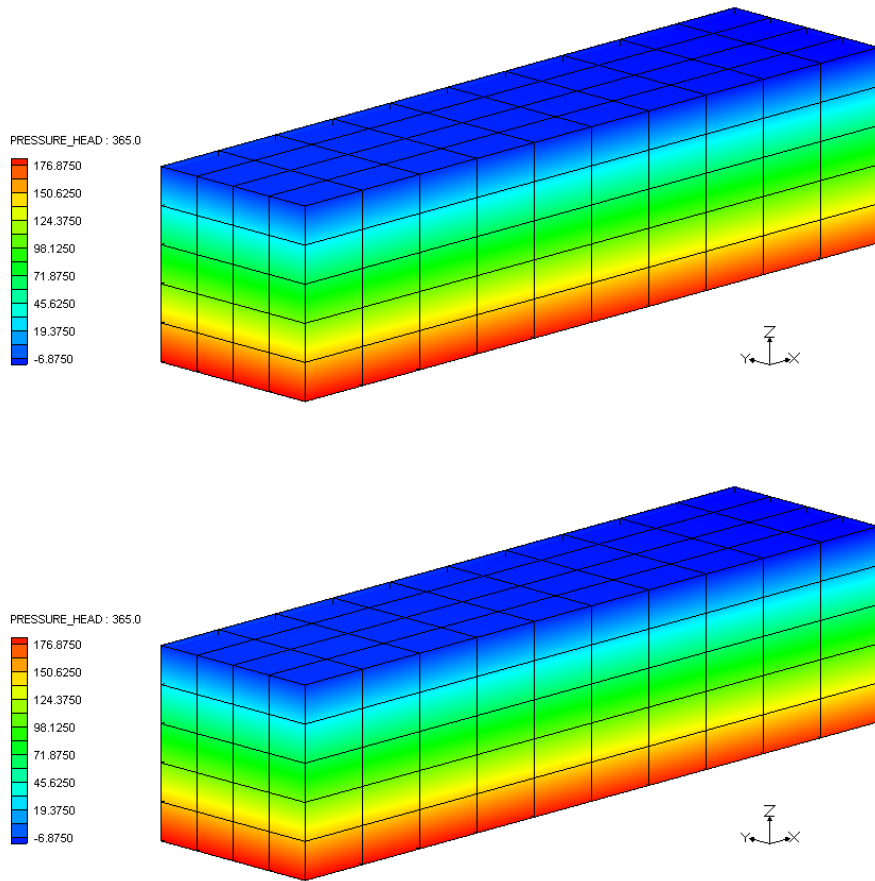


Figure 5.4 Simulated pressure head at year 1  
 Upper: WASH123D version 1.5 Lower: WASH123D version 3.0

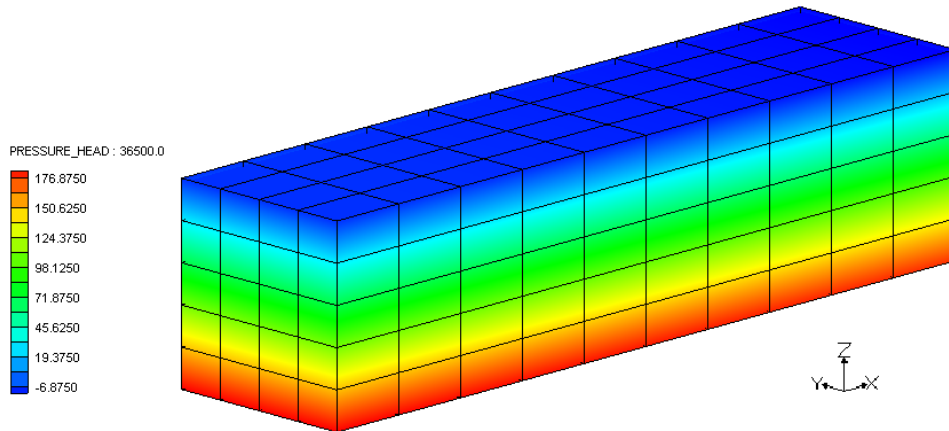
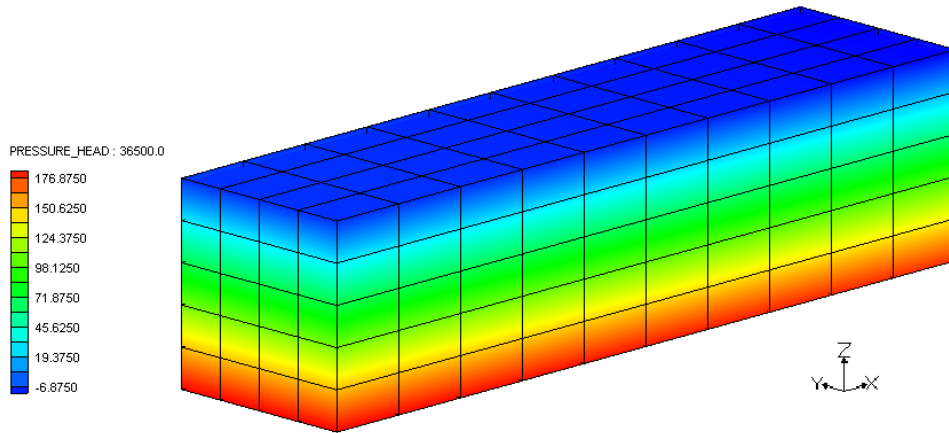


Figure 5.5 Simulated pressure head at year 100  
 Upper: WASH123D version 1.5 Lower: WASH123D version 3.0

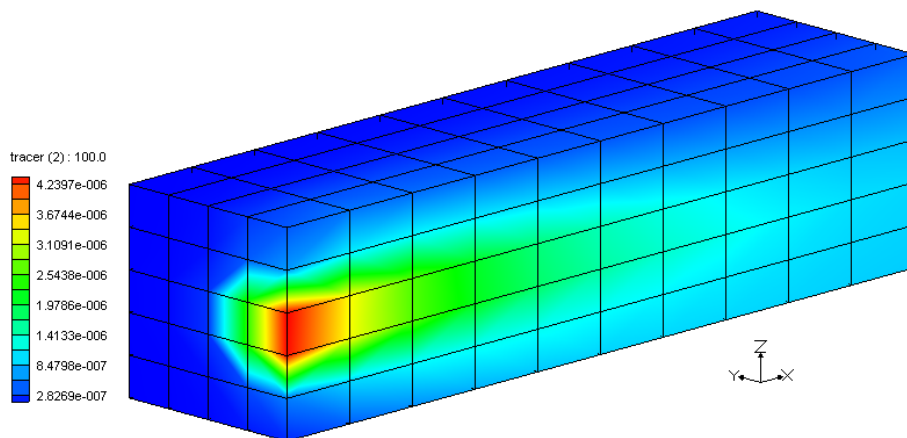
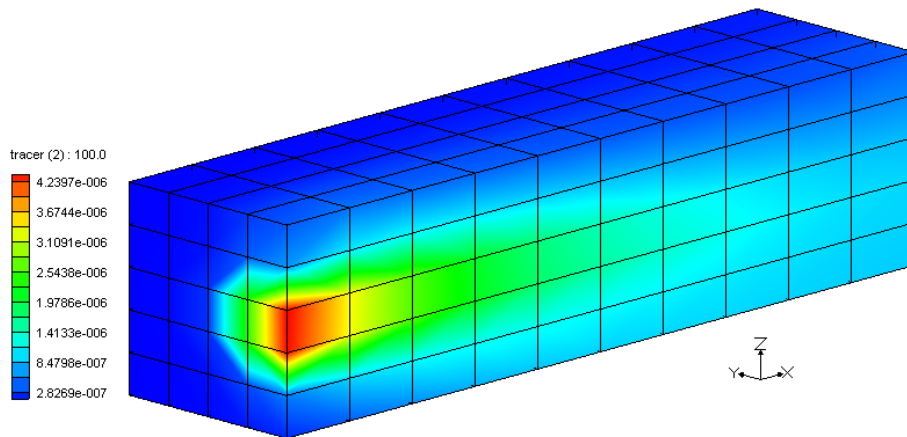


Figure 5.6 Simulated Tracer concentration at year 100  
 Upper: paradigm Lower: WASH123D version 3.0

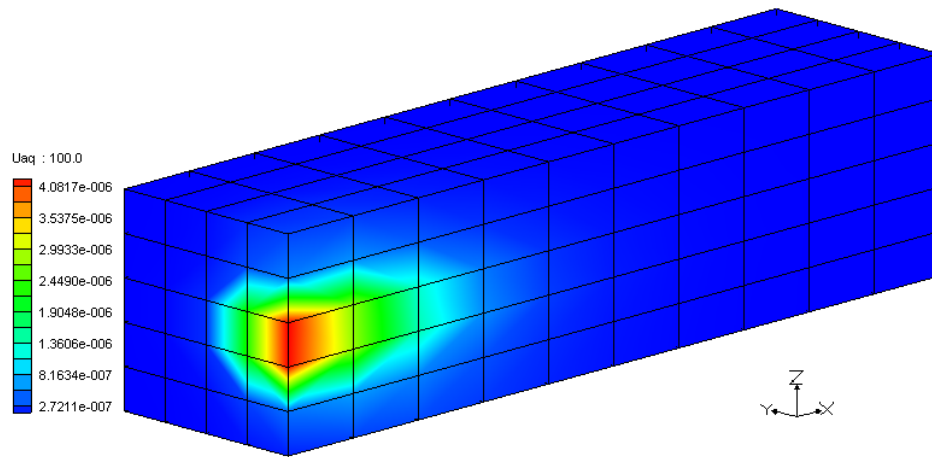
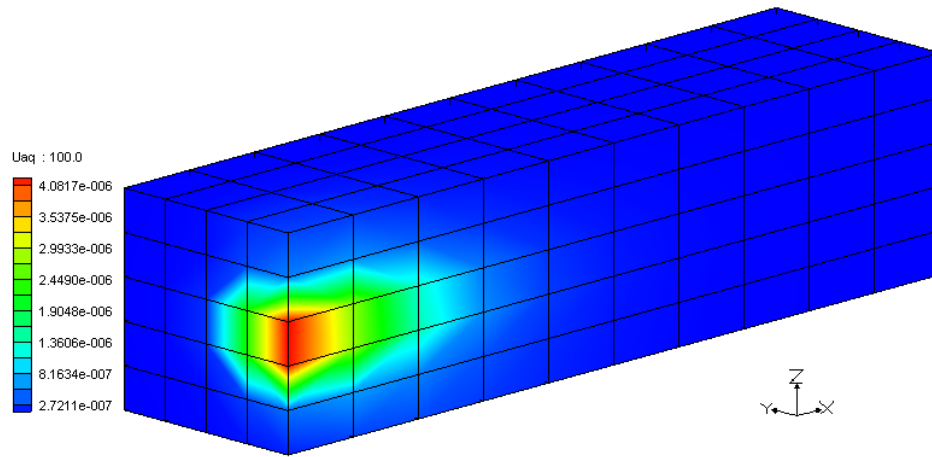


Figure 5.7 simulated aqueous Uranium concentration at year 100  
 Upper: paradigm Lower: WASH123D version 3.0

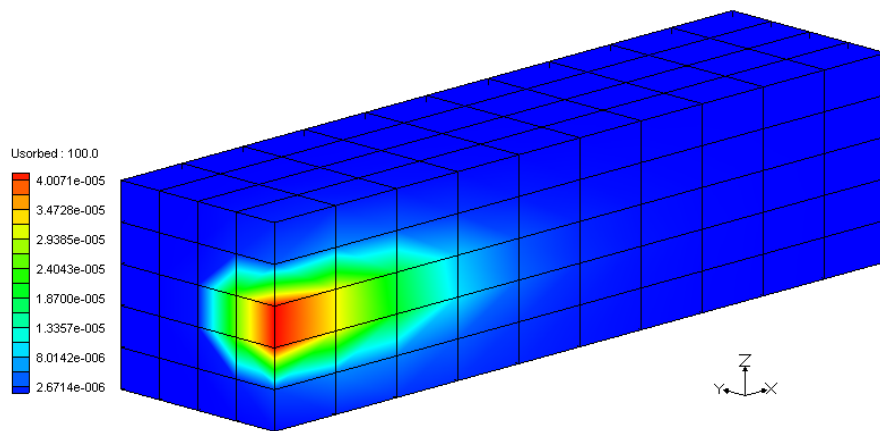
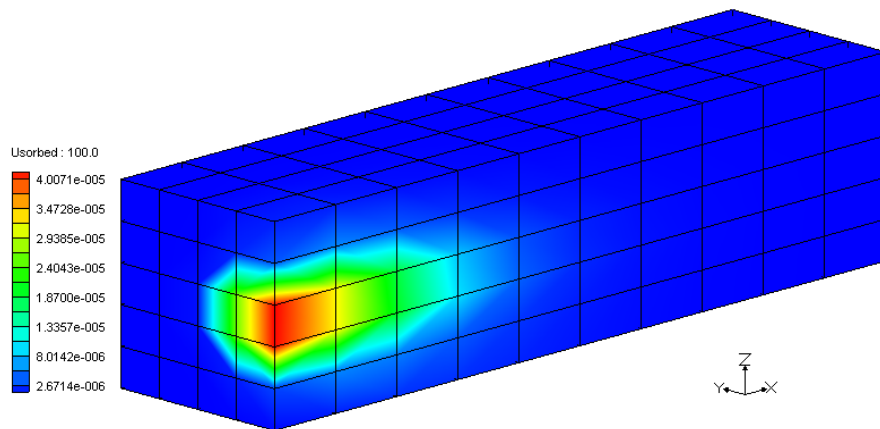


Figure 5.8 Simulated adsorbed Uranium concentration year 100  
 Upper: Paradigm Lower: WASH123D version 3.0

## 5.6 Conclusion

This chapter presents the development of a numerical model for fluid flow and reactive water quality simulation in subsurface water system by incorporating a general water quality simulation paradigm into the current version of WASH123D model. The model is one of three major components of an integrated hydrology/hydraulic water quality model for watershed scale simulations.

The coupling of water flow and water quality simulations provides the model with a full range of simulation capability and saves computer storage compared with the commonly used indirectly linked models. The coupling of water quality transport with an arbitrary number of mixed equilibrium and kinetic reactions makes the model general and flexible enough to simulate water quality problems subject to any number of chemical reactions.

Through the diagonalization of the reactive transport equation via Gauss-Jordan column reduction of the chemical reaction network, equilibrium reactions are decoupled from the kinetic reactions. Species reactive transport equations are transformed into two sets: reactive transport equations of kinetic-variables and algebraic equations of equilibrium variables. Kinetic variable is adopted as primary dependent variable in solving the transport equation rather than individual species to reduce the number of transport equations and simplify the reaction terms. Three coupling strategies, fully implicit scheme, mixed predictor-corrector/operator-splitting scheme, and operator-splitting scheme, are included in the model to deal with the coupling of transport and biogeochemical reactions at different levels of efficiency and accuracy. Five spatial discretization approaches are utilized to solve the advection-dispersion transport equation

describing the kinetic variable transport.

In each time step, hydrologic/hydraulic variables are solved in the flow module; kinetic variables are then solved in the transport module. This is followed by solving the reactive chemical system node by node to yield concentrations of all species. One hypothetical example is employed to verify the correctness of the coupling between hydrodynamics and reactive water quality model and to demonstrate the simulation capability of the model.

### 5.7 References

- Ambrose, R.B., Wool, T.A. and Martin, J.L., 1993. The water quality analysis simulation program, WASP5 Part A: model documentation Environmental Research Laboratory, US Environmental Protection Agency, Athens, GA.
- Brown, L.C. and Barnwell, T.O., 1987. The enhanced stream water quality models QUAL2E and QUAL2E-UNCAS: Documentation and user Manual. EPA/600/3-87/007.
- Brooks, S.C., 2001. Waste Characteristics of the former S-3 ponds and outline of Uranium chemistry relevant to NABIR FRC studies, Oak Ridge National Laboratory, Oak Ridge, Tennessee.
- Cheng, H.P., 1995. Development and Application of a Three-Dimensional Finite Element Model of Subsurface Flow, Heat Transfer, and Reactive Chemical Transport, The Pennsylvania State University, University Park, PA.
- Cheng, J.R. and Yeh, G.T., 1994. Modeling three-dimensional subsurface flow, fate and transport of microbes and chemicals (3DFATMIC), X-th Int. Conf. on Numerical Methods in Water

- Resources, Heidelberg, Germany, pp. 217-224.
- Fang, Y.L., Yeh, G.T. and Burgos, W.D., 2003. A Generic Paradigm to Model Reaction-Based Biogeochemical Processes in Batch Systems. *Water Resources Research*, 33(4): 1083-1118.
- Guo, W. and Langevin, C.D., 2002. User's guide to SEAWAT: a computer program for simulation of three-dimensional variable-density ground-water flow, U.S. .
- Jr. Kipp, K.L., 1997. Guide to the revised heat and solute transport simulator, HST3D (version 2), U.S. Geological Survey Water-Resources Investigations Report 97-4157.
- Keum, D.K. and Hahn, P.S., 2003. A coupled reactive chemical transport model: mixing cell model with two solid phases and its application. *Computer & Geosciences*, 29: 431-445.
- Langmuir, D., 1997. *Aqueous Environmental Geochemistry*. Prentice Hall
- Lichtner, P.C., 1996. Continuum Formulation of Multicomponent-Multiphase Reactive Transport. In: P.C. Lichtner, C.I. Steefel and E.H. Oelkers (Editors), *Reactive Transport in Porous Media, Reviews in Mineralogy*. Mineralogical Society of America, Washington, D.C.
- Lin, H.-C., Richards, D.R., Yeh, G.T., Cheng, J.R., Cheng, H.P. and Jones, N.L., 1997. FEMWATER, a three-dimensional finite element computer model for simulating density-dependent flow and transport in variably saturated media, U.S. Army Corps of Engineer Waterway Experiment Station Technical Report CHL-97-12, Vicksburg, MS.
- Mao, X., Prommer, H., Barry, D.A., Langevin, C.D., Panteleit, B. and Li, L., 2006. Three-dimensional model for multi-component reactive transport with variable density groundwater flow. *Environmental Modelling & Software*, 21: 615-628.
- Parkhurst, D.L. and Appelo, C.A.J., 1999. User's guide to PHREEQC - a computer program for

- speciation, reaction-path, 1D-transport, and Inverse Geochemical Calculations, U.S. Geological Survey, USA.
- Prommer, H., Barry, D.A. and Zheng, C., 2003. MODFLOW/MT3DMS-based reactive multicomponent transport modeling. *Ground Water*, 41(2): 247-257.
- Salvage, K.M., Yeh, G.T., Cheng, H.P. and Cheng, J.R., 1996. Development of a model of subsurface hydrologic transport and biogeochemical reactions (HYDROBIOGEOCHEM), *Computational Methods in Water Resources XI*.
- Steeffel, C.I. and van Cappellen, P., 1998. Preface: reactive transport modeling of natural systems. *journal of Hydrology*, 209: 1-7.
- Steeffel, C.I. and Yabusaki, S.B., 1996. OS3D/GIMRT, Software for Modeling Multi-Component-Multidimensional Reactive Transport, Pacific Northwest Laboratory, Richland, WA.
- Szecsody, J.E., Zachara, J.M., Chilakapati, A., Jardine, P.M. and Ferreny, A.S., 1998. Importance of flow and particle-scale heterogeneity on Co(II/III)EDTA reactive transport. *journal of Hydrology*, 209(1): 112-136.
- Trefry, M.G. and Muffels, C., 2007. FEFLOW: a finite-element ground water flow and transport modeling tool. *Ground Water*, 45(5): 525-528.
- VOSS, C.I., 1984. A finite element simulation model for saturated-unsaturated, fluid-density-dependent ground water flow with energy transport or chemical reactive single-species solute transport, U.S. Geological Survey Water-Resources Investigation Report 84-4369.
- Waite, T.D., 1994. Uranium (VI) adsorption to ferrihydrite: Application of a surface

- complexation model. *Geochemica et Cosmochimica Acta*, 58(24)
- Wood, B.D., Dawson, C.N., Szecsody, J.E. and Streile, G.P., 1994. Modeling contaminant transport and biodegradation in a layered porous media system. *Water Resources Research*, 30(6): 1833-1845.
- Yeh, G.-T., Burgosb, W.D. and Zacharac, J.M., 2001a. Modeling and measuring biogeochemical reactions: system consistency, data needs, and rate formulations. *Advances in Environmental Research*, 5: 219-237.
- Yeh, G.-T., Fang, Y., Zhang, F., Sun, J., Li, Y., Li, M.-H. and Siegel, M.D., 2009. Numerical modeling of coupled fluid flow and thermal and reactive biogeochemical transport in porous and fractured media. *Computational Geosciences*.
- Yeh, G.-T., Huang, G., Cheng, H.-P., Zhang, F., Lin, H.-C., Edris, E. and Richards, D., 2006. A first-principle, physics-based watershed model: WASH123D. In: V.P. Singh and D.K. Frevert (Editors), *Watershed Models*. CRC Press, Boca Raton, FL.
- Yeh, G.-T., Huang, G., Zhang, F., Cheng, H.P. and Lin, H.-C., 2005. WASH123D: A numerical model of flow, thermal transport, and salinity, sediment, and water quality transport in WAterSHed systems of 1-D stream-river network, 2-D overland regime, and 3-D subsurface media, Office of Research and Development, Orlando, FL.
- Yeh, G.T., Salvage, K. and Choi, W.H., 1996. Reactive Multispecies-Multicomponent Chemical Transport Controlled by both Equilibrium and Kinetic Reactions, XI-th Int. Conf. on Numerical Methods in Water Resources, Cancun, Mexico, pp. 585-592.
- Yeh, G.T., Siegel, M.D. and Li, M.H., 2001b. Numerical Modeling of Coupled Fluid Flows and Reactive Transport Including Fast and Slow Chemical Reactions. *Journal of Contaminant*

- Hydrology, 47: 379-390.
- Yeh, G.T., Sun, J., Jardine, P.M., Burgos, W.D., Fang, Y.L., Li, M.H. and Siegel, M.D., 2004. HYDROGEOCHEM 5.0: A Three-Dimensional Model of Coupled Fluid Flow, Thermal Transport, and HYDROGEOCHEMical Transport through Variably Saturated Conditions - Version 5.0, OAK RIDGE NATIONAL LABORATORY, Oak Ridge, Tennessee.
- Yeh, G.T. and Tripathi, V.S., 1991. A model for simulating transport of reactive multispecies components: model development and demonstration. *Water Resources Research*, 27: 3075-3094.
- Zhang, F., 2005. A new paradigm of modeling watershed water quality. Ph.D Dissertation. Depart. of Civil, Environmental, & Construction Engineering, University of Central Florida, Orlando, FL
- Zhang, F., Yeh, G.T., Parker, J.C., Brooks, S.C., Pace, M.N., Kim, Y.J., Jardine, P.M. and Watson, D.B., 2007. A reaction-based paradigm to model reactive chemical transport in groundwater with general kinetic and equilibrium reactions. *Journal of Contaminant Hydrology*, 92(1-2): 10-32.

## CHAPTER 6 SUMMARY AND FUTURE WORK

### 6.1 Summary

This dissertation presents the design of a first principle, physics-based watershed-scale model which integrates hydrology/hydraulics and water quality transport. The numerical model developed in this thesis comprises of three modules: (1) a one-dimensional simulation module for dendritic river networks, (2) a two-dimensional simulation module for land surfaces, and (3) a three-dimensional simulation module for subsurface media. All three modules are capable of simulating separated and integrated fluid flow, water quality transport, and/or sediment transport.

The Saint Venant equation and its simplified versions, diffusion wave and kinematic wave forms, are employed for surface fluid flow simulations and the modified Richards equation is applied for subsurface flow simulation. The governing equations for fluid flow, their associated boundaries conditions and the numerical approaches used to solve the governing equation for water flow have been addressed in detail elsewhere (Huang, 2006; Yeh et al., 2005).

The reaction-based advection-dispersion equation is used as the governing equation for water quality transport. Three coupling strategies: fully implicit mixed predictor-corrector and operator-splitting, and operator-splitting schemes are included in the model to deal with the reactive chemistry and five numerical approaches are provided to solve the advective-dispersive transport equation. These five numerical approaches are (1) finite element method on the

conservative form of the transport equation, (2) finite element method on the advective form of the transport equation, (3) modified Lagrangian-Eulerian approach, (4) Lagrangian-Eulerian approach for the interior nodes and downstream boundary nodes with finite element method on the conservative form of transport equation for the upstream boundary nodes, (5) Lagrangian-Eulerian approach for the interior nodes and downstream boundary nodes with finite element method on the advective form of transport equation for the upstream boundary nodes,

The surface-subsurface water interactions are considered in the flow module and simulated on the basis of continuity of interface. In the transport simulations, fast/equilibrium reactions are decoupled from slow/kinetic reactions by the decomposition of reaction networks; this enables robust numerical integration of the governing equations. Kinetic variables are adopted as primary dependent variables rather than biogeochemical species to reduce the number of transport equations and simplify the reaction terms. In each time step, hydrologic/hydraulic variables are solved in the flow module; kinetic variables are then solved in the transport module. This is followed by solving the reactive chemical system node by node to yield concentrations of all species.

One unique feature included in the new developed model is its inclusion of several levels of integration or coupling. They are (1) coupling of water flow and water quality simulations, providing the model with a full range of simulation capabilities, allowing density-dependent water flow simulation, and saving significant computer storage compared to the commonly used external link of water flow model and water quality model; (2) coupling of surface and groundwater flow simulation, which allows the model to include the interaction of water flow

from 1-D, 2-D and 3-D media, so that the users can conduct complete watershed-based simulations, this feature has been addressed in detail by Huang and Yeh (2009), and (3) coupling of water quality transport with an arbitrary number of mixed equilibrium and kinetic reactions, which makes the model general and flexible enough to simulate water quality problems subject to any number of chemical reactions.

## 6.2 Future works

Currently the model can simulate the reactive water quality transport only in each single media, either in 1-D river/stream network systems, or 2-D overland regimes, or 3-3 subsurface systems although the interaction among media has been taken into account in the flow module. One of the critical issues in a first principle physics-based watershed model is its treatment of coupling among various media (Huang and Yeh, 2009). A rigorous consideration of coupling of reactive transport among media based on the continuity of material flux and species concentration would enable the model to calculate the exchange of material mass among media and extend the capability of the model so that the model can be used to simulation the whole hydrological processes.

The model presented in this dissertation does not have a component for uncertainty analysis. The inclusion of uncertainty analysis will improve the usability of model and provide the users with more actionable results.

The full implementation of the comprehensive simulation capabilities of the model requires intensive computation effort. The current code of the model does not support parallel computing.

The parallelization of the current code will help improve the model performance and save computational effort. This improvement will lead to the ability to simulate the large scale field problems more readily.

The model has been applied to only a few field studies. Further validation of the new integrated watershed model for hydrologic and reactive water quality transport processes in the field with actual data is needed.

### 6.3 References

Huang, G., 2006. Physics based, integrated modeling of hydrology and hydraulics at watershed scales, The Pennsylvania State University, College Park, PA, 199 pp.

Huang, G.B. and Yeh, G.T., 2009. Comparative study of coupling approaches for surface water and subsurface interactions. *Journal of Hydrologic Engineering*, 14(5): 453-462.

Yeh, G.-T., Huang, G., Zhang, F., Cheng, H.P. and Lin, H.-C., 2005. WASH123D: A numerical model of flow, thermal transport, and salinity, sediment, and water quality transport in WATerSHed systems of 1-D stream-river network, 2-D overland regime, and 3-D subsurface media, Office of Research and Development, Orlando, FL.